TUMOR IMMUNITY

CD4$^+$ T cells with convergent TCR recombination reprogram stroma and halt tumor progression in adoptive therapy

Steven P. Wolf[1,2]*, Matthias Leisegang[1,3,4], Madeline Steiner[2]†, Veronika Wallace[2], Kazuma Kiyotani[5,6], Yifei Hu[7,8], Leonie Rosenberger[3], Jun Huang[7,9], Karin Schreiber[1,2], Yusuke Nakamura[5,6], Andrea Schietinger[10], Hans Schreiber[1,2,9]

Cancers eventually kill hosts even when infiltrated by cancer-specific T cells. We examined whether cancer-specific T cell receptors of CD4$^+$ T cells (CD4TCRs) from tumor-bearing hosts can be exploited for adoptive TCR therapy. We focused on CD4TCRs targeting an autochthonous mutant neoantigen that is only presented by stroma surrounding the MHC class II–negative cancer cells. The 11 most common tetramer-sorted CD4TCRs were tested using TCR-engineered CD4$^+$ T cells. Three TCRs were characterized by convergent recombination for which multiple T cell clonotypes differed in their nucleotide sequences but encoded identical TCR α and β chains. These preferentially selected TCRs destroyed tumors equally well and halted progression through reprogramming of the tumor stroma. TCRs represented by single T cell clonotypes were similarly effective only if they shared CDR elements with preferentially selected TCRs in both α and β chains. Selecting candidate TCRs on the basis of these characteristics can help identify TCRs that are potentially therapeutically effective.

INTRODUCTION

Somatic mutations cause cancer and therefore are found in all types of malignancies (*1*). Many of these mutations represent nonsynonymous single nucleotide variants (nsSNVs) in tumor DNA, absent from the germline genome. These nsSNVs cause single–amino acid substitutions, are the basis of individually distinct ("unique") tumor-specific antigens (*2*, *3*), and are targetable by adoptive transfer of mutation-specific T cells (*2*). These mutation-encoded, tumor-specific antigens are now usually referred to as "neoantigens." Findings from patients treated with immune checkpoint inhibitors (ICIs) or adoptively transferred tumor-infiltrating lymphocytes (TILs) support the notion that these neoantigens are effective T cell targets in humans (*4*). Unfortunately, such immunotherapies achieve long-term survival only in a fraction of patients with certain types of cancers, and relapse remains common (*5*, *6*). ICI and TIL therapies seem to rely on converting the endogenous tumor-specific T cells into an active, tumor-killing state. However, reactivated T cells may return to an inactive state once re-exposed to the cancer cells and the tumor microenvironment (*7*, *8*).

An alternative approach, now also being applied in humans (*9*, *10*), is to isolate T cell receptors (TCRs) from neoantigen-specific CD8$^+$ T cells (CD8TCRs) and express these CD8TCRs in healthy T cells from peripheral blood for adoptive transfer. Neoantigen-specific CD8TCR-engineered T cells can eliminate large, established solid tumors in mice after adoptive T cell transfer (*11*, *12*). However, the targeted neoantigen needs to be artificially overexpressed for eradication, whereas cancer cells expressing the unmanipulated autochthonous neoantigen regularly escape immune-mediated destruction (*11*).

Some clinical data using neoantigen-specific TILs suggest the potential use of CD4$^+$ T cells in immunotherapy (*13*–*15*). TIL populations usually consist of various effector cells, and it has been unclear from clinical studies whether one or multiple TCRs of tumor-infiltrating CD4$^+$ T cells (CD4TCRs) are sufficient for effective immunotherapy. We have shown recently that a single CD4TCR expressed by engineered CD4$^+$ T cells can destroy established tumors when targeting an unmanipulated autochthonous neoantigen (*16*). However, it remains unclear how to predict therapeutic efficacy of CD4TCRs from a polyclonal T cell response of a tumor-bearing host (mouse and human) and how effective CD4TCRs mediate tumor destruction when used in adoptive therapy settings.

Here, we use the autochthonous and syngeneic ultraviolet (UV)–induced cancer cell model 6132A (*17*) to explore the selection of therapeutically effective neoantigen-specific CD4TCRs isolated from tumors and/or peripheral blood of cancer-bearing mice. Among the 11 most frequently occurring CD4TCRs, three TCRs were each made by multiple T cell clonotypes (*18*) differing in their α and β chain nucleotide sequences but encoding identical amino acid sequences, which is also referred to as convergent recombination (*19*). Adoptive transfer of T cells engineered with either one of these preferentially selected TCRs (*20*) resulted in destruction of aggressively growing tumors and the reprogramming of its stroma. This effect was dependent solely on stroma recognition and not on direct cancer cell targeting. The other eight TCRs, represented by single T cell clonotypes, were only effective therapeutically when they shared complementarity-determining region (CDR) elements with at least one preferentially selected TCR in both chains. Thus, our study identifies characteristics of neoantigen-specific CD4TCRs

[1]David and Etta Jonas Center for Cellular Therapy, University of Chicago, Chicago, IL, USA. [2]Department of Pathology, University of Chicago, Chicago, IL, USA. [3]Institute of Immunology, Charité–Universitätsmedizin Berlin, Campus Berlin Buch, Berlin, Germany. [4]German Cancer Consortium (DKTK), partner site Berlin, and German Cancer Research Center (DKFZ), Heidelberg, Germany. [5]Project for Immunogenomics, Cancer Precision Medicine Center, Japanese Foundation for Cancer Research, Tokyo, Japan. [6]Laboratory of Immunogenomics, Center for Intractable Diseases and ImmunoGenomics (CiDIG), National Institute of Biomedical Innovation, Health and Nutrition (NIBIOHN), Ibaraki-shi, Osaka, Japan. [7]Pritzker School of Molecular Engineering, University of Chicago, Chicago, IL, USA. [8]Pritzker School of Medicine, University of Chicago, Chicago, IL, USA. [9]Committees on Cancer Biology and Immunology and Cancer Center, University of Chicago, Chicago, IL, USA. [10]Immunology Program, Memorial Sloan Kettering Cancer Center, New York, NY, USA.
*Corresponding author. Email: wolfs@uchicago.edu
†Present address: Department of Immunology, University of Texas MD Anderson Cancer Center, Houston, TX, USA.

that can help to predict therapeutic efficacy against progressing solid tumors.

RESULTS

Hosts with progressing tumors respond with multiple CD4$^+$ TCRs to an immunodominant neoantigen

6132A cancer cells harbor an immunodominant L47H mutation in the ribosomal protein L9 (mL9) that is presented on the major histocompatibility complex (MHC) class II haplotype I-E^k (*2*). To understand whether tumor-bearing hosts generate a response to this unmanipulated autochthonous neoantigen, we used an mL9–I-E^k–tetramer to analyze tumors and spleens from normal syngeneic mice bearing 6132A tumors that had grown for more than 2 weeks (Fig. 1A). 6132A tumors were infiltrated with mL9–I-E^k–tetramer–binding CD4$^+$ T cells (median frequency, 1.4%) (Fig. 1B and fig. S1). Single-cell TCR sequencing of mL9-tetramer–binding CD4$^+$ T cells showed the relative frequencies of TCRs (Fig. 1C). On average, we obtained 162 T cells from a tumor sample harboring 45 different TCRs and 202 T cells from a spleen sample harboring 55 different TCRs (table S1). Our aim was to determine which of these CD4TCRs could be used for adoptive transfer of TCR-engineered CD4$^+$ T cells, and, if any, by which mechanisms these TCRs mediate antitumor activity.

Convergent recombination by multiple T cell clonotypes indicates TCRs preferentially selected by hosts with autochthonous or transplanted progressive tumors

We analyzed the 11 most common TCRs found in tumors and spleens of six mice (Fig. 1C). The two most frequent TCRs (H6 and H9) from mice #1, #2, #3, #5, and #6 were found in tumor and spleen tissue. The amino acid sequences of the CDR3s of the H6- and H9-TCR were generated by multiple different T cell clonotypes as determined by different N nucleotides between the V(D)J joints (Fig. 1D). Seven different T cell clonotypes in at least four different mice encoded the H6-TCR, whereas six different T cell clonotypes in at least three different mice encoded the H9-TCR (Fig. 1E). This convergent recombination by multiple T cell clonotypes encoding identical TCRs is in agreement with preferential selection. Compellingly, even though mouse #4 had very few mL9–I-E^k–tetramer–binding T cells, we still detected in the spleen a less frequent TCR (H13) that was again characterized by recombinational convergence of multiple T cell clonotypes. Six different T cell clonotypes found in at least four different mice encoded TCR H13 (Fig. 1, D and E). Furthermore, H13 was also among the TCR response detected in the spleen of the 6132 mouse that developed the original 6132A tumor, indicating that convergent recombination was not restricted to mice with transplanted tumors (fig. S2).

Convergent recombination defined therapeutically effective TCRs

All three preferentially selected TCRs were cloned into retroviral vectors and transduced into splenic T cells from C3H CD8$^{-/-}$ mice. TCR-engineered CD4$^+$ T cells were adoptively transferred into C3H Rag$^{-/-}$ mice bearing large and established solid 6132A tumors (Fig. 2A). TCR H6 destroyed tumors within 10 days after transfer (Fig. 2B). Transfer of αmL26-TCR T cells, a CD4TCR T cell targeting the irrelevant mutant ribosomal protein L26 (*21*) (found in another UV-induced C3H tumor, 6139B) had no effects because 6132A tumors progressed similarly to untreated controls (Fig. 2B). TCRs H9 and H13 had therapeutic efficacies similar to that of H6 (Fig. 2C), even though five of eight mice treated with H13 relapsed after 50 days.

TCRs from single clonotypes can also be therapeutically effective when sharing CDR elements in both TRA and TRB with TCRs identified by convergent recombination

We also cloned all eight TCRs represented by single T cell clonotypes (fig. S3) into retroviral vectors and used again TCR-transduced CD4$^+$ T cells for adoptive transfer into C3H Rag$^{-/-}$ mice bearing large, established solid 6132A tumors. Only H12 was as effective as H6 and H9, whereas H11, H14, H15, and H16 also destroyed tumors, but most of the mice relapsed more rapidly. TCRs H7, H8, and H10 had almost no antitumor effects (Fig. 2C).

When further evaluating the amino acid sequence of TCRs made by single T cell clonotypes, we found that some TCRs share CDR elements with preferentially selected TCRs (Fig. 2D): The V(D)J elements of H11 and H14 are almost identical to those of H6 except for a single–amino acid difference in the α chains and a single–amino acid difference in the β chains precisely at the site of V(D)J rearrangement. TCR H12 uses the identical β chain of H6 and an α chain in which the V region from H6 was recombined with the J region of H9. TCR H15 is almost identical to H13 except for two amino acid differences in the α chain, precisely at the site of V(D)J rearrangement. TCR H16 uses the same α chain V gene as H6 combined with a different J gene and the same β chain V gene as H13 combined with a different J gene. The therapeutically failing TCR H7 shared an identical β chain with H6 but had a unique α chain. TCRs H8 and H10 had completely unique V(D)J usages and thus completely different amino acid sequences in their respective α and β chains.

On the basis of therapeutic success and representation by either multiple or single clonotypes, the 11 TCRs fell into three groups (Fig. 2E). Group 1 encompasses the preferentially selected TCRs (H6, H9, and H13). Each of these TCRs was therapeutically effective but has its own unique amino acid sequence characterized by convergent recombination of multiple clonotypes. Group 2 (H11, H12, H14, H15, and H16) is composed of TCRs that are also therapeutically effective but derived from single T cell clonotypes. All TCRs in group 2 share CDR elements in both chains with the preferentially selected TCRs (group 1). Group 3 TCRs (H7, H8, and H10) are also derived from single clonotypes but fail therapeutically. These group 3 TCRs lack CDR elements of group 1 TCRs in either one or both chains. Therapeutic success was similar between mice treated with TCRs from groups 1 and 2 (Fig. 2E), except that relapse occurred earlier with TCRs from group 2 (Fig. 2F). By contrast, mice treated with TCRs from group 3 had no statistically significant survival improvements compared to mice treated with the control TCR αmL26 (Fig. 2E).

These results using H6 (preferentially selected and therapeutically effective), H10 (single clonotype, lacking elements, and therapeutically failing), H12 (single clonotype, with shared elements, and therapeutically effective), and the control TCR αmL26 were confirmed in another UV-induced tumor model, 4102 (*17*), which was engineered to express the mL9 neoantigen (fig. S4).

We found that the well-studied model antigen moth cytochrome c (MCC) also induces a CD4TCR response that consists of TCRs characterized by convergent recombination and TCRs from single clonotypes with shared elements (*22*) (fig. S5). When introducing MCC into 6132A and 4102, mice treated with TCRs characterized

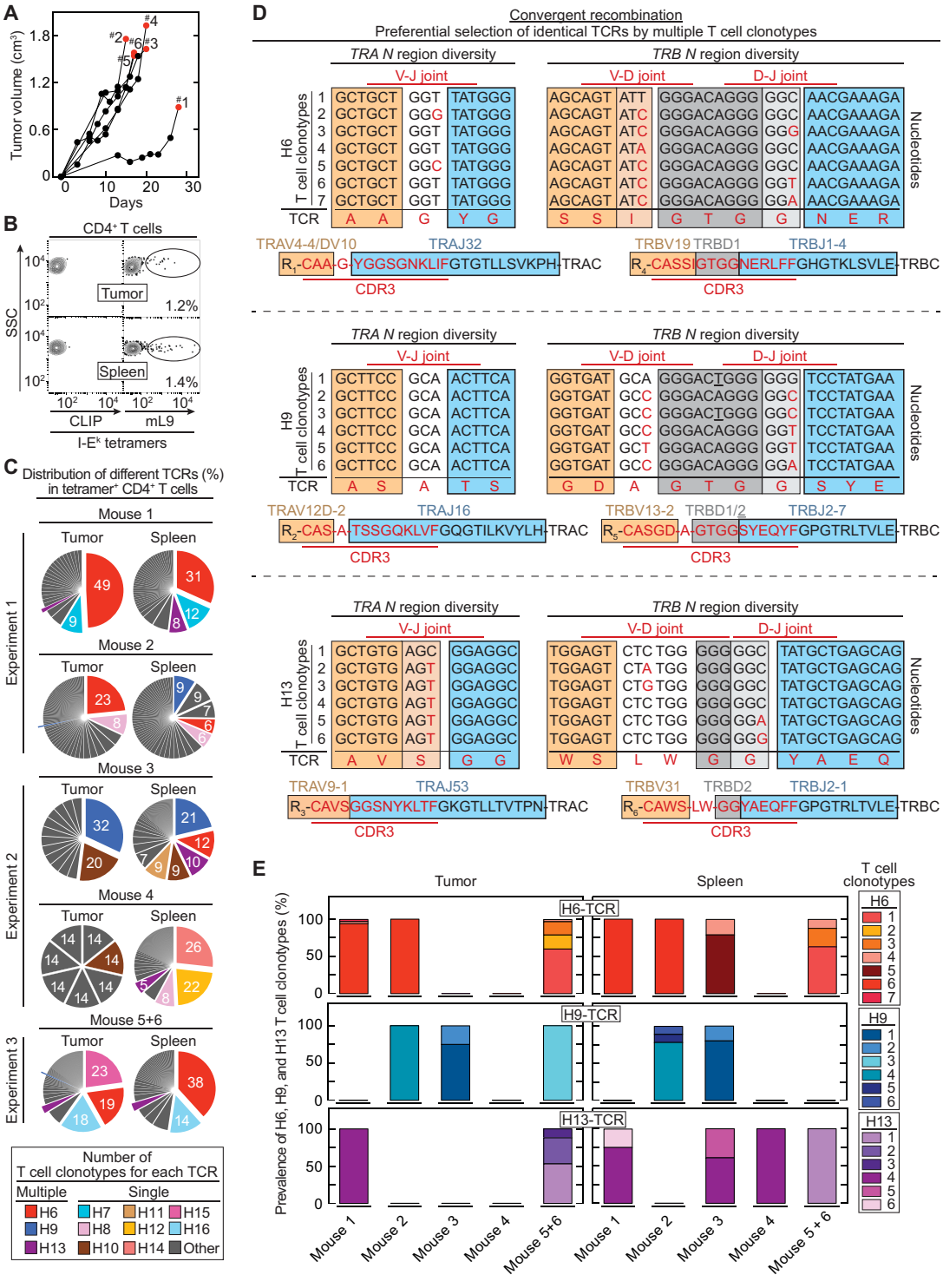

Fig. 1. Convergent recombination of different T cell clonotypes encoding identical, preferentially selected TCRs against the mutant neoantigen mL9. (**A**) 6132A tumor fragments were injected subcutaneously into C3H/HeN mice. Six mice are shown that developed tumors after fragment injection (55%, 11 of 20 injected C3H/HeN mice) and were used for TCR analysis. Results were compiled from three independent experiments. Red dots indicate day of T cell analysis. (**B**) An example is shown of T cells isolated from spleen and tumor sorted for live, $CD3^+$, $CD4^+$, and mL9-tetramer$^+$ specificity. Percentages of mL9-tetramer–positive T cells are indicated. CLIP-tetramer staining was used as negative control. (**C**) Frequencies of paired TCR CDR3 amino acid sequences in mL9-teramer–sorted $CD4^+$ T cells obtained from tumors and spleens of the six analyzed mice. (**D**) Identification of different T cell clonotypes encoding an identical TCR based on N nucleotide sequence diversity in the *TRA* (T cell receptor alpha locus) and *TRB* (T cell receptor beta locus) V(D)J joints. This was determined for the TCRs H6 (upper TCR), H9 (middle TCR), and H13 (bottom TCR). (**E**) Frequency of the different T cell clonotypes encoding an identical TCR (either H6, H9, or H13) among the analyzed mice.

by convergent recombination (group 1) showed again a significant ($P = 0.005$) therapeutic advantage over mice treated with TCRs from single clonotypes with shared elements (group 2) or mice treated with the control TCR αmL26 ($P = 0.0001$; fig. S6). Thus, in two distinct tumor systems targeting autochthonous neoantigen or model antigen, convergent recombination identified TCRs that mediated superior antitumor immunity upon adoptive transfer.

CD4TCRs cause destruction of tumor vessels but not of preexistent vasculature

To determine how neoantigen-specific CD4TCRs caused tumor shrinkage, we used the tumor window technology and longitudinal confocal microscopy (*23*) to follow the cellular and vascular events that occurred in the first 3 weeks after CD4TCR T cell transfer. Window frames were implanted into a dorsal skinfold of mice. We

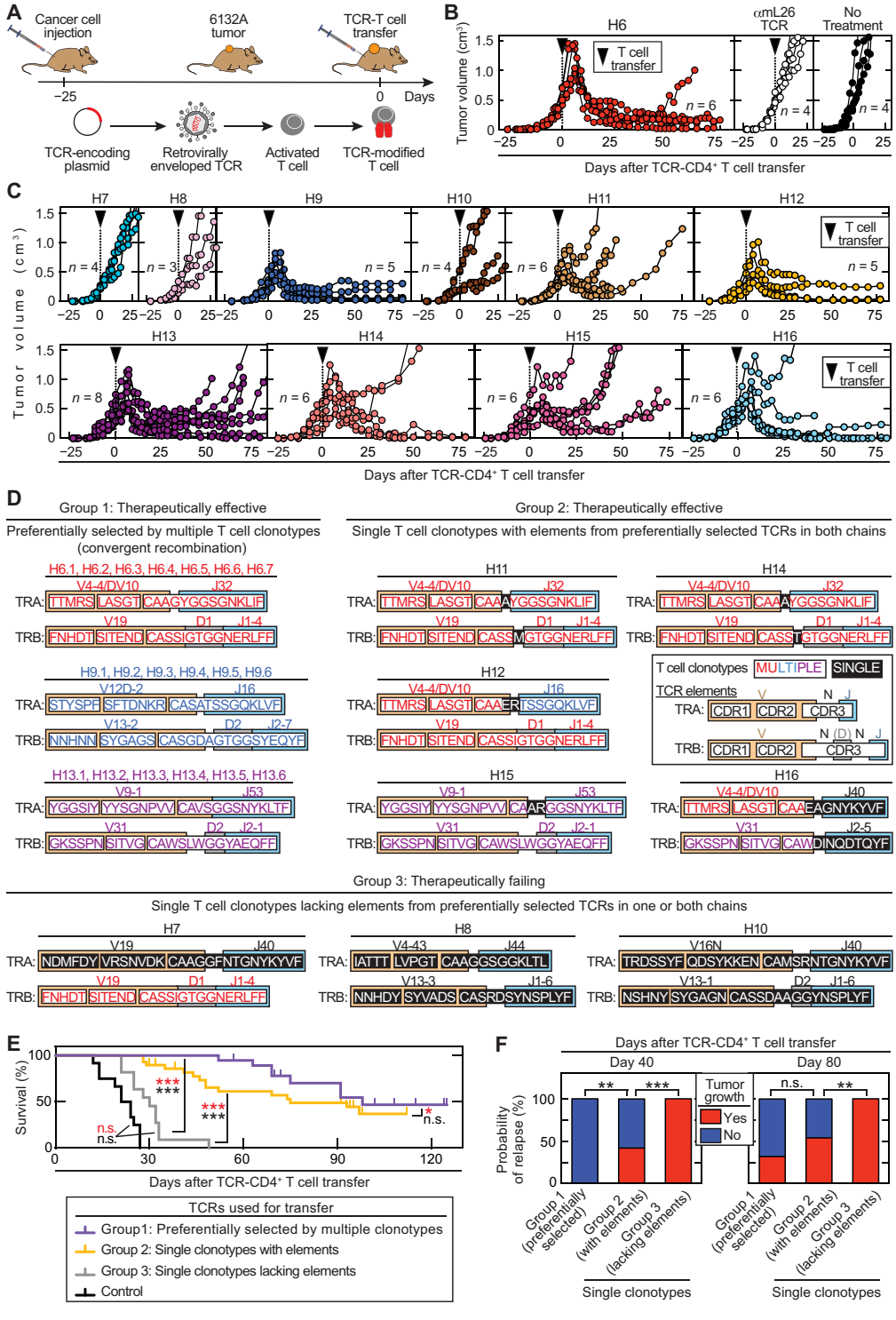

Fig. 2. Therapeutically effective TCRs cause tumor destruction followed by long-term growth arrest and can be predicted by CDR elements of preferentially selected TCRs. (**A**) Outline of adoptive transfer using TCR-engineered T cells. (**B** and **C**) Spleens from C3H CD8$^{-/-}$ mice were used as a CD4^{+} T cell source for TCR engineering. C3H Rag$^{-/-}$ mice bearing 6132A tumors were treated with TCR-engineered CD4^{+} T cells 21 to 25 days after cancer cell injection as indicated by the arrowhead. Total number of mice (*n*) is indicated. (B) Average tumor sizes were 0.558 ± 0.122 cm^3 SD at day of treatment. Data are summarized from three independent experiments. (Left) Treatment was performed with H6-T cells ($n = 6$). (Middle) Mice treated with αmL26-T cells, which are specific against an irrelevant antigen ($n = 4$), have the same outcome as (right) untreated mice ($n = 4$). (C) Average tumor sizes were 0.378 ± 0.156 cm^3 SD at day of treatment. Data are summarized from two independent experiments. Treatment with different TCR-engineered CD4^{+} T cells is indicated from left to right, top to bottom: H7 ($n = 4$), H8 ($n = 3$), H9 ($n = 5$), H10 ($n = 4$), H11 ($n = 6$), H12 ($n = 5$), H13 ($n = 8$), H14 ($n = 6$), H15 ($n = 6$), and H16 ($n = 6$). (**D**) The 11 TCRs fell into three groups on the basis of therapeutic failure or efficacy (defined by >25% shrinkage of tumor volume) and whether they were generated by multiple or single clonotypes. Color coding indicates whether CDR elements were shared in TRA and/or TRB with preferentially selected TCRs. (**E** and **F**) TCR treatment group 1: H6, H9, H13 (total $n = 16$). Group 2: H11, H12, H14, H15, and H16 (total $n = 29$). Group 3: H7, H8, and H10 (total $n = 11$). (E) The three groups were compared in a survival analysis (*$P \leq 0.5$, ***$P \leq 0.001$ significance, n.s., not significant). Log-rank test was used to determine significance indicated in black, whereas significance indicated in red used the Wilcoxon test. (F) Probability of relapse at day 40 or 80 after start of T cell transfer among the three TCR-treatment groups. **$P \leq 0.01$ and ***$P \leq 0.001$ significance determined using a two-tailed Fisher's exact test.

dissected a circular hole of 1-cm diameter from one side of the skin flap by removing the skin with its fascial plane while leaving intact the opposite skin layer with its fascial plane and associated vasculature. Cerulean-labeled 6132A cancer cells were then injected under the remaining fascia before covering the opening with a glass pane. During the following 14 to 16 days, tumors developed dorsal to the window. When mice were treated with H6-T cells, DiD (1,1′-dioctadecyl-3,3,3′,3′-tetramethylindodicarbocyanine,4-chlorobenzenesulfonate salt)–labeled red blood cells were also injected to visualize the blood flow. A custom-made precision holder was used for the window frames to be able to focus on the exact same positions of multiple different areas in the tumors and to revisit these areas on different days. Thus, we could examine longitudinally the progressive changes of vasculature, blood flow, and cancer cells in a defined area over time after treatment with H6-T cells (Fig. 3A). Macroscopic regression of the tumors began about 4 to 5 days after T cell transfer and correlated with the disappearance of the flow of the DiD-labeled red blood cells in the tortuous tumor vessels. Quantification of the images during the early/first phase of tumor shrinkage showed that the area covered by vessels regressed by about 50% comparing day 4 with day 6 after H6-T cell transfer, whereas the area covered by cancer cells regressed on average by 70% (Fig. 3B). Flow cytometric analyses revealed an increase in dead endothelial cells in tumor tissue 6 to 8 days after transfer of H6-T cells (Fig. 3C). Furthermore, these tumor tissues had significantly ($P = 0.02$) higher interferon-γ (IFN-γ) and tumor necrosis factor (TNF) values compared with the control tumors from mice that received no or mL26-specific T cells (Fig. 3, D and E). During the later/second phase of tumor shrinkage, the windows appeared flooded with unstained particles and assumed a ground-glass appearance consistent with debris resulting from cellular destruction (Fig. 3A). Histology of tumor tissue taken at day 6 after T cell transfer verified large areas of destroyed vessels and dead cells mainly in the tumor center. By contrast, pre-existing vessels stayed intact in the surrounding normal tissue at the tumor margin where cancer cells survived and T cells accumulated (figs. S7 and S8A). However, starting around day 10 after T cell transfer, the windows cleared, and patches of cancer cells became visible within regular nontortuous thinner vasculature. This characterized the fully arrested stage in which the cancer cells remained long term.

CD4TCRs cause long-term tumor growth arrest

After the bulk of the tumor mass had been destroyed and shrunken to small sizes, the remaining tumors persisted over the entire observation period (≥75 days) (Fig. 2C). H6-T cells persisted in the peripheral blood for months (fig. S8B), and there was no notable decrease in the intensity of $CD4^+$ T cell infiltration even at the longest observation time point (124 days; fig. S8C). To determine whether the stable size was the result of an equilibrium between cancer cell growth and death, we injected mice with 5-bromo-2′-deoxyuridine (BrdU) for 3 consecutive days. We found that proliferation of 6132A cancer cells had ceased almost completely in the tumors remaining small after treatment with the H6-TCR (Fig. 3F, left). Unexpectedly, a large fraction of 6132A cancer cells showed cleavage of caspase 3 as determined by flow cytometry (Fig. 3F, right). Both findings were exclusively dependent on using the mL9-specific H6-TCR (Fig. 3G). Because the tumor stayed at a small size even though cancer cells were nonproliferative and positive for cleaved caspase 3, we investigated whether cancer cells could be readapted in vitro. When removing tumors from the H6-T cell–treated host, cancer cells started to grow in vitro 60 days later, and a stable cell line was recovered that repeatedly induced tumors in vivo and also could be treated again with H6-T cells (fig. S9). Because cleaved caspase 3 can also be associated with DNA instability (*24*), we compared DNA damage in 6132A tumors when arrested after H6-T cell treatment with damage when actively growing after treatment with αmL26-T cells (Fig. 3, H and I). No elevated DNA damage was detected in the arrested tumor using terminal deoxynucleotidyl transferase–mediated deoxyuridine triphosphate nick end labeling (TUNEL) stain for either of the two situations. In addition, we determined whether the number of mutations had changed by performing whole-exome sequencing and RNA sequencing (RNA-seq; table S2) of in vitro readapted 6132A cancer cells from untreated, H6-treated, or αmL26-treated tumors. The expression of nsSNVs by these three cell lines was nearly indistinguishable, showing that growth arrest and its reversion in vitro did not lead to any notable acquisition of additional mutations.

Stromal recognition is sufficient for tumor destruction and long-term growth arrest

6132A cancer cells lack expression of MHC class II (*25*) and are therefore representative of most human cancers. Thus, 6132A cancer cells are not recognized directly by H6-$CD4^+$ T cells, but H6-T cells recognize similarly well $CD11b^+$ cells and $F4/80^+$ cells isolated from the stroma of 6132A tumors (*16*), indicating that stromal dendritic cells and macrophages become $CD4^+$ T cell targets by presenting neoantigen. To determine whether the effect of $CD4^+$ T cells depended solely on stroma recognition, we genetically deleted the β chain of the I-E MHC class II molecule in 6132A cancer cells. H6-T cells were similarly capable of permanently shrinking and halting tumor progression of both parental and I-E^k–deficient 6132A cancer cells (Fig. 3J).

TCR efficacy in vivo was not reliably predicted by in vitro responses of TCR-transduced T cells

We aimed to understand whether in vitro characterizations of our CD4TCRs correlate with features of preferential selection and in vivo efficacy. We stimulated all 11 CD4TCR-engineered T cell populations in vitro with dilutions of either mutant L9 (mL9) or wild-type L9 (wtL9) peptide presented by spleen cells from wild-type C3H/HeN mice and compared IFN-γ secretion values (Fig. 4A). None of the 11 CD4TCRs recognized wtL9 peptide. Within the group of preferentially selected TCRs, H6 was able to detect very low amounts of mL9 peptide [median effective concentration (EC_{50}), 0.1 nM] whereas H9 (EC_{50}, 10 nM) and H13 (EC_{50}, 1 nM) needed 100× or 10× more peptide for effective stimulation. The single-clonotype TCRs H11, H12, H14, H15, and H16, which share elements with preferentially selected TCRs, all detected low mL9 peptide amounts (EC_{50}, 0.5 nM) almost as well as H6 and were more sensitive than H9 and H13. Single-clonotype TCRs lacking elements from preferentially selected TCRs either showed no IFN-γ response (H7 and H8) or were only stimulated by very high amounts of mL9 peptides (H10; EC_{50}, 1000 nM).

The IFN-γ response in combination with other cytokines might more reliably predict the in vivo efficacy of our CD4TCRs. Therefore, we also determined cytokine values of TNF, interleukin-2 (IL-2), IL-4, IL-10, IL-17, and IL-22 after stimulation with different amounts of mL9 peptide (Fig. 4B). Again, T cells engineered with

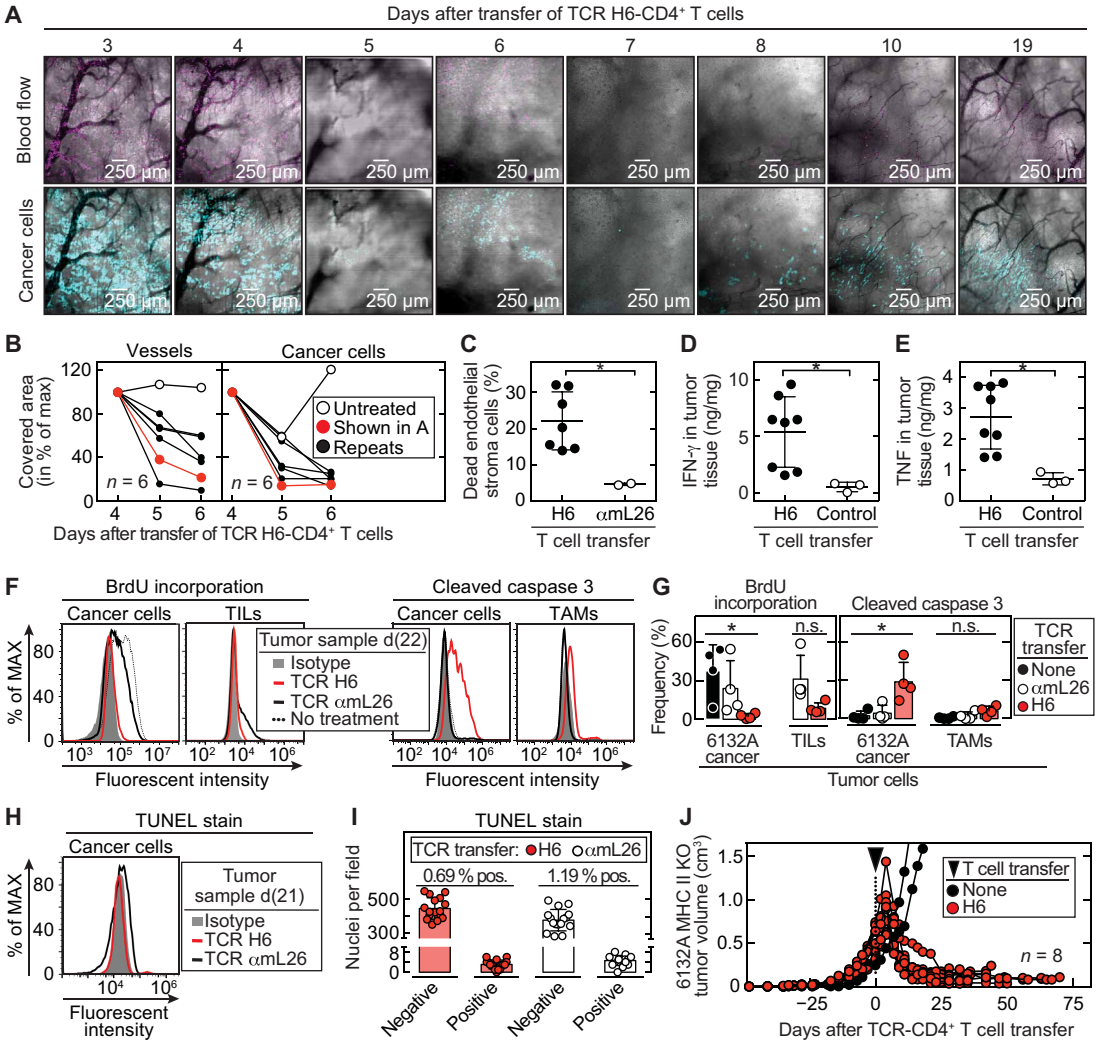

Fig. 3. Stroma recognition by CD4$^+$ T cells is sufficient to cause tumor destruction followed by growth arrest. (**A**) Example of longitudinal microscopy in 6132A-cerulean tumor–bearing C3H Rag$^{-/-}$ mice after transfer of H6-T cells. Tumor areas were randomly chosen before therapy and analyzed for (**B**) vessel and cancer cell reduction (total $n = 6$). DiD-labeled erythrocytes were used to visualize blood flow. Imaged area (in pixels) that was covered by vessels (black) or cancer cells (blue) from day 4 was set to 100%. Following days were assigned as percentage of maximum covered area. Indicated are an untreated control mouse (open circle) and the H6-treated mouse (red) shown in (A). Histology of tumor and vessel destruction on day 6 are shown in fig. S7. (**C** to **E**) Tumor tissue was analyzed on days 6, 7, and 8 after therapy by flow cytometry. Control tumors received either no T cells (total $n = 1$) or αmL26-T cells (total $n = 2$) and were analyzed at day 8. Results are means ± SD from two independent experiments. Significance between groups was determined by a two-tailed Student's t test with $^*P \leq 0.05$. (C) Tumors were analyzed for dead endothelial cells (Sytox-positive, CD146–, and CD31–double-positive cell populations) (total $n = 7$). (D) IFN-γ and (E) TNF concentrations in tumor tissue were determined (total $n = 8$). (**F** to **I**) 6132A-ECFP was used for injection into C3H Rag$^{-/-}$ mice. (F and G) Tumors were left untreated (total $n = 4$) or treated with either H6- (total $n = 4$) or αmL26-T cells (total $n = 4$). Mice were injected with BrdU twice a day for 3 consecutive days before tumor tissue was isolated at days 20 to 25 after T cell transfer. (F) A representative flow cytometry analysis is shown. Left: 6132A-ECFP cancer cells and TILs (CD3$^+$, CD4$^+$ and mL9-tetramer$^+$) were analyzed by flow cytometry for frequency of BrdU incorporation. Right: 6132A-ECFP cancer cells and TAMs (CD11b$^+$ and F4/80$^+$) were analyzed by flow cytometry for activation of cleaved caspase 3. (G) Significance between groups of 6132A cancer cells was determined by an ordinary one-way analysis of variance (ANOVA) with $^*P \leq 0.05$. Results are compiled from three independent experiments. (H and I) Tumors were treated either with H6- or αmL26-T cells. Tumor tissue was isolated at days 20 to 22 after T cell transfer. (H) Live 6132A-ECFP cancer cells were analyzed by TUNEL staining using flow cytometry. One representative flow cytometry analysis is shown out of two independent experiments. (I) DNA damage on formalin-fixed paraffin-embedded 6132A tumor slides was determined using TUNEL staining by immunohistochemistry. Eight fields were counted per slide. Shown is the total number of nuclei that were either stained negative or positive for TUNEL. The proportion (%) of TUNEL-positive nuclei was slightly higher ($P = 0.0017$) in αmL26-treated control samples (1.19 ± 0.45%) compared with H6-treated samples (0.69 ± 0.39%). (**J**) C3H Rag$^{-/-}$ mice bearing 6132A MHC II KO tumors (red, total $n = 8$) were treated with H6-T cells 31 to 35 days after cancer cell injection, indicated by the arrowhead. Spleens from C3H CD8$^{-/-}$ mice were used as a CD4$^+$ T cell source for TCR engineering. Average tumor sizes were 0.530 ± 0.170 cm^3 SD at day of treatment. Data are summarized from two independent experiments. Shown are untreated tumors (black, total $n = 2$) as control.

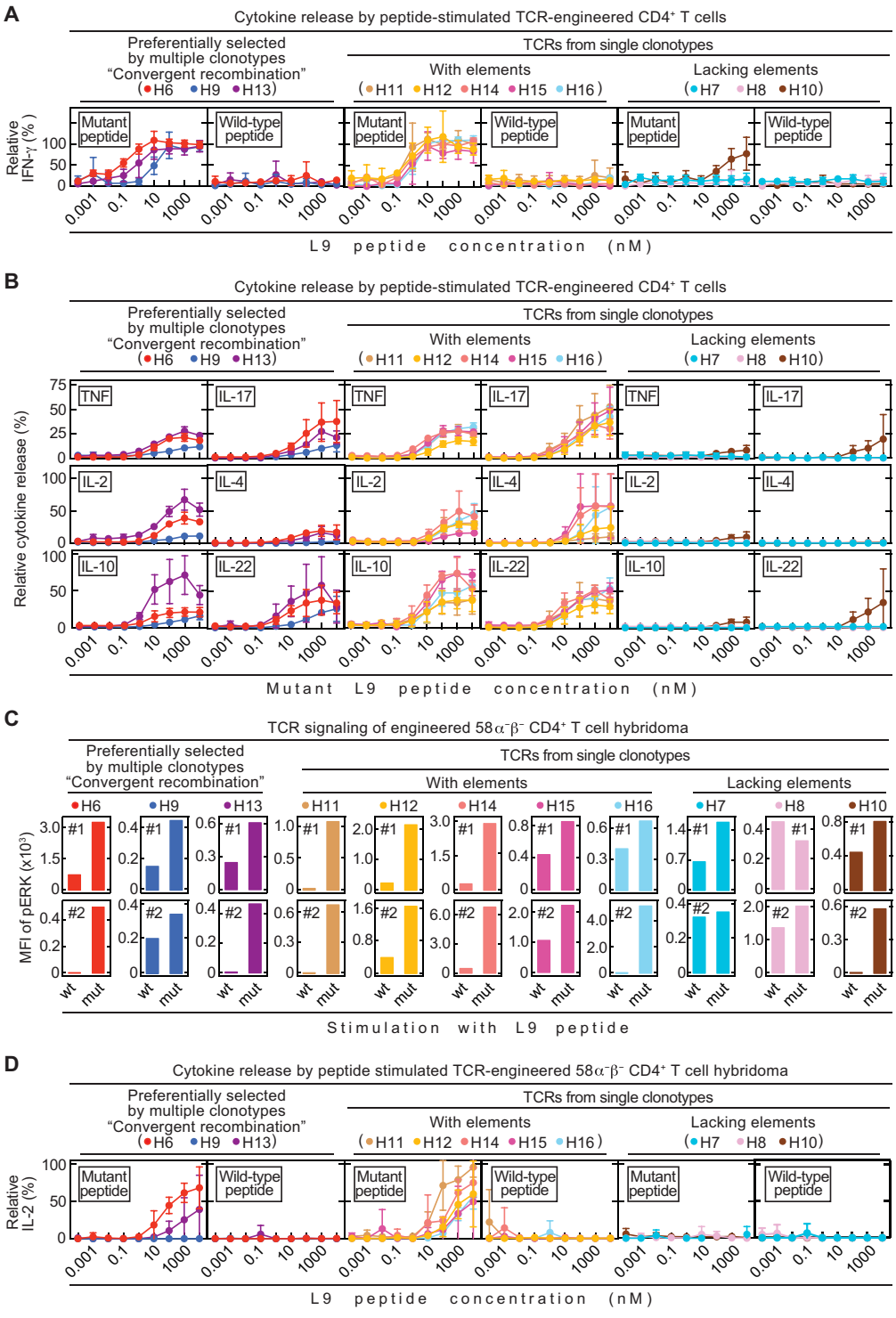

Fig. 4. Analysis of TCR-engineered CD4$^+$ T cells in vitro did not reliably predict therapeutic value in vivo. All 11 TCRs were tested in vitro. (**A** and **B**) Spleens from C3H CD8$^{-/-}$ mice were used as a source for CD4$^+$ T cells. TCR-engineered CD4$^+$ T cells were cocultured for 24 hours with C3H/HeN spleen cells and various mL9 or wtL9 peptide concentrations. Data are means ± SD and were compiled from two independent experiments. (A) Supernatants were analyzed for IFN-γ concentrations by ELISA. (B) Supernatants were analyzed for various cytokines by flow cytometry. (**C** and **D**) TCR-engineered 58α$^-$β$^-$ CD4$^+$ T cell hybridomas were used for cocultures together with LK35 B cell hybridoma as APC of either mL9 or wtL9 peptide. (C) Phosphorylation of ERK1/2, as a measure of TCR signaling, was determined by flow cytometry (MFI). Live, TCR β chain–positive 58α$^-$β$^-$ cells were analyzed. Shown are both (#1 and #2) independently performed experiments. (D) Cocultures were performed for 24 hours using various mL9 or wtL9 peptide concentrations. Supernatants were analyzed for IL-2 by ELISA. Data are means ± SD and were compiled from two independent experiments.

the TCRs H11, H12, H14, H15, and H16, which have shared elements, reliably produced as much TNF, IL-2, IL-17, and IL-22 as T cells engineered with the preferentially selected TCRs H6 and H13, whereas H9 always led to secretion of low cytokine values. However, there seems to be a difference in release of IL-4 and IL-10. The preferentially selected TCRs secreted almost no IL-4, which is in contrast with single-clonotype TCRs with shared elements. The same seems to be true for IL-10. The preferentially selected TCR H13 also induces a stronger release of IL-10 and is associated with eventual relapse in vivo that is in contrast to H6 and H9. Furthermore, H11 and H12 as single-clonotype TCRs with shared elements also resulted in only low values of IL-4 and IL-10. Yet, tumors treated with H12 stay in long-term growth arrest, whereas tumors treated with H11 relapse regularly within 25 days after T cell transfer. In

addition, TCRs H11, H14, H15, and H16 outperformed TCR H9 in the comprehensive cytokine analysis in vitro, yet in vivo, treatment with H11, H14, H15, and H16 was fraught with early relapse. The TCR engineering of bulk T cells from the spleen can bias in vitro assays because the endogenous TCR may influence the strength of the response (*26*). Therefore, we made use of the TCR-negative 58α$^-$β$^-$ CD4$^+$ T cell hybridoma (*27*) to normalize the peptide L9 T cell response in vitro and generated 11 TCR-engineered 58α$^-$β$^-$ CD4$^+$ T cell lines (fig. S10). We first determined the strength of TCR signaling by phosphorylation of extracellular signal–regulated kinase (ERK), which is an indicator for T cell activation (*28*), using flow cytometry (Fig. 4C). Preferentially selected TCRs (H6, H9, and H13) and single-clonotype TCRs with shared elements (H11, H12, H14, H15, and H16) as well as the TCR H10 (lacking elements) all had increased mean fluorescent intensity (MFI) values of phosphorylated ERK when stimulated with mL9 peptide in comparison with wtL9 peptide. We did not observe a consistent increase in MFI of phosphorylated ERK in the TCRs H7 and H8. In addition, we also analyzed the ability of the 11 TCR-engineered 58α$^-$β$^-$ CD4$^+$ T cell lines to secrete IL-2 (Fig. 4D). As before, none of the TCR-engineered 58α$^-$β$^-$ cells recognized wtL9. Yet again, the single-clonotype TCRs H11, H12, H14, H15, and H16 demonstrated a strong IL-2 response, and only the preferentially selected TCR H6 worked comparably well in vitro.

Because in vitro assays using peptide seem to be inconsistent for the understanding of in vivo efficacy of CD4TCRs, we investigated the cytokine response of TCR-engineered CD4$^+$ T cells when stimulated with 6132A tumor-associated macrophages (TAMs) isolated from established tumors (TAMs, Fig. 5A). The preferentially selected TCRs H6 and H13 released high amounts of IFN-γ, IL-2, and IL-10 and some degree of IL-17, whereas H9 only showed high release of IL-10, small secretion of IFN-γ and IL-17, and almost no IL-2. Single-clonotype TCRs with shared elements (H11, H12, H14, H15, and H16) responded similarly well to TAMs as H6 and H13. High secretion of IFN-γ, IL-2, and IL-10 and some degree of IL-17 were detected. The single-clonotype TCRs H7, H8, and H10 (lacking elements) failed to release any cytokines except for IL-10 at amounts that were comparable to the preferentially selected TCRs. Overall, the cytokine response of TCR-transduced T cells to TAMs correlated as poorly as responses to peptide with in vivo efficacy.

CD4TCR efficacy correlates with ability to reprogram TAMs

Because in vitro stimulation of TCR-transduced T cells unreliably predicts in vivo efficacy of CD4TCRs, we focused on the interaction between stroma and CD4$^+$ T cells required for tumor shrinkage and growth arrest. More than 80% of all CD11b$^+$ cells in the 6132A microenvironment were F4/80$^+$ TAMs (fig. S11A). Thus, we examined which effect the different CD4TCRs might have on TAMs. Stromal recognition of TAMs by CD4TCRs was not associated with an increased death rate of TAMs because the number of nonviable TAMs did not differ significantly between untreated, H6-treated, or αmL26-treated tumors (fig. S11B). Two different TAM phenotypes, M1 and M2, have been described in the tumor microenvironment (*29*). In general, M2-TAMs promote tumor growth and are immunosuppressive, whereas M1-TAMs are proinflammatory and tissue damaging (*29*). Therefore, we examined 6132A-TAMs for phenotypic changes in response to T cell transfer. Tumors were isolated at days 0, 6, and 20 after transfer of either H6- or αmL26-T cells, and TAMs were found to express the M2-type protein arginase (fig. S12). We observed an increase in MHC class II I-E^k in almost all TAMs by day 20 after T cell transfer. However, this up-regulation was not antigen specific because it was similar after transfer of either H6- or αmL26-T cells (fig. S12). In addition, the fraction of TAMs expressing arginase also increased by day 20, but this again occurred independent of the antigen specificity of the transferred T cells. Instead, H6-T cell transfer resulted in significant ($P = 0.0001$) induction of nitric oxide (NO) expression in almost all TAMs by day 20. This antigen-specific NO expression was absent when tumors were treated with αmL26 control T cells (fig. S12). For a more comprehensive analysis on how phenotypic changes in TAMs predict the outcome of treatment, we analyzed TAMs for the expression of arginase, CD40, CD163, CD204, CD206, IDO, IL-10, IL-12, NO, and TNF around 20 days after transfer of therapeutically effective, preferentially selected TCRs H6, H9, and H13; the single clonotype and therapeutically effective TCR H12; or the single clonotype but therapeutically failing TCR H10 using the αmL26-specific TCR as control (Fig. 5B). We only observed a significant ($P = 0.0001$) change in NO production of TAMs from 6132A tumors treated with therapeutically effective TCRs (72% of all TAMs are NO positive). Even the therapeutically effective TCR H9, which performed poorly in all of our in vitro stimulations, was able to induce NO production in TAMs, whereas the therapeutically failing TCR H10, which also performed poorly in our in vitro stimulations, faltered. For further understanding of the TAM subpopulations, we analyzed the I-E^k–expressing TAMs for their NO and arginase proportions. We found that TAMs from tumors treated with therapeutically effective TCRs consisted on average of 41% NO-producing TAMs, whereas this cell population was minor (6%) in TAMs from mice treated with failing or control TCRs (Fig. 5, C and D). This indicates that most TAMs present in an arrested tumor are of the M1 phenotype, whereas TAMs found in growing tumors are mostly M2. However, TAMs that are double positive for NO and arginase were also detected in arrested tumors (28% versus 5% in growing tumors), showing that M2-TAMs are capable of producing NO without losing their M2-type identity. Thus, reprogramming of TAMs to produce NO correlated with therapeutically effective CD4TCRs.

DISCUSSION

In this study, we show that selecting candidate TCRs on the basis of convergent recombination can help identify TCRs that are therapeutically effective. Not only the TCRs made by multiple T cell clonotypes but also TCRs made by a single T cell clonotype had therapeutic value when they shared CDR elements in paired α and β chains with the TCRs characterized by convergent recombination. Identical TCRs encoded by different nucleotide sequences have been considered to be "preferentially selected" (*20*), because different T cell clonotypes expressing the same TCR developed independently multiple times in vivo. Thus, convergent recombination adds an important host-generated quality indicator for a "best-fit" TCR (*30*). Beneficial clinical outcome has been linked statistically to the increased occurrence of convergent recombination in bulk TCR β chain sequencing only (*31*–*33*). However, presence of convergent recombination only in TCR β chain sequences did not distinguish the therapeutically effective TCR H6 from the failing TCR H7. Therefore, predicting a therapeutic TCR depended on finding convergence in T cell clonotypes by paired α and β chain analyses.

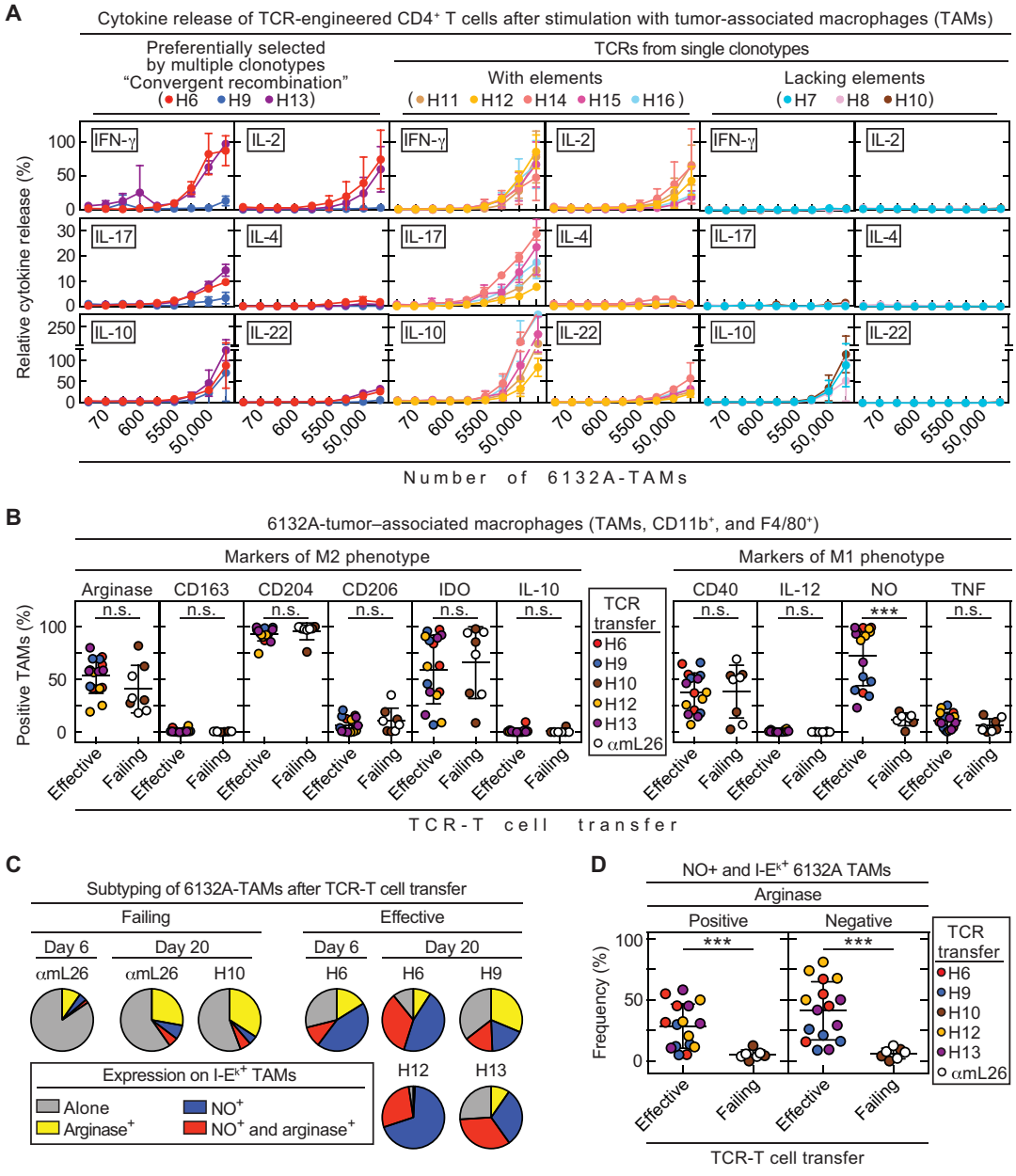

Fig. 5. NO expression in 6132A TAMs is induced by T cells when transduced with therapeutically effective CD4TCRs. (**A** to **D**) Spleens from C3H CD8$^{-/-}$ mice were used as a CD4^{+} T cell source for TCR engineering. (A) TCR-engineered CD4^{+} T cells were cocultured for 24 hours with threefold dilutions of TAMs (F4/80^{+} cells) isolated from 6132A tumors grown in C3H Rag$^{-/-}$ mice. Supernatants were analyzed for various cytokines by flow cytometry. Data are means ± SD and were compiled from two independent experiments. (B to D) C3H Rag$^{-/-}$ mice bearing 6132A tumors were treated with H6- ($n = 4$), H9- ($n = 4$), H10- ($n = 4$), H12- ($n = 4$), H13- ($n = 4$), or αmL26- ($n = 4$) TCR-engineered T cells 21 to 23 days after cancer cell injection. Tumor tissue was isolated at days 20 to 22 after T cell transfer. Tumors were analyzed by flow cytometry for frequency of life CD11b^{+} and F4/80^{+} 6132A TAMs expressing M1-type (CD40, IL-12, NO, and TNF) or M2-type (arginase, CD163, CD204, CD206, IDO, and IL-10) markers. TCR treatment was divided into effective (H6, H9, H12, and H13; $n = 16$) and failing (H10 and αmL26, $n = 8$) therapy groups. Therapeutically effective TCRs are able to induce tumor shrinkage by more than >25% volume within 12 days after T cell transfer. All other TCRs are considered therapeutically failing, which also includes the control TCR αmL26. Number (n) indicates the total number of tumors analyzed from independent mice. (B) Comparison of M1- and M2-type markers of TAMs from effective or failing TCR-T cell therapy. Significance between groups was determined by an unpaired, two-tailed Student's t test with ***$P \leq 0.001$. Data were compiled from two independent experiments. (C) MHC class II I-E^{k}–positive TAMs were further analyzed by their frequency of expressing either arginase, NO, both, or none. Data were compiled from three independent experiments (D) Frequency of NO- and I-E^{k}–expressing TAMs that were either positive or negative for arginase. Significance between groups was determined by an unpaired, two-tailed Student's t test with ***$P \leq 0.001$. Data were compiled from two independent experiments.

Currently, the focus is on finding in vitro assays that can predict which TCR will be successful for immunotherapeutic interventions (*34*). Our in vitro analyses did not reliably predict the in vivo outcome. Both CD4TCRs H6 and H9 caused long-term growth arrest after tumor destruction, although H6 responded well and H9 poorly to peptide or TAMs that present the tumor antigen. However, we do not know whether TCRs from single T cell clonotypes with strong responses to the mutant peptide or other types of in vitro activity could fail in vivo. Using mice that lacked endogenous T cells was essential to exclude the participation of such T cells (*35*, *36*) and to evaluate stromal reprogramming as well as long-term outcome between preferentially selected TCRs and TCRs generated by single T cell clonotypes. However, this reductionist approach also has limitations because it does not examine how the efficiency of our T cell therapy might be affected by preconditioning regimens in immunocompetent mice (*37*).

Most human epithelial cancers do not express MHC class II and do not allow for direct recognition by $CD4^+$ T cells, as observed in our tumor models (*25*) even though melanoma represents a notable exception (*38*–*40*). Nevertheless, adoptive transfer of $CD4^+$ T cells has been shown to eradicate disseminated Friend virus–induced erythroleukemia, and these cancer cells were found to be MHC class II negative (*41*). A decrease in targeted lesions and growth control of the persistent cancer has also been achieved in patients after transfer of in vitro–expanded mutation-specific $CD4^+$ TIL populations (*13*, *14*). Loss of antigen or MHC is a common cause of relapse after immune therapy with $CD8^+$ T cells (*42*). In our model, relapse after CD4TCR therapy retained the targeted neoantigen (*16*). Although the CD4TCRs targeted the neoantigen only on stroma, spatial restriction in the tumor environment can favor the escape of antigen-loss variants (*43*). Therefore, another reason why we did not observe antigen loss variants might be that we targeted an antigen essential for cell survival and growth that is characterized by genetic loss of the wild-type allele (*21*). Loss of heterozygosity of essential genes is increasingly being recognized as an underestimated potent class of cancer-specific targets (*21*, *44*, *45*) and can become a paradigm shift for cancer therapy (*46*). Previous reports showed destruction of tumor vessels followed by ischemic necrosis of large areas of solid tumors by effects of IFN-γ and/or TNF (*47*–*50*), which we also observe through antigen-specific release of IFN-γ and TNF by tumor-infiltrating CD4TCR-T cells. After tumor destruction, the surviving cancer cells persisted at tumor margins nourished by the pre-existent nontumor vasculature that is resistant to IFN-γ and TNF (*51*). The tumor microenvironment is widely considered to be tumor promoting (*52*), immunosuppressive (*53*), and a barrier for effective $CD8^+$ T cell therapy. A part of stromal TAMs in untreated or control TCR–treated mice expressed arginase, but few expressed NO, consistent with an immunosuppressive environment (*54*, *55*). Changes in MHC II expression on TAMs in tumors treated with nonspecific T cells were observed, which is consistent with bystander infiltration and activation of nonspecific T cells in cancer and viral diseases (*56*–*58*). Nonetheless, we observed antigen-specific reprogramming of M2-type TAMs together with appearance of M1-type TAMs. Therefore, our approach of identifying and using CD4TCRs for adoptive T cell transfer gives evidence for the concept that the immunosuppressive, tumor-promoting microenvironment can be targeted and reprogrammed by tumor-infiltrating neoantigen-specific $CD4^+$ T cells.

NO is known for its reversible cytostatic effect on cancer cells (*59*), and previous studies showed that $CD4^+$ T cells producing IFN-γ and TNF signal TAMs to activate nitric oxide synthase (*60*, *61*), thereby preventing the outgrowth of cancer cell inocula. This is in line with our observation that effective T cells secreting IFN-γ and TNF occur together with TAMs that produce NO. Histochemistry showed T cells densely infiltrating nonproliferating cancer cells forming a "stalemate" with T cells maintaining cancer cells in growth arrest without eradicating them. Thus, growth arrest was not due to an equilibrium of growth and death of cancer cells as in previous studies targeting tumor stroma with $CD8^+$ T cells (*62*, *63*). The reversibility we observed also appears to exclude growth arrest due to $CD4^+$ T cell–induced senescence (*64*). Instead, we found that cleaved caspase 3–positive arrested cancer cells without damaged DNA could recover. This has been reported in other studies (*65*), is consistent with NO being an antiapoptotic regulator of caspase 3 activity in vivo (*66*), and is now referred to as "anastasis" (*67*, *68*). It also had been proposed that cleaved caspase 3 could cause genetic instability and might be involved in carcinogenesis (*24*, *65*). However, one reason for accumulation of mutations is errors during DNA replication (*69*). Because the cancer cells in our model are growth arrested, no DNA replication occurs, and thus the acquisition of new mutations is hindered. We found no significant increase in mutations, which is consistent with lack of DNA damage, in cancer cells readapted after treatment.

Together, our study shows that the clonally diverse $CD4^+$ T cell response in progressive cancers harbors some CD4TCRs that are of therapeutic value in adoptive therapy settings. We suggest that convergent recombination in paired TCR chains can be used to identify these therapeutically effective CD4TCRs and that this strategy can become applicable when treating human cancers.

MATERIALS AND METHODS

Study design

Objective of the study was to determine therapeutically effective TCRs used for adoptive transfer of TCR-engineered $CD4^+$ T cells against established solid tumors. Animal experiments were approved by the University of Chicago Institutional Animal Care and Use Committee (IACUC). Cancer cells were injected subcutaneously in the shaved backs of mice. Tumor volumes were measured along three orthogonal axes every 2 to 3 days and were calculated as $(a \times b \times c) \div 2$. Mice were treated around 3 weeks after cancer cell injection when tumors were established. The number of TCR^+ T cells was calculated on the basis of transduction rate (determined by TCR Vβ stain, on average ~ 30%) on the day of treatment before T cell transfer. Per recipient, 2×10^6 TCR^+ $CD4^+$ T cells were injected intraperitoneally. Mice were randomized into different treatment groups on the day of adoptive T cell transfer. Mice were euthanized when tumor sizes reached more than 2 cm^3 or mice appeared hunched and weak. Relapsing tumors were allowed to reach 1.5 cm^3 before mice needed to be euthanized. TCRs were defined as being therapeutically effective when tumor volume shrunk by more than 25% within 12 days after T cell transfer; otherwise, TCRs were defined as therapeutically failing. Therefore, the control αmL26 TCR was also included in the therapeutically failing TCR group. Experimental replicates are included in figure legends.

Mice

Three- to 8-month-old female and male mice were used in this study. Mice were bred and maintained in a specific pathogen–free barrier facility at the University of Chicago according to IACUC

guidelines. C3H/HeN mice were obtained from Envigo [Huntingdon, Cambridgeshire, UK, research resource identifier (RRID): MGI:2160972]. C3H Rag2$^{-/-}$ (C3H.129S6-Rag2^{tm1Fwa}) mice were obtained from D. Hanahan (University of California, San Francisco, CA, USA). C3H CD8$^{-/-}$ (C3H.129S2-Cd8a^{tm1Mak}) mice were generated in house by crossing C3H/HeN mice with C57BL/6 CD8$^{-/-}$ mice purchased from the Jackson Laboratory (B6.129S2-Cd8a^{tm1Mak}, RRID: MGI:3789587) and then backcrossed with C3H/HeN for 20 generations. Spleens of C3H CD8$^{-/-}$ mice were used as T cell sources for TCR engineering.

Cell lines

6132A and 4102 cancer cell lines originated from UV-treated C3H/HeN mice and were generated in our laboratory together with heart-lung fibroblasts as autologous normal tissue controls for each cancer cell line (*17*). The original primary tumors were minced, and fragments were used to establish uncloned primary cultures of 6132A and 4102 cancer cells. These primary tumor cell cultures were only minimally expanded and used for cell culture experiments and tumor induction in vivo. The 6132A-ECFP was generated by using retroviral transduction with the pMFG-ECFP vector as described before (*23*). 6132A-Cerulean was described before (*70*). Knockout of the H2-Eb1 gene results in I-E β chain loss and therefore loss of MHC class II expression. The 6132A-H2-Eb1 knockout cell line was generated using CRISPR-Cas9. Single guide RNAs (sgRNAs) targeting exon 1 of the murine C3H H2-Eb1 gene were designed using the sgRNA design tool from the Broad Institute. The corresponding sense and antisense DNA oligomers (IDT, Coralville, IA, USA) were compared with other publications that also targeted H2-Eb1 to generate murine MHC class II knockout cancer cell lines. The DNA oligomers were annealed and cloned over a Bbs I side into PX458. The sgRNA 5′–AGGAGACACGAGAGTCAGAG–3′ was successfully used to generate 6132A-H2-Eb1$^{-/-}$ cancer cells, which were verified by Sanger sequencing to have an indel and frameshift in exon 1. The 25-mer of MCC and mL9 was cloned into the retroviral vector pMP71 (pMP71-mL9-P2A-eGFP and pMP71-MCC25-P2A-eGFP) and used to generate 6132A-MCC-GFP as well as 4102-MCC-GFP and 4102-mL9-GFP cell lines. Phoenix-ampho cells were transfected by calcium phosphate precipitation. Repeated rounds of transduction of either 6132A or 4102 with viral supernatants followed by fluorescence-based cell sorting (FACS) (FACSAria II, BD Biosciences, San Jose, CA, USA) derived highly green fluorescent protein (GFP) fluorescent cell lines that were cloned for homogeneous expression. The B cell hybridoma LK35 (*71*) was provided by A. Sant from the University of Rochester and maintained in Dulbecco's modified Eagle's medium (DMEM) supplemented with 10% fetal bovine serum (FBS), 2 mM L-glutamine, and 0.1 mM nonessential amino acids and cultured at 10% CO_2 in a 37°C dry incubator. Cancer cells were maintained in DMEM supplemented with 5% FBS (Gemini Bio-Products) and 2 mM L-glutamine (Life Technologies, Carlsbad, CA, USA) and cultured at 10% CO_2 in a 37°C dry incubator. Plat-E packaging cells (*72*) used for TCR gene transfer and Phoenix ampho used for gene transfer of neoantigens were maintained in DMEM supplemented with 10% FBS, 2 mM L-glutamine, puromycin (1 μg/ml), and blasticidin (1 mg/ml; Invivogen, San Diego, CA, USA) and cultured at 5% CO_2 in a 37°C dry incubator. The 58α$^-$β$^-$ CD4$^+$ T cell hybridoma was provided by D. Kranz from the University of Illinois Urbana-Champaign (*27*), and its TCR-engineered variants were maintained in RPMI 1640 (Corning, Corning, NY, USA) 10% FBS (Gemini, Sacramento, CA, USA), 2 mM L-glutamine, 1 mM sodium pyruvate, 0.1 mM nonessential amino acids, penicillin (100 U/ml), streptomycin (100 μg/ml; all purchased from Life Technologies, Carlsbad, CA, USA), 50 μM 2-mercaptoethanol (Thermo Fisher Scientific, Waltham, MA, USA), and gentamicin (50 μg/ml; VWR, Radnor, PA, USA) and cultured at 5% CO_2 in a 37°C dry incubator. Before use, cancer cell lines were authenticated by sequencing and/or coculture with antigen-specific T cells and by morphology. All cell lines were shortly passaged after thawing of the initial frozen stock to generate master cell banks. Working batches were passaged no longer than 4 weeks.

Cell sorting, single-cell sequencing, and isolation of TCR genes

After harvesting tumor and spleen tissue between days 18 and 28 after injection of cancer cell fragments, single-cell suspensions were prepared and stained for Sytox Blue (Helix NP Blue, Biolegend, San Diego, CA, USA, life/dead stain), CD3, CD4, and tetramer, respectively, before viable tetramer binding CD4$^+$ T cells were sorted (FACSAria II, BD Bioscience, Franklin Lakes, NJ, USA). Samples from different mice were stained with TotalSeq-C Hashtag antibodies #4, #6, and #8 (Biolegend, San Diego, CA, USA) and combined before sorting. The 10x Genomics (10x Genomics, Pleasanton, CA, USA) Chromium controller and the single-cell 5′ dual index platform was used to generate TCR libraries following the manufacturer's protocol. Next-generation sequencing was performed at the University of Chicago Genomics facility using NovaSeq 6000 (Illumina, San Diego, CA, USA). TotalSeq-C Hashtag antibodies were used to demultiplex the different mice. Therefore, only four data points are shown in fig. S1B. These data points are from tetramer sorts of mice #1, #2, #3, #4, #5, and #6. Unfortunately, the TotalSeq-C Hashtag procedure failed for mice #5 and #6. Therefore, the two mice could not be separated. Obtained TCR sequences were codon-optimized (GeneArt, Thermo Fisher Scientific, Waltham, MA, USA) and integrated into the pMP71 vector using Not I–and Eco RI–flanked restriction sides as described (*73*). The control TCR αmL26 was isolated from a T cell clone specific for the H96Y mutation in the ribosomal protein L26 that was identified in 6139B cancer cells and has been characterized before (*16*, *21*). In addition, the TCR H6 isolated from tumor-bearing mice is identical to a TCR identified in immunized mice (*2*, *16*). MCC-specific TCR sequences 5c.c7, AND, M2.3, and M4.3 have been described before (*22*) and were also codon-optimized and integrated into the pMP71 vector.

TCR engineering of primary CD4$^+$ T cells

TCR engineering was conducted as previously described (*74*). A separate retroviral vector was generated for each TCR: pMP71-H6, pMP71-H7, pMP71-H8, pMP71-H9, pMP71-H10, pMP71-H11, pMP71-H12, pMP71-H13, pMP71-H14, pMP71-H15, pMP71-H16, pMP71-5c.c7, pMP71-AND, pMP71-M2.3, pMP71-M4.3, or pMP71-αmL26. Potential mispairing of transduced TCRs (*75*) was prevented by using a P2A element in TCR-vector designs. Plat-E packaging cells were transfected with pMP71-H6, pMP71-H7, pMP71-H8, pMP71-H9, pMP71-H10, pMP71-H11, pMP71-H12, pMP71-H13, pMP71-H14, pMP71-H15, pMP71-H16, pMP71-5c.c7, pMP71-AND, pMP71-M2.3, pMP71-M4.3, or pMP71-αmL26 by calcium phosphate precipitation. Forty-two hours after transfection, virus supernatant was removed and filtrated through a 0.45-μm syringe filter (VWR, Radnor, PA, USA). Spleens were isolated,

and erythrocytes were lysed for 3 min with 0.017 M tris and 0.14 M ammonium chloride (both Sigma-Aldrich, St. Louis, MO, USA). Cells were cultured in complete medium containing Roswell Park Memorial Institute medium (RPMI 1640, Corning, Corning, NY, USA) 10% FBS (Gemini, Sacramento, CA, USA), 2 mM L-glutamine, 1 mM sodium pyruvate, 0.1 mM nonessential amino acids, penicillin (100 U/ml), streptomycin (100 μg/ml; all purchased from Life Technologies, Carlsbad, CA, USA), 50 μM 2-mercaptoethanol (Thermo Fisher Scientific, Waltham, MA, USA), and gentamicin (50 μg/ml; VWR, Radnor, PA, USA) and were supplemented with recombinant human IL-2 (40 U/ml; PeproTech, Rocky Hill, NJ, USA). The cell suspension was transferred into a 24-well plate (Greiner Bio-One, Kremsmuenster, Austria) coated with αCD3 (1.4 μg/ml; University of Chicago, Frank W. Fitch Monoclonal Antibody Facility, clone 145-2C11.1) and αCD28 (0.2 μg/ml; clone 37.51, Biolegend, San Diego, CA, USA) at a concentration of 3×10^6 cells/ml. On the subsequent day, 0.5 ml of corresponding virus supernatant containing protamine sulfate (8 μg/ml; Sigma-Aldrich, St. Louis, MO, USA) was added per well, and cells were spinoculated (800*g*, 90 min, 32°C). Overnight, a 12-well plate (Greiner Bio-One, Kremsmuenster, Austria) was coated with RetroNectin [12.5 μg/ml (TaKaRa)] and centrifuged with 1.5 ml of virus supernatant (3000*g*, 90 min, 4°C) on the next day. The virus supernatants were removed, and 5×10^6 of $CD4^+$ T cells in complete medium containing IL-2 (40 U/ml) were transferred to the virus-coated 12-well plate and followed by spinoculation (800*g*, 90 min, 32°C). Transduction rate was confirmed by flow cytometry using NovoCyte Quanteon (Agilent, Santa Clara, CA, USA), and T cells were used 3 days after transduction for adoptive transfer. For in vitro analyses, TCR-engineered $CD4^+$ T cells were maintained in complete medium with IL-2 (40 U/ml) and used after 4 days.

TCR engineering of the 58α$^-$β$^-$ CD4$^+$ T cell hybridoma

Plat-E packaging cells were transfected with pMP71-H6, pMP71-H7, pMP71-H8, pMP71-H9, pMP71-H10, pMP71-H11, pMP71-H12, pMP71-H13, pMP71-H14, pMP71-H15, and pMP71-H16 by calcium phosphate precipitation. Forty-two hours after transfection, virus supernatant was removed and filtrated through a 0.45-μm syringe filter (VWR, Radnor, PA, USA). A 24-well plate was coated overnight with RetroNectin [500 μl per well; 12.5 μg/ml (TaKaRa)]. The coated plate was centrifuged with 0.5 ml of virus supernatant (3000*g*, 90 min, 4°C). Supernatant was removed, and 2×10^5 58α$^-$β$^-$ cells in RPMI 1640 (1 ml per well; Corning, Corning, NY, USA) 10% FBS (Gemini, Sacramento, CA, USA), 2 mM L-glutamine, 1 mM sodium pyruvate, 0.1 mM nonessential amino acids, penicillin (100 U/ml), streptomycin (100 μg/ml; all purchased from Life Technologies, Carlsbad, CA, USA), 50 μM 2-mercaptoethanol (Thermo Fisher Scientific, Waltham, MA, USA), and gentamicin (50 μg/ml; VWR, Radnor, PA, USA) were added. The plate was centrifuged at 800*g* for 30 min and 32°C. On the subsequent day, 0.5 ml of corresponding virus supernatant containing protamine sulfate (8 μg/ml; Sigma-Aldrich, St. Louis, MO, USA) was added per well, and cells were again spinoculated (800*g*, 90 min, 32°C). Three days later, 58α$^-$β$^-$ cells were stained for TCR β chain and sorted using FACSAria II (BD Bioscience, Franklin Lakes, NJ, USA). After cells recovered in vitro, the level of expression of the TCRs among the different TCR-engineered 58α$^-$β$^-$ cells was determined by TCR β chain staining using flow cytometry with NovoCyte Quanteon (Agilent, Santa Clara, CA, USA).

Cancer cell injection in mice

For generation of tumor-bearing C3H/HeN wild-type mice, 6132A fragments were generated and injected subcutaneously as previously described (*76*). For treatment of established 6132A, 6132A-MCC-GFP, 4102-mL9-GFP, or 4102-MCC-GFP tumors, 1×10^7 cancer cells were injected subcutaneously into the shaved backs of C3H Rag2$^{-/-}$ mice.

Tumor preparation and isolation of CD11b$^+$ and F4/80$^+$ cells

6132A tumors, either grown in C3H/HeN mice for isolation of tetramer-binding $CD4^+$ T cells or grown in C3H Rag2$^{-/-}$ mice for isolation of antigen-presenting cells (APCs), were removed, and single-cell suspensions were generated by enzymatic digestion (*77*). Tumors were minced, collagenase D (2 mg/ml) and deoxyribonuclease I (100 U/ml; both Roche, Indianapolis, IN, USA) were added, and suspension was incubated for 20 min at 37°C in RPMI 1640 on a horizontal shaker. After the addition of trypsin in Hanks' balance salt solution (MP Biomedicals LLC, Solon, OH, USA) to a final concentration of 0.025%, cell suspension was incubated for additional 15 min at 37°C on a horizontal shaker. Tumor cell suspension was filtered over a 40-μm cell strainer (Thermo Fisher Scientific, Waltham, MA, USA) and used subsequently. For the isolation of APCs, CD11b$^+$ and F4/80$^+$ cells were collected by magnetic cell sorting (Miltenyi, Bergisch Gladbach, Germany) following the manufacturer's protocol. Successful isolation was confirmed by FACS before both cell populations were used for T cell stimulation.

Tumor tissue analysis

At days 6, 7, and 8 after ATT, tumors were isolated, and about 100 mg was homogenized using Polytron (Kinematica, Lucern, Swiss) and spun down. Supernatants were used for determination of cytokines by flow cytometry using Legendplex according to the manufacturer's protocol (Biolegend, San Diego, CA, USA). For endothelial cell analysis, single-cell suspension from tumor tissue was generated as described in the "Tumor preparation and isolation of CD11b$^+$ and F4/80$^+$ cells" section. Tumor single-cell suspensions were analyzed for dead CD31$^+$ and CD146$^+$ cell populations with Sytox Blue (Helix NP Blue, Biolegend, San Diego, CA, USA) by flow cytometry.

T cell stimulation and cytokine analysis

TCR-engineered T cells or TCR-engineered 58α$^-$β$^-$ cells were cocultured for 24 hours with APCs to determine specificity and sensitivity. In brief, 1×10^5 T cells were added to 1×10^5 stromal cells isolated from tumor. For TCR-independent stimulation, αCD3 (8 μg/ml; University of Chicago, Frank W. Fitch Monoclonal Antibody Facility, clone 145-2C11.1) and αCD28 (2 μg/ml; clone 37.51, Biolegend, San Diego, CA, USA) was used. In addition, T cells were also cocultured with spleen cells isolated from C3H/HeN mice and 26-mer mL9, wtL9, or MCC peptides at various concentrations indicated in the figure legends. After 24 hours, supernatants were removed and tested for IFN-γ or IL-2 concentrations by enzyme-linked immunosorbent assay (ELISA, Ready-SET-Go!, eBioscience, San Diego, CA, USA), following the manufacturer's protocol. Light absorbance at 450 nm was read with the microplate reader VERSAmax (Molecular Devices LLC, San Jose, CA, USA), respectively. Furthermore, supernatants were used for determination of various cytokines by flow cytometry using Legendplex according to the manufacturer's protocol (Biolegend, San Diego, CA, USA).

Analysis of TCR signaling by phosphorylation of ERK

To measure strength of TCR signaling, 1×10^5 TCR-engineered $58\alpha^-\beta^-$ T cell hybridomas were cocultured with 1×10^5 LK35 cells. The LK35 cells were cultured overnight with 1 μM mL9 or 1 μM wtL9 peptide in 96-well U-bottom plates. TCR-engineered $58\alpha^-\beta^-$ cells were live/dead-stained with fixation-resistant dye 510 (BD Bioscience, Franklin Lakes, NJ, USA) before addition to LK35 cells. Cocultures were stopped at 0, 5, 10, 15, 20, 25, and 30 min after addition of TCR-engineered $58\alpha^-\beta^-$ cells. Plates were centrifuged for 20 s at 400*g* after each T cell addition to initiate contact and placed in a 37°C humidified incubator at 5% CO_2. After the last time point, the plate was centrifuged at 400*g* for 4 min, supernatants were discarded, and cells were immediately fixed with ice-cold 10% formalin solution (containing 4% formaldehyde) (100 μl per well) for 15 min on ice. Phosphate-buffered saline (PBS) (100 μl per well) was added, cells were centrifuged for 4 min at 400*g*, and supernatants were discarded. Cells were then permeabilized with ice-cold 90% methanol (100 μl per well) for 15 min on ice. PBS (100 μl per well) was added, cells were centrifuged for 4 min at 400*g*, and supernatants were discarded. Cells were then FcR-blocked [anti-FcR clone 2G4 (50 μl per well) in PBS] for 10 min at 4°C, washed, and stained at a 1:50 dilution intracellularly for phosphorylated ERK1/2 and at a 1:100 dilution for the I-E^k and TCR β chain to distinguish LK35 cells from TCR-engineered $58\alpha^-\beta^-$ cells for 30 min at room temperature, before resuspending in PBS and analyzing phosphorylated ERK1/2 by flow cytometry. The MFI of TCR-engineered $58\alpha^-\beta^-$cells stimulated by wtL9 peptide was averaged from all time points and considered background. The time point that showed the peak response to mL9 peptide was used, and background was subtracted from both samples (stimulation with wtL9 or mL9).

Analysis of TAMs

6132A tumor tissue was harvested at days 0, 6, and 20 after transfer of T cells. Single-cell suspensions were prepared as described in the "Tumor preparation and isolation of $CD11b^+$ and $F4/80^+$ cells" section and incubated with 4-amino-5-methylamino-2',7'-difluorescein (DAF-FM) diacetate (Life Technologies, Carlsbad, CA, USA) following the manufacturer's protocol for detection of NO. The viability dye 780 (BD Bioscience, Franklin Lakes, NJ, USA) was used for detection of live/dead cells following the manufacturer's protocol. Afterwards, cells were fixed and permeabilized using Cytofix/Cytoperm solution (BD Bioscience, Franklin Lakes, NJ, USA) following the manufacturer's protocol followed by 1 μg of Fc receptor block. At the end, intracellular stain was performed together with αCD11b, and αF4/80 antibodies and TAMs were analyzed by flow cytometry using NovoCyte Quanteon (Agilent, Santa Clara, CA, USA).

BrdU injection and cleaved caspase 3

6132A-ECFP–labeled cancer cells were used. Mice were injected intraperitoneally twice a day with 100 μl of BrdU (Sigma-Aldrich, Burlington, MA, USA) at a concentration of 10 μg/μl for three consecutive days. Mice were euthanized, and tumors and spleens were taken out as described in the "Tumor preparation and isolation of $CD11b^+$ and $F4/80^+$ cells" section. BrdU stain was performed using the BD BrdU Flow kit (BD Bioscience, Franklin Lakes, NJ, USA) following the manufacturer's protocol. In addition, dye 780 (BD Bioscience, Franklin Lakes, NJ, USA) was used for detection of live/dead cells. The rabbit antibody clone 9661 (Cell Signaling Technology, Danvers, MA, USA) was used for detection of cleaved caspase 3, and anti-rabbit immunoglobulin G clone 79408 [R-phycoerythrin (PE), Cell Signaling Technology, Danvers, MA, USA] was used for detection by flow cytometry. Furthermore, αCD11b and αF4/80 antibodies were used to detect TAMs, and αCD3, αCD4 antibodies together with mL9-tetramer were used to detect TILs.

Tumor infiltration and peripheral blood analysis

Blood was taken by buccal bleeding between days 45 and 75 as indicated in the figure legends with a 5-mm animal lancet (Medipoint Inc., Mineola, NY, USA). Blood (100 μl) was collected in tubes containing 50 μl of heparin (80 U/ml, Pfizer, New York, NY, USA). Red blood cells were lysed, and remaining peripheral blood cells were stained with Sytox Blue (Helix NP Blue, Biolegend, San Diego, CA, USA) for live/dead cells and for CD3, CD4, and Vβ6 before being analyzed by flow cytometry with the NovoCyte Quanteon (Agilent, Santa Clara, CA, USA).

Longitudinal confocal imaging

The method was described previously (*63*). Windows were implanted on the shaved backs of C3H $Rag^{-/-}$ mice. 6132A-cerulean cancer cells were injected at three different sites between the fascia and dermis of the rear skin layer. Mice were treated 15 days after window implantation with H6-engineered $CD4^+$ T cells. For longitudinal in vivo imaging, mice were anesthetized and positioned on a custom-made stage adaptor. The three screws used to hold the window frame also fixed the mouse onto the stage adaptor. A motorized microscope XY scanning stage and Leica LAS-AF software allowed recording of individual three-dimensional positions per field of view and returning to them later with high precision (stated accuracy, ±3 μm; reproducibility, <1.0 μm). Blood vessels were used as "landmarks" and could be located within 50 μm on the same day and within 100 μm on the next day. Data were acquired using a Leica SP5 II TCS tandem scanner two-photon spectral confocal microscope [long-working distance 20×/numerical aperture (NA) 0.45 and 4×/NA 0.16 dry lenses, Olympus]. Tumor blood flow was visualized by retro-orbital injection of 100 μl of red blood cells labeled with DiD (Thermo Fisher Scientific, Waltham, MA, USA). To determine the fraction of area occupied by vessels or cerulean fluorescent cancer cells, acquired images were analyzed using Fiji software (Laboratory for Optical and Computational Instrumentation; University of Wisconsin-Madison, WI, RRID: SCR_002285).

Flow cytometry and antibodies

Fc receptor block (1 μg; anti-mouse 2.4G2) was added to samples, and cells were incubated with 50 μl of PBS containing 0.2 μg of indicated anti-mouse antibodies for 20 min at 4°C. Then, samples were washed twice with PBS and acquired using NovoCyte Quanteon (Agilent, Santa Clara, CA, USA). Data analysis was performed using FlowJo software (TreeStar, Ashland, OR, USA, RRID: SCR_008520). The following fluorophores were used: allophycocyanin (APC), fluorescein isothiocyanate (FITC), Peridinin chlorophyll protein-cyanine5.5 (PerCp/Cy5.5), allophycocyanin-cyanine7 (APC/Cy7), Brilliant Violet 421 (BV421), R-phycoerythrin (PE), and Alexa Fluor 647 (AF647). The following antibodies were used: arginase 1 (A1exF5, APC, eFluor 450, eBioscience, Hatfield, GB, RRID: AB_2734833), anti-BrdU (3D4, FITC, RRID: AB_396304), $CD3^+$ (145-2C11, FITC, PerCp/Cy5.5, RRID: AB_312671), $CD4^+$ (GK1.5, APC, APC/Cy7, BV421, FITC, RRID: AB_312697), $CD11b^+$ (M1/70, APC, APC/Cy7, BV421, PE, RRID: AB_312794), $CD31^+$ (390, PE, RRID: AB_312902),

CD40 (3/23, FITC, RRID: AB_1134090), CD146$^+$ (ME-9F1, APC, RRID: AB_2563088), CD163 (S15049F, PE, RRID: AB_2860724), CD204 (1F8C33, APC, RRID: AB_2892311), CD206 (C068C2, BV421, RRID: AB_2562232), F4/80$^+$ (BM8, FITC, PerCp/Cy5.5, RRID: AB_893502), IDO (mIDO-4B, PE, Invitrogen Carlsbad, CA, USA), I-E^k (14-4-4S, FITC, PerCp/Cy5.5, AF647, RRID: AB_313470), IL-10 (JES5-16E3, BV421, RRID: AB_2563240), IL-12 (C15.6, APC, RRID: AB_315369), pERK1/2 (4B11B69, AF647, RRID: AB_2571894), TGFβ (TW7-20B9, PE, PerCp/Cy5.5, RRID: AB_10720866), TCR β chain (H57-597, PE, RRID: AB_313430), TNF (MP6-XT22, APC, PE, RRID: AB_315429), TCR Vb2 (B20.6, PE, RRID: AB_1227785), TCR Vb3 (KJ25, PE, BD Bioscience, Franklin Lakes, NJ, USA, RRID: AB_394709), TCR Vb6 (RR4-7, PE, RRID: AB_10643583), TCR Vb8.1,8.2 (KJ16-133.18, PE, RRID: AB_1134109), and TCR Vb8.3 (1B3.3, PE, RRID: AB_2800699). Unless indicated otherwise, antibodies were purchased from Biolegend (San Diego, CA, USA). Tetramers (I-E^k–mL9 and I-E^k–CLIP) were provided by the NIH Tetramer Core Facility. Samples were stained with tetramer (1.4 μg/ml) for 1 hour at 4°C in RPMI 1640 (Corning, NY, USA) containing 10% FBS (Gemini, Sacramento, CA, USA). For live/dead distinction, Sytox Blue (Helix NP Blue, Biolegend, San Diego, CA, USA) or fixation-resistant dye 510 or 780 (BD Bioscience, Franklin Lakes, NJ, USA) was used. Gating strategy for Fig. 1B is included in fig. S1. Gating strategies for Figs. 3 to 5 and supplementary figures are explained in the first part of the Supplementary Materials.

Histology and immunohistochemistry

Tumor-bearing and/or moribund mice were euthanized by cervical dislocation and were subjected to a full necropsy. Tissue samples were fixed for 24 hours in 10% buffered formalin (Sigma-Aldrich, Burlington, MA, USA) and then transferred to 70% ethanol. Tissue processing and immunohistochemistry stainings were performed by the Human Tissue Resource Center at the University of Chicago. Tissues were processed and paraffin-embedded, and 5-μm sections mounted on glass slides were subsequently stained with hematoxylin and eosin. Histopathological analysis was performed blinded and independently by two experienced pathologists. Microscopic images were captured using an Olympus BX43 microscope equipped with a ProgRes Speed XT core5 camera (Jenoptik) or a Leitz Laborlux D (W. Nuhsbaum Inc., Mc Henry, IL, USA) microscope with a Retiga 2000R (QImaging) camera and Adobe Photoshop 2014 2.2 (San Jose, CA) to compose images. Serial sections were stained for CD3 with rabbit monoclonal antibody SP162 (abcam ab135372). The slides were stained using Leica Bond RX automated stainer. After dewax and rehydration, tissue section was heat-treated for 20 min with antigen retrieval solution (Leica Biosystems, AR9961). Anti-CD3 antibody (1:100) was applied on tissue sections for 60-min incubation at room temperature, and the antigen-antibody binding was detected with the Bond Polymer Refine Detection HRP detection system (Leica Biosystems, DS9800) without postprimary antibody amplification. The peroxidase reaction was developed using liquid diaminobenzidine brown substrate chromogen provided in the kit. Sections were counterstained with hematoxylin, dehydrated in alcohol, cleared in xylene, and mounted in Tissue-Tek Glas Mounting Medium (Sakura Finetek Japan Co, Ltd., Tokyo, Japan) for microscopic evaluation.

Detection of DNA damage using TUNEL

6132A-ECFP–labeled cancer cells were injected subcutaneously in the backs of C3H Rag2$^{-/-}$ mice and around 40 days later treated with either H6- or αmL26-engineered CD4$^+$ T cells. About 20 days after T cell transfer, tumors were isolated. For analysis of DNA damage using flow cytometry, tumor single-cell suspensions were prepared (see the "Tumor preparation and isolation of CD11b$^+$ and F4/80$^+$ cells" section). Samples were stained with the viability dye 780 (BD Bioscience, Franklin Lakes, NJ, USA). TUNEL staining was performed using APO-BrdU TUNEL Assay Kit (Life Technologies/Invitrogen, Carlsbad, CA, USA) according to the manufacturer's protocol. Cells were fixed and permeabilized as described in TCR signaling. Detection of live, TUNEL-positive 6132A-ECFP cancer cells was done by flow cytometry using NovoCyte Quanteon (Agilent, Santa Clara, CA, USA). For detection of TUNEL-positive cells by immunohistochemistry, formalin-fixed, paraffin-embedded slides were stained using ApopTag plus peroxidase in situ (Millipore, Burlington, MA, USA) and counterstained with hematoxylin, dehydrated in alcohol, cleared in xylene, and mounted in Tissue-Tek Glas Mounting Medium (Sakura Finetek Japan Co, Ltd., Tokyo, Japan) for microscopic evaluation using ×40 magnification.

TCR sequencing analysis

The raw sequencing data were processed using the 10x Genomics Cell Ranger Software (v6.0.0, RRID: SCR_023221) with the command cellranger multi; the provided config csv files contain the information of the mm10 reference genome, vdj GRCm38 reference, and TotalSeq-C surface markers. The output from cellranger multi contains the TCR diversity metric that includes clonotype frequency and barcode information.

Whole-exome sequencing and RNA-seq of cancer cells

Both genomic DNA and total RNA were extracted from in vitro readapted 6132A cell lines, using AllPrep DNA/RNA mini kit (Qiagen, Venlo, Netherlands). For whole-exome sequencing, 3 μg of genomic DNA was subjected to library construction using SureSeletXT Mouse All Exon V1 (Agilent Technologies, Santa Clara, CA, USA). RNA-seq libraries were prepared from 1 μg of total RNA using TruSeq Stranded Total RNA Library Prep kit (Illumina, San Diego, CA, USA). The prepared whole-exome-sequencing and RNA-seq libraries were quantified by 2200 Tape Station (Agilent Technologies, Santa Clara, CA, USA) and then sequenced by 150-bp paired-end reads on NextSeq 500 Sequencer (Illumina, San Diego, CA, USA).

Statistics

All statistical analyses, including survival data, were performed using GraphPad Prism software (GraphPad, San Diego, CA, USA, RRID: SCR_002798). Data points either indicate means of biological duplicates of a representative experiment or are experimental replicates summarized as means ± SD. An unpaired, two-tailed Student's *t* test was used to determine significance between TUNEL-positive and TUNEL-negative samples. In all other experiments, the method used to present the statistical significance of the data is indicated in the figure legend. In all experiments, statistical significance was indicated as follows: n.s., not significant with $P > 0.5$, $*P \leq 0.5$, $**P \leq 0.01$, and $***P \leq 0.001$.

Supplementary Materials

The PDF file includes:

Figs. S1 to S12
Tables S1 and S2

Other Supplementary Material for this manuscript includes the following:
Data file S1
MDAR Reproducibility Checklist

REFERENCES AND NOTES

1. B. Vogelstein, N. Papadopoulos, V. E. Velculescu, S. Zhou, L. A. Diaz Jr., K. W. Kinzler, Cancer genome landscapes. *Science* **339**, 1546–1558 (2013).
2. P. A. Monach, S. C. Meredith, C. T. Siegel, H. Schreiber, A unique tumor antigen produced by a single amino acid substitution. *Immunity* **2**, 45–59 (1995).
3. T. Wölfel, M. Hauer, J. Schneider, M. Serrano, C. Wölfel, E. Klehmann-Hieb, E. De Plaen, T. Hankeln, K. H. Meyer zum Buschenfelde, D. Beach, A $p16^{INK4a}$-insensitive CDK4 mutant targeted by cytolytic T lymphocytes in a human melanoma. *Science* **269**, 1281–1284 (1995).
4. E. Tran, P. F. Robbins, S. A. Rosenberg, 'Final common pathway' of human cancer immunotherapy: Targeting random somatic mutations. *Nat. Immunol.* **18**, 255–262 (2017).
5. A. Haslam, V. Prasad, Estimation of the percentage of US patients with cancer who are eligible for and respond to checkpoint inhibitor immunotherapy drugs. *JAMA Netw. Open* **2**, e192535 (2019).
6. S. A. Rosenberg, N. P. Restifo, Adoptive cell transfer as personalized immunotherapy for human cancer. *Science* **348**, 62–68 (2015).
7. A. Schietinger, J. J. Delrow, R. S. Basom, J. N. Blattman, P. D. Greenberg, Rescued tolerant CD8 T cells are preprogrammed to reestablish the tolerant state. *Science* **335**, 723–727 (2012).
8. M. Philip, L. Fairchild, L. Sun, E. L. Horste, S. Camara, M. Shakiba, A. C. Scott, A. Viale, P. Lauer, T. Merghoub, M. D. Hellmann, J. D. Wolchok, C. S. Leslie, A. Schietinger, Chromatin states define tumour-specific T cell dysfunction and reprogramming. *Nature* **545**, 452–456 (2017).
9. S. P. Kim, N. R. Vale, N. Zacharakis, S. Krishna, Z. Yu, B. Gasmi, J. J. Gartner, S. Sindiri, P. Malekzadeh, D. C. Deniger, F. J. Lowery, M. R. Parkhurst, L. T. Ngo, S. Ray, Y. F. Li, V. Hill, M. Florentin, R. V. Masi, B. C. Paria, N. Levin, A. Bera, E. A. Hedges, A. Choi, P. D. Chatani, A. Y. Parikh, S. Levi, S. Seitter, Y. C. Lu, Z. Zheng, T. D. Prickett, L. Jia, J. M. Hernandez, C. D. Hoang, P. F. Robbins, S. L. Goff, R. M. Sherry, J. C. Yang, S. A. Rosenberg, Adoptive cellular therapy with autologous tumor-infiltrating lymphocytes and T-cell receptor-engineered T cells targeting common p53 neoantigens in human solid tumors. *Cancer Immunol. Res.* **10**, 932–946 (2022).
10. R. Leidner, N. Sanjuan Silva, H. Huang, D. Sprott, C. Zheng, Y. P. Shih, A. Leung, R. Payne, K. Sutcliffe, J. Cramer, S. A. Rosenberg, B. A. Fox, W. J. Urba, E. Tran, Neoantigen T-cell receptor gene therapy in pancreatic cancer. *N. Engl. J. Med.* **386**, 2112–2119 (2022).
11. M. Leisegang, B. Engels, K. Schreiber, P. Y. Yew, K. Kiyotani, C. Idel, A. Arina, J. Duraiswamy, R. R. Weichselbaum, W. Uckert, Y. Nakamura, H. Schreiber, Eradication of large solid tumors by gene therapy with a T-cell receptor targeting a single cancer-specific point mutation. *Clin. Cancer Res.* **22**, 2734–2743 (2016).
12. M. Leisegang, T. Kammertoens, W. Uckert, T. Blankenstein, Targeting human melanoma neoantigens by T cell receptor gene therapy. *J. Clin. Invest.* **126**, 854–858 (2016).
13. E. Tran, S. Turcotte, A. Gros, P. F. Robbins, Y. C. Lu, M. E. Dudley, J. R. Wunderlich, R. P. Somerville, K. Hogan, C. S. Hinrichs, M. R. Parkhurst, J. C. Yang, S. A. Rosenberg, Cancer immunotherapy based on mutation-specific CD4+ T cells in a patient with epithelial cancer. *Science* **344**, 641–645 (2014).
14. J. R. Veatch, S. M. Lee, M. Fitzgibbon, I. T. Chow, B. Jesernig, T. Schmitt, Y. Y. Kong, J. Kargl, A. M. Houghton, J. A. Thompson, M. McIntosh, W. W. Kwok, S. R. Riddell, Tumor-infiltrating BRAFV600E-specific CD4+ T cells correlated with complete clinical response in melanoma. *J. Clin. Invest.* **128**, 1563–1568 (2018).
15. N. Zacharakis, H. Chinnasamy, M. Black, H. Xu, Y. C. Lu, Z. Zheng, A. Pasetto, M. Langhan, T. Shelton, T. Prickett, J. Gartner, L. Jia, K. Trebska-McGowan, R. P. Somerville, P. F. Robbins, S. A. Rosenberg, S. L. Goff, S. A. Feldman, Immune recognition of somatic mutations leading to complete durable regression in metastatic breast cancer. *Nat. Med.* **24**, 724–730 (2018).
16. S. P. Wolf, V. Anastasopoulou, K. Drousch, M. I. Diehl, B. Engels, P. Y. Yew, K. Kiyotani, Y. Nakamura, K. Schreiber, H. Schreiber, M. Leisegang, One $CD4^+$TCR and one $CD8^+$TCR targeting autochthonous neoantigens are essential and sufficient for tumor eradication. *Clin. Cancer Res.* **30**, 1642–1654 (2024).
17. P. L. Ward, H. Koeppen, T. Hurteau, H. Schreiber, Tumor antigens defined by cloned immunological probes are highly polymorphic and are not detected on autologous normal cells. *J. Exp. Med.* **170**, 217–232 (1989).
18. M. B. Yassai, Y. N. Naumov, E. N. Naumova, J. Gorski, A clonotype nomenclature for T cell receptors. *Immunogenetics* **61**, 493–502 (2009).
19. V. Venturi, K. Kedzierska, D. A. Price, P. C. Doherty, D. C. Douek, S. J. Turner, M. P. Davenport, Sharing of T cell receptors in antigen-specific responses is driven by convergent recombination. *Proc. Natl. Acad. Sci. U.S.A.* **103**, 18691–18696 (2006).
20. K. Kedzierska, S. J. Turner, P. C. Doherty, Conserved T cell receptor usage in primary and recall responses to an immunodominant influenza virus nucleoprotein epitope. *Proc. Natl. Acad. Sci. U.S.A.* **101**, 4942–4947 (2004).
21. G. B. Beck-Engeser, P. A. Monach, D. Mumberg, F. Yang, S. Wanderling, K. Schreiber, R. Espinosa III, M. M. Le Beau, S. C. Meredith, H. Schreiber, Point mutation in essential genes with loss or mutation of the second allele: Relevance to the retention of tumor-specific antigens. *J. Exp. Med.* **194**, 285–300 (2001).
22. L. J. McHeyzer-Williams, J. F. Panus, J. A. Miksztа, M. G. McHeyzer-Williams, Evolution of antigen-specific T cell receptors in vivo: Preimmune and antigen-driven selection of preferred complementarity-determining region 3 (CDR3) motifs. *J. Exp. Med.* **189**, 1823–1838 (1999).
23. A. Schietinger, A. Arina, R. B. Liu, S. Wells, J. Huang, B. Engels, V. Bindokas, T. Bartkowiak, D. Lee, A. Herrmann, D. W. Piston, M. J. Pittet, P. C. Lin, T. Zal, H. Schreiber, Longitudinal confocal microscopy imaging of solid tumor destruction following adoptive T cell transfer. *Onco. Targets Ther.* **2**, e26677 (2013).
24. X. Liu, Y. He, F. Li, Q. Huang, T. A. Kato, R. P. Hall, C. Y. Li, Caspase-3 promotes genetic instability and carcinogenesis. *Mol. Cell* **58**, 284–296 (2015).
25. D. Mumberg, P. A. Monach, S. Wanderling, M. Philip, A. Y. Toledano, R. D. Schreiber, H. Schreiber, CD4(+) T cells eliminate MHC class II-negative cancer cells in vivo by indirect effects of IFN-gamma. *Proc. Natl. Acad. Sci. U.S.A.* **96**, 8633–8638 (1999).
26. R. J. Orentas, L. A. Bircher, S. Roskopf, Retroviral transfer of T-cell receptor genes produces cells with a broad range of lytic activity. *Scand. J. Immunol.* **58**, 33–42 (2003).
27. K. S. Weber, D. L. Donermeyer, P. M. Allen, D. M. Kranz, Class II-restricted T cell receptor engineered in vitro for higher affinity retains peptide specificity and function. *Proc. Natl. Acad. Sci. U.S.A.* **102**, 19033–19038 (2005).
28. K. Adachi, M. M. Davis, T-cell receptor ligation induces distinct signaling pathways in naive vs. antigen-experienced T cells. *Proc. Natl. Acad. Sci. U.S.A.* **108**, 1549–1554 (2011).
29. S. K. Biswas, A. Mantovani, Macrophage plasticity and interaction with lymphocyte subsets: Cancer as a paradigm. *Nat. Immunol.* **11**, 889–896 (2010).
30. P. Dash, A. J. Fiore-Gartland, T. Hertz, G. C. Wang, S. Sharma, A. Souquette, J. C. Crawford, E. B. Clemens, T. H. O. Nguyen, K. Kedzierska, N. L. La Gruta, P. Bradley, P. G. Thomas, Quantifiable predictive features define epitope-specific T cell receptor repertoires. *Nature* **547**, 89–93 (2017).
31. T. J. Looney, D. Topacio-Hall, G. Lowman, J. Conroy, C. Morrison, D. Oh, L. Fong, L. Zhang, TCR convergence in individuals treated with immune checkpoint inhibition for cancer. *Front. Immunol.* **10**, 2985 (2019).
32. M. Pan, B. Li, T cell receptor convergence is an indicator of antigen-specific T cell response in cancer immunotherapies. *eLife* **11**, e81952 (2022).
33. W. J. Storkus, D. Maurer, Y. Lin, F. Ding, A. Bose, D. Lowe, A. Rose, M. DeMark, L. Karapetyan, J. L. Taylor, M. Chelvanambi, R. J. Fecek, J. N. Filderman, T. J. Looney, L. Miller, E. Linch, G. M. Lowman, P. Kalinski, L. H. Butterfield, A. Tarhini, H. Tawbi, J. M. Kirkwood, Dendritic cell vaccines targeting tumor blood vessel antigens in combination with dasatinib induce therapeutic immune responses in patients with checkpoint-refractory advanced melanoma. *J. Immunother. Cancer* **9**, e003675 (2021).
34. S. Guedan, M. Luu, D. Ammar, P. Barbao, C. Bonini, P. Bousso, C. J. Buchholz, M. Casucci, B. De Angelis, E. Donnadieu, D. Espie, B. Greco, R. Groen, J. B. Huppa, C. Kantari-Mimoun, B. Laugel, M. Mantock, J. L. Markman, E. Morris, C. Quintarelli, M. Rade, K. Reiche, A. Rodriguez-Garcia, J. R. Rodriguez-Madoz, E. Ruggiero, M. Themeli, M. Hudecek, I. Marchiq, Time 2EVOLVE: Predicting efficacy of engineered T-cells - how far is the bench from the bedside? *J. Immunother. Cancer* **10**, e003487 (2022).
35. S. E. Brightman, A. Becker, R. R. Thota, M. S. Naradikian, L. Chihab, K. S. Zavala, A. L. Ramamoorthy Premlal, R. Q. Griswold, J. S. Dolina, E. E. W. Cohen, A. M. Miller, B. Peters, S. P. Schoenberger, Neoantigen-specific stem cell memory-like CD4(+) T cells mediate CD8(+) T cell-dependent immunotherapy of MHC class II-negative solid tumors. *Nat. Immunol.* **24**, 1345–1357 (2023).
36. M. O. Schaettler, R. Desai, A. Z. Wang, A. J. Livingstone, D. K. Kobayashi, A. T. Coxon, J. A. Bowman-Kirigin, C. J. Liu, M. Li, D. E. Bender, M. J. White, D. M. Kranz, T. M. Johanns, G. P. Dunn, TCR-engineered adoptive cell therapy effectively treats intracranial murine glioblastoma. *J. Immunother. Cancer* **11**, e006121 (2023).
37. C. A. Klebanoff, H. T. Khong, P. A. Antony, D. C. Palmer, N. P. Restifo, Sinks, suppressors and antigen presenters: How lymphodepletion enhances T cell-mediated tumor immunotherapy. *Trends Immunol.* **26**, 111–117 (2005).
38. N. N. Hunder, H. Wallen, J. Cao, D. W. Hendricks, J. Z. Reilly, R. Rodmyre, A. Jungbluth, S. Gnjatic, J. A. Thompson, C. Yee, Treatment of metastatic melanoma with autologous CD4+ T cells against NY-ESO-1. *N. Engl. J. Med.* **358**, 2698–2703 (2008).
39. P. Muranski, A. Boni, P. A. Antony, L. Cassard, K. R. Irvine, A. Kaiser, C. M. Paulos, D. C. Palmer, C. E. Touloukian, K. Ptak, L. Gattinoni, C. Wrzesinski, C. S. Hinrichs, K. W. Kerstann, L. Feigenbaum, C. C. Chan, N. P. Restifo, Tumor-specific Th17-polarized cells eradicate large established melanoma. *Blood* **112**, 362–373 (2008).
40. S. A. Quezada, T. R. Simpson, K. S. Peggs, T. Merghoub, J. Vider, X. Fan, R. Blasberg, H. Yagita, P. Muranski, P. A. Antony, N. P. Restifo, J. P. Allison, Tumor-reactive CD4(+) T cells develop cytotoxic activity and eradicate large established melanoma after transfer into lymphopenic hosts. *J. Exp. Med.* **207**, 637–650 (2010).
41. P. D. Greenberg, D. E. Kern, M. A. Cheever, Therapy of disseminated murine leukemia with cyclophosphamide and immune Lyt-1+,2- T cells. Tumor eradication does not require participation of cytotoxic T cells. *J. Exp. Med.* **161**, 1122–1134 (1985).

42. D. J. Zahavi, L. M. Weiner, Tumor mechanisms of resistance to immune attack. *Prog. Mol. Biol. Transl. Sci.* **164**, 61–100 (2019).
43. A. A. Tveita, F. H. Schjesvold, O. Sundnes, O. A. W. Haabeth, G. Haraldsen, B. Bogen, Indirect $CD4^+$ T-cell-mediated elimination of MHC II^{NEG} tumor cells is spatially restricted and fails to prevent escape of antigen-negative cells. *Eur. J. Immunol.* **44**, 2625–2637 (2014).
44. C. A. Nichols, W. J. Gibson, M. S. Brown, J. A. Kosmicki, J. P. Busanovich, H. Wei, L. M. Urbanski, N. Curimjee, A. C. Berger, G. F. Gao, A. D. Cherniack, S. Dhe-Paganon, B. R. Paolella, R. Beroukhim, Loss of heterozygosity of essential genes represents a widespread class of potential cancer vulnerabilities. *Nat. Commun.* **11**, 2517 (2020).
45. M. S. Hwang, B. J. Mog, J. Douglass, A. H. Pearlman, E. H. Hsiue, S. Paul, S. R. DiNapoli, M. F. Konig, D. M. Pardoll, S. B. Gabelli, C. Bettegowda, N. Papadopoulos, B. Vogelstein, S. Zhou, K. W. Kinzler, Targeting loss of heterozygosity for cancer-specific immunotherapy. *Proc. Natl. Acad. Sci. U.S.A.* **118**, e2022410118 (2021).
46. X. Zhang, T. Sjoblom, Targeting loss of heterozygosity: A novel paradigm for cancer therapy. *Pharmaceuticals* **14**, 57 (2021).
47. T. Kammertoens, C. Friese, A. Arina, C. Idel, D. Briesemeister, M. Rothe, A. Ivanov, A. Szymborska, G. Patone, S. Kunz, D. Sommermeyer, B. Engels, M. Leisegang, A. Textor, H. J. Fehling, M. Fruttiger, M. Lohoff, A. Herrmann, H. Yu, R. Weichselbaum, W. Uckert, N. Hubner, H. Gerhardt, D. Beule, H. Schreiber, T. Blankenstein, Tumour ischaemia by interferon-γ resembles physiological blood vessel regression. *Nature* **545**, 98–102 (2017).
48. M. N. Teng, B. H. Park, H. K. Koeppen, K. J. Tracey, B. M. Fendly, H. Schreiber, Long-term inhibition of tumor growth by tumor necrosis factor in the absence of cachexia or T-cell immunity. *Proc. Natl. Acad. Sci. U.S.A.* **88**, 3535–3539 (1991).
49. D. Pennica, G. E. Nedwin, J. S. Hayflick, P. H. Seeburg, R. Derynck, M. A. Palladino, W. J. Kohr, B. B. Aggarwal, D. V. Goeddel, Human tumour necrosis factor: Precursor structure, expression and homology to lymphotoxin. *Nature* **312**, 724–729 (1984).
50. J. Shen, Z. Xiao, Q. Zhao, M. Li, X. Wu, L. Zhang, W. Hu, C. H. Cho, Anti-cancer therapy with TNFα and IFNγ: A comprehensive review. *Cell Prolif.* **51**, e12441 (2018).
51. J. L. Rothstein, H. Schreiber, Synergy between tumor necrosis factor and bacterial products causes hemorrhagic necrosis and lethal shock in normal mice. *Proc. Natl. Acad. Sci. U.S.A.* **85**, 607–611 (1988).
52. L. P. Seung, D. A. Rowley, P. Dubey, H. Schreiber, Synergy between T-cell immunity and inhibition of paracrine stimulation causes tumor rejection. *Proc. Natl. Acad. Sci. U.S.A.* **92**, 6254–6258 (1995).
53. M. Binnewies, E. W. Roberts, K. Kersten, V. Chan, D. F. Fearon, M. Merad, L. M. Coussens, D. I. Gabrilovich, S. Ostrand-Rosenberg, C. C. Hedrick, R. H. Vonderheide, M. J. Pittet, R. K. Jain, W. Zou, T. K. Howcroft, E. C. Woodhouse, R. A. Weinberg, M. F. Krummel, Understanding the tumor immune microenvironment (TIME) for effective therapy. *Nat. Med.* **24**, 541–550 (2018).
54. K. Singer, E. Gottfried, M. Kreutz, A. Mackensen, Suppression of T-cell responses by tumor metabolites. *Cancer Immunol. Immunother.* **60**, 425–431 (2011).
55. S. J. Yu, C. Ma, B. Heinrich, Z. J. Brown, M. Sandhu, Q. Zhang, Q. Fu, D. Agdashian, U. Rosato, F. Korangy, T. F. Greten, Targeting the crosstalk between cytokine-induced killer cells and myeloid-derived suppressor cells in hepatocellular carcinoma. *J. Hepatol.* **70**, 449–457 (2019).
56. S. Li, S. Zhuang, A. Heit, S.-L. Koo, A. C. Tan, I. T. Chow, W. W. Kwok, I. B. Tan, D. S. W. Tan, Y. Simoni, E. W. Newell, Bystander $CD4^+$ T cells infiltrate human tumors and are phenotypically distinct. *Oncoimmunology* **11**, 2012961 (2022).
57. S. L. Meier, A. T. Satpathy, D. K. Wells, Bystander T cells in cancer immunology and therapy. *Nat. Cancer* **3**, 143–155 (2022).
58. H. G. Lee, M. J. Cho, J. M. Choi, Bystander CD4(+) T cells: Crossroads between innate and adaptive immunity. *Exp. Mol. Med.* **52**, 1255–1263 (2020).
59. D. J. Stuehr, C. F. Nathan, Nitric oxide. A macrophage product responsible for cytostasis and respiratory inhibition in tumor target cells. *J. Exp. Med.* **169**, 1543–1555 (1989).
60. M. Fauskanger, O. A. W. Haabeth, F. M. Skjeldal, B. Bogen, A. A. Tveita, Tumor killing by CD4(+) T cells is mediated via induction of inducible nitric oxide synthase-dependent macrophage cytotoxicity. *Front. Immunol.* **9**, 1684 (2018).
61. B. Bogen, M. Fauskanger, O. A. Haabeth, A. Tveita, CD4(+) T cells indirectly kill tumor cells via induction of cytotoxic macrophages in mouse models. *Cancer Immunol. Immunother.* **68**, 1865–1873 (2019).
62. B. Zhang, N. A. Bowerman, J. K. Salama, H. Schmidt, M. T. Spiotto, A. Schietinger, P. Yu, Y. X. Fu, R. R. Weichselbaum, D. A. Rowley, D. M. Kranz, H. Schreiber, Induced sensitization of tumor stroma leads to eradication of established cancer by T cells. *J. Exp. Med.* **204**, 49–55 (2007).
63. B. Zhang, Y. Zhang, N. A. Bowerman, A. Schietinger, Y. X. Fu, D. M. Kranz, D. A. Rowley, H. Schreiber, Equilibrium between host and cancer caused by effector T cells killing tumor stroma. *Cancer Res.* **68**, 1563–1571 (2008).
64. H. Braumuller, T. Wieder, E. Brenner, S. Assmann, M. Hahn, M. Alkhaled, K. Schilbach, F. Essmann, M. Kneilling, C. Griessinger, F. Ranta, S. Ullrich, R. Mocikat, K. Braungart, T. Mehra, B. Fehrenbacher, J. Berdel, H. Niessner, F. Meier, M. van den Broek, H. U. Haring, R. Handgretinger, L. Quintanilla-Martinez, F. Fend, M. Pesic, J. Bauer, L. Zender, M. Schaller, K. Schulze-Osthoff, M. Rocken, T-helper-1-cell cytokines drive cancer into senescence. *Nature* **494**, 361–365 (2013).
65. H. L. Tang, H. M. Tang, K. H. Mak, S. Hu, S. S. Wang, K. M. Wong, C. S. Wong, H. Y. Wu, H. T. Law, K. Liu, C. C. Talbot Jr., W. K. Lau, D. J. Montell, M. C. Fung, Cell survival, DNA damage, and oncogenic transformation after a transient and reversible apoptotic response. *Mol. Biol. Cell* **23**, 2240–2252 (2012).
66. L. Rössig, B. Fichtlscherer, K. Breitschopf, J. Haendeler, A. M. Zeiher, A. Mülsch, S. Dimmeler, Nitric oxide inhibits caspase-3 by *S*-nitrosation in vivo. *J. Biol. Chem.* **274**, 6823–6826 (1999).
67. G. Sun, E. Guzman, V. Balasanyan, C. M. Conner, K. Wong, H. R. Zhou, K. S. Kosik, D. J. Montell, A molecular signature for anastasis, recovery from the brink of apoptotic cell death. *J. Cell Biol.* **216**, 3355–3368 (2017).
68. Y. N. Gong, J. C. Crawford, B. L. Heckmann, D. R. Green, To the edge of cell death and back. *FEBS J.* **286**, 430–440 (2019).
69. B. D. Preston, T. M. Albertson, A. J. Herr, DNA replication fidelity and cancer. *Semin. Cancer Biol.* **20**, 281–293 (2010).
70. M. I. Diehl, S. P. Wolf, V. P. Bindokas, H. Schreiber, Automated cell cluster analysis provides insight into multi-cell-type interactions between immune cells and their targets. *Exp. Cell Res.* **393**, 112014 (2020).
71. J. Kappler, J. White, D. Wegmann, E. Mustain, P. Marrack, Antigen presentation by Ia+ B cell hybridomas to H-2-restricted T cell hybridomas. *Proc. Natl. Acad. Sci. U.S.A.* **79**, 3604–3607 (1982).
72. S. Morita, T. Kojima, T. Kitamura, Plat-E: An efficient and stable system for transient packaging of retroviruses. *Gene Ther.* **7**, 1063–1066 (2000).
73. B. Engels, A. S. Chervin, A. J. Sant, D. M. Kranz, H. Schreiber, Long-term persistence of $CD4^+$ but rapid disappearance of $CD8^+$ T cells expressing an MHC class I-restricted TCR of nanomolar affinity. *Mol. Ther.* **20**, 652–660 (2012).
74. B. Engels, V. H. Engelhard, J. Sidney, A. Sette, D. C. Binder, R. B. Liu, D. M. Kranz, S. C. Meredith, D. A. Rowley, H. Schreiber, Relapse or eradication of cancer is predicted by peptide-major histocompatibility complex affinity. *Cancer Cell* **23**, 516–526 (2013).
75. G. M. Bendle, C. Linnemann, A. I. Hooijkaas, L. Bies, M. A. de Witte, A. Jorritsma, A. D. M. Kaiser, N. Pouw, R. Debets, E. Kieback, W. Uckert, J.-Y. Song, J. B. A. G. Haanen, T. N. M. Schumacher, Lethal graft-versus-host disease in mouse models of T cell receptor gene therapy. *Nat. Med.* **16**, 565–570 (2010).
76. P. L. Ward, H. K. Koeppen, T. Hurteau, D. A. Rowley, H. Schreiber, Major histocompatibility complex class I and unique antigen expression by murine tumors that escaped from CD8+ T-cell-dependent surveillance. *Cancer Res.* **50**, 3851–3858 (1990).
77. M. T. Spiotto, D. A. Rowley, H. Schreiber, Bystander elimination of antigen loss variants in established tumors. *Nat. Med.* **10**, 294–298 (2004).

Acknowledgments: We thank V. P. Bindokas, T. Krausz, C. Nathan, L. Zhou, M. Diehl, D. Feng, E. Kim, C.-E. Lee, and T. Tate for technical support and valuable suggestions. This work used the NIH tetramer core facility (contract number 75N93020D00005) for tetramers. This work was supported by the Cytometry and Antibody Technology Core Facility, the Center for Research Informatics, the Integrated Light Microscopy Core, and the Genomics Core at the University of Chicago. The core facilities are supported by the Cancer Center Support Grant (P30CA014599) at the University of Chicago. **Funding:** This work was supported by NIH grants (R01-CA22677 to H.S.), the David and Etta Jonas Center for Cellular Therapy (to S.P.W., M.L. and H.S.), Harriet and Allan Wulfstat (to H.S.), the Gerald O. Mann Foundation (to H.S.), a gift of N. Carey (to H.S.), and a gift of J. D. Rowley (to H.S.). **Author contributions:** The authors contributed as follows. Conceptualization: S.P.W., M.L., A.S., and H.S. Methodology: S.P.W., M.L., and H.S. Investigation: S.P.W., M.L., M.S., V.W., K.K., Y.H., L.R., and K.S. Performing experiments: S.P.W., M.S., V.W., K.K., Y.H., L.R., and K.S. Visualization: S.P.W. and H.S. Data curation: S.P.W., M.S., K.K., Y.H., L.R., J.H., K.S., and Y.N. Funding acquisition: M.L. and H.S. Project administration: M.L., J.H., Y.N., A.S., and H.S. Supervision: M.L. and H.S. Writing—original draft: S.P.W. and H.S. Writing—review and editing: S.P.W., M.L., V.W., K.S., A.S., and H.S. **Competing interests:** S.P.W., M.L., K.S., and H.S. have patent WO2023049733A3 pending. The authors declare that they have no other competing interests. **Data and materials availability:** All data needed to evaluate the conclusions in the paper are present in the paper or the Supplementary Materials and in data file S1. Materials used to conduct this study will be made available upon request. Sequencing data are accessible at the Sequence Read Archive (SRA). Project number PRJNA1113628 includes original TCR-sequencing data, and project number PRJNA1113704 includes original whole-exome-sequencing data for reisolated and readapted 6132A cancer cell lines referenced in table S2.

Submitted 5 April 2024
Accepted 19 August 2024
Published 13 September 2024
10.1126/sciimmunol.adp6529

Science Immunology
AAAS

Supplementary Materials for

CD4$^+$ T cells with convergent TCR recombination reprogram stroma and halt tumor progression in adoptive therapy

Steven P. Wolf *et al.*

Corresponding author: Steven P. Wolf, wolfs@uchicago.edu

Sci. Immunol. **9**, eadp6529 (2024)
DOI: 10.1126/sciimmunol.adp6529

The PDF file includes:

Other Supplementary Material for this manuscript includes the following:

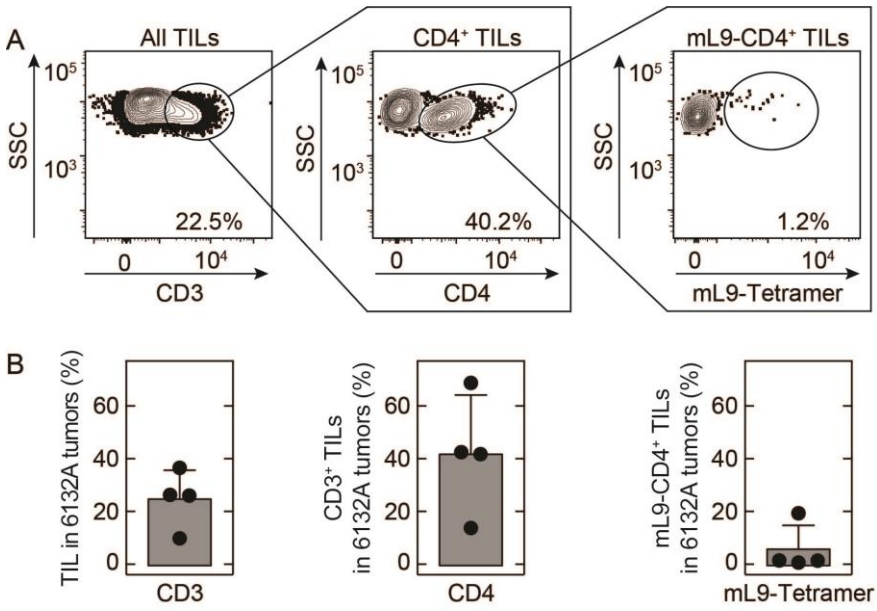

Fig. S1. Progressively growing 6132A tumors are heavily infiltrated by T cells. (A – B) 6132A tumors grown in C3H/HeN mice were analyzed by flow cytometry for $CD3^+$ tumor infiltrating lymphocytes (**left**, all TILs), proportion of (**middle**) $CD4^+$ TILs and (**right**) mL9-specific $CD4^+$ TILs. **(A)** Gating strategy of sample shown in **Fig. 1B**. **(B)** Results summarized from a total of n = 4 mL9-tetramer sortings in four independent experiments.

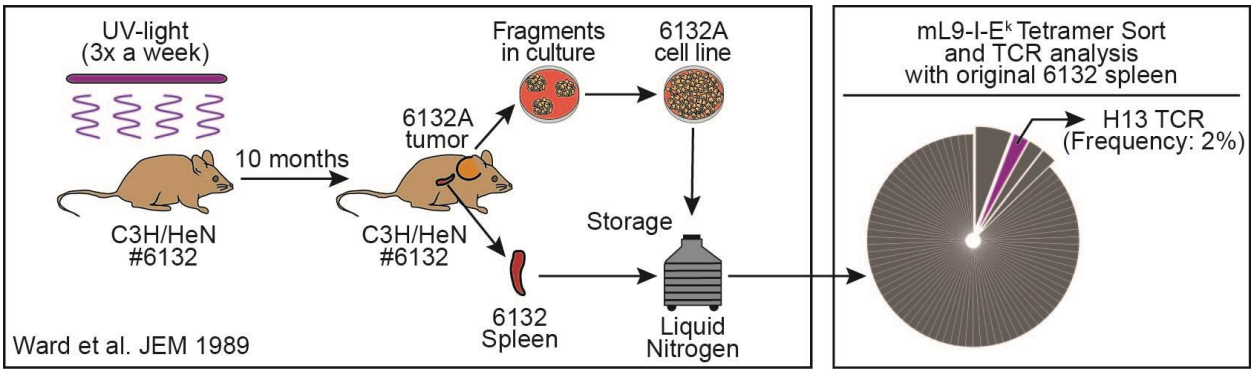

Fig. S2. The spleen of the original 6132-tumor bearing mouse contained a preferentially selected TCR. (left) Depiction of the generation of the 6132A cancer cell line. The spleen of the original 6132 mouse, that developed the autochthonous 6132A cancer after exposure to UV-light, was taken out, frozen and stored in liquid nitrogen as cell suspension. **(right)** The spleen was thawed and $CD3^+$, $CD4^+$ and mL9-I-E^k-$tetramer^+$ cells were sorted and used for single cell TCR analysis which identified the preferentially selected TCR H13.

Fig S3. TCR sequences of single T cell clonotypes found in 6132A-tumor bearing mice. Amino acid CDR3 sequences of paired TCR α- and β-chains of the **(A)** single T cell clonotype TCRs H7, H8, H10, H11, H12, H14, H15 and H16 which were frequent among tumor and spleen in the six analyzed 6132A-tumor bearing mice.

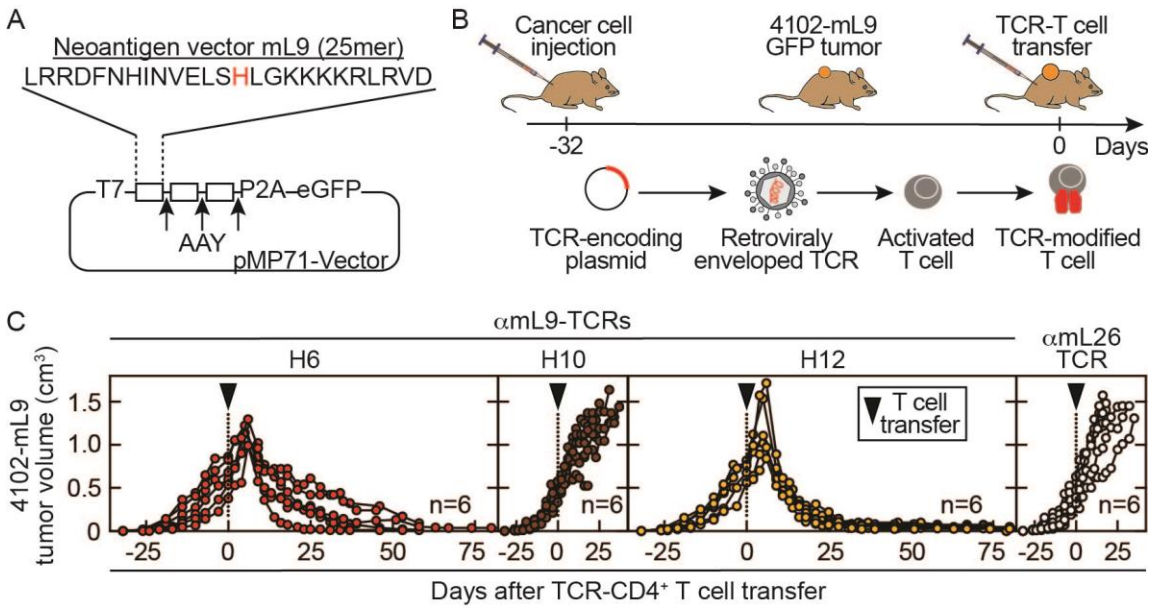

Fig. S4. CD4TCRs therapeutic in the 6132A tumor model are also effective in a second UV-induced tumor model. (A) Vector design to introduce the neoantigen mL9 as a trimeric 25mer, separated by the proteasomal cleavage side AAY and linked over a P2A element to eGFP, into the UV-induced cancer cell line 4102. **(B)** The 4102-mL9-GFP cancer cells were injected *s.c.* on the back of C3H Rag$^{-/-}$ mice. Around 32 days later, established tumors were treated with TCR-engineered CD4^{+} T cells. **(C)** 4102-mL9-GFP bearing C3H Rag$^{-/-}$ mice were treated with CD4^{+} T cells from the spleen of C3H CD8$^{-/-}$ mice that were TCR-engineered with either H6 (n = 6), H10 (n = 6), H12 (n = 6) or the mL26-specific (n = 6) control TCR. TCRs H6 and H12 caused 4102 tumor destruction followed by long-term growth arrest, while the TCR H10 failed, which is a similar outcome as observed in the 6132A tumor model. Mice treated with the mL26-specific TCR-engineered CD4^{+} T cells were used as outgrowth controls. Number (n) indicates total number of mice used. Data are compiled from two independent experiments.

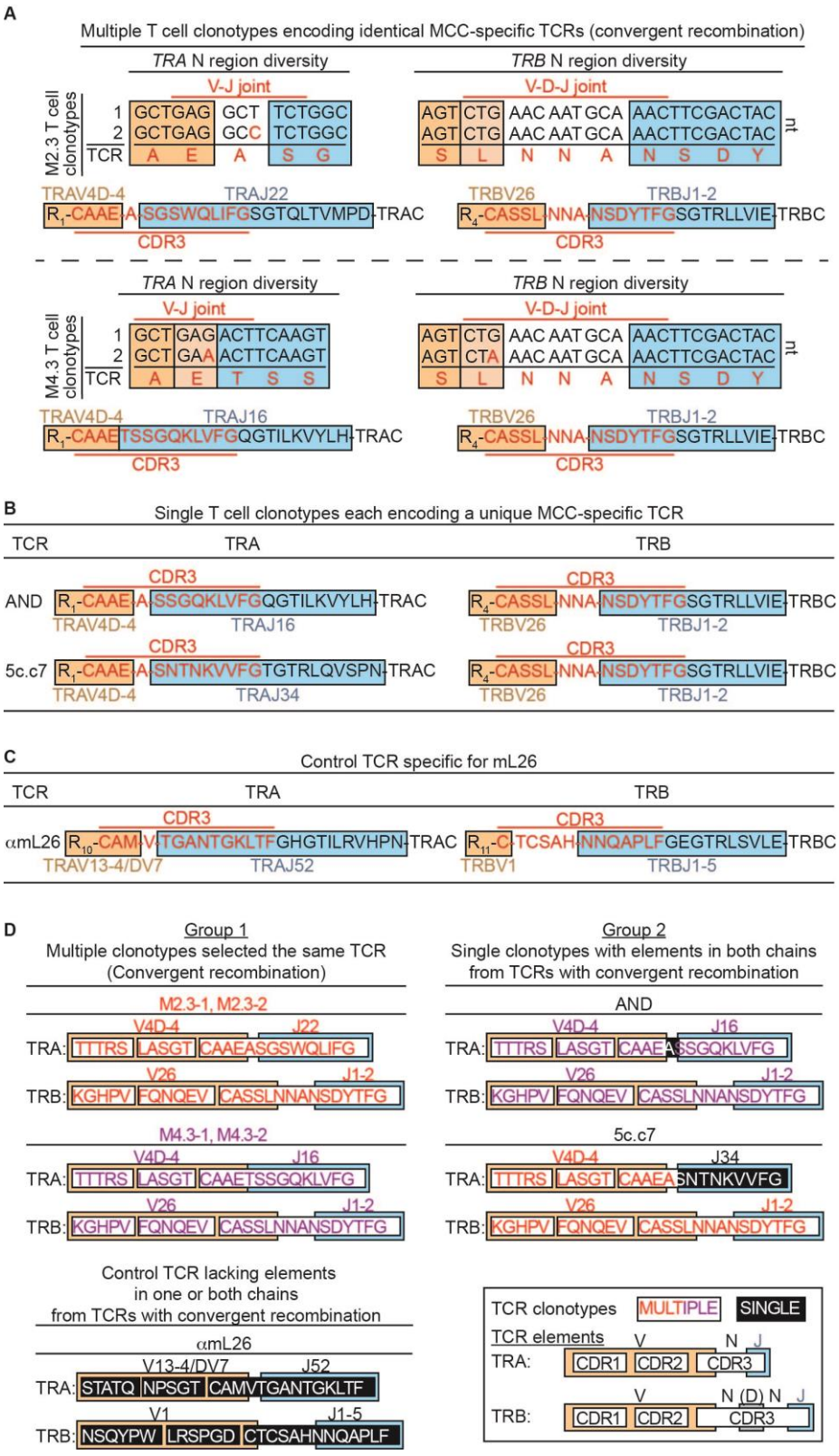

Fig. S5. The immune response against moth cytochrome c induces TCRs encoded by multiple or single T cell clonotypes. Nucleotide sequences of the TCRs were reported by McHeyzer-

Williams et. al. (22). **(A)** TCRs M2.3 and M4.3 are each encoded by two different T cell clonotypes based on N nucleotide (nt) sequence diversity in the *TRA* and *TRB* V(D)J joints. **(B)** CDR3 amino acid sequences of the single T cell clonotype TCRs AND and 5c.c7 as well as (**C**) the control TCR αmL26. **(D)** Based on representation by either multiple or single T cell clonotypes, the four MCC-specific TCRs fell into two groups. Group 1: TCRs M2.3 and M4.3 are each characterized by convergent recombination of multiple T cell clonotypes. Group 2: TCRs AND and 5c.c7 are each represented by single T cell clonotypes. Control group: Control TCR αmL26. Color coding indicates whether CDR elements were shared in TRA and/or TRB between the different TCR groups.

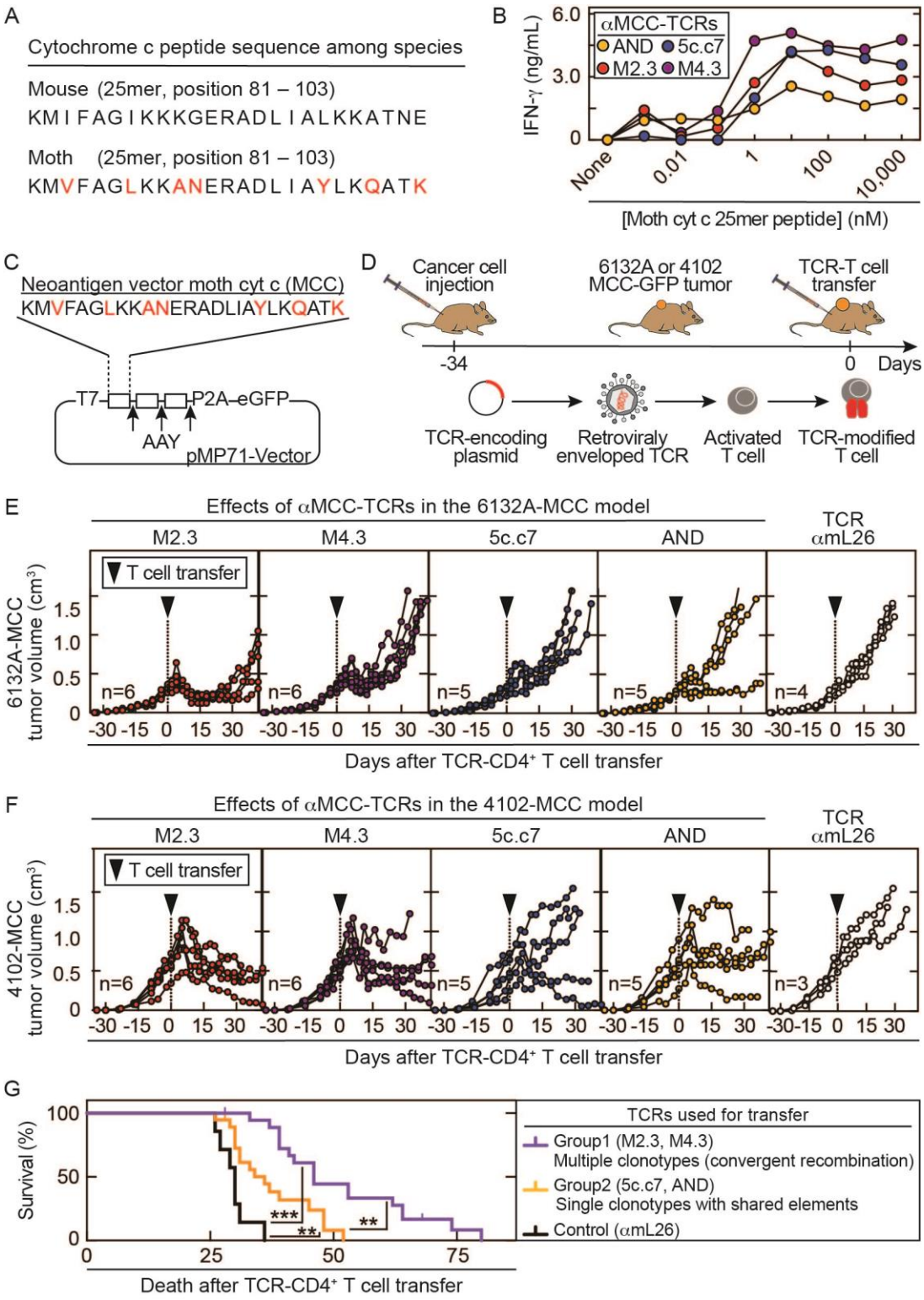

Fig. S6. Comparing the therapeutic effects of MCC-specific TCRs encoded by multiple T cell clonotypes with MCC-specific TCRs from single T cell clonotypes. (A) Comparison of the 25mer peptide sequence of mouse and moth cytochrome c (MCC). Differences in the amino acid

sequence are highlighted in red. **(B – F)** We ordered the four different moth cytochrome c (MCC) specific TCRs and cloned them into the retroviral vector pMP71. Spleens of C3H $CD8^{-/-}$ were used as $CD4^+$ T cell source for TCR-engineering. **(B)** TCR-engineered $CD4^+$ T cells were used for co-cultures with C3H/HeN spleen cells as APCs and various concentrations of the MCC 25mer peptide. Supernatants were analyzed for IFN-γ by ELISA. Shown is one representative out of two independent experiments. **(C)** Vector design to introduce the neoantigen MCC as a trimeric 25mer, separated by the proteasomal cleavage side AAY and linked over a P2A to eGFP, into the UV-induced cancer cell lines 6132A and 4102. **(D)** 6132A- or 4102-mL9-GFP cancer cells were injected *s.c.* on the back of C3H $Rag^{-/-}$ mice. Around 34 days later, established tumors were treated with TCR-engineered $CD4^+$ T cells. **(E – G)** Data are compiled from two independent experiments. Number (n) indicates total number of mice used. **(E)** 6132A-MCC-GFP bearing C3H $Rag^{-/-}$ mice were treated with TCR-engineered $CD4^+$ T cells: M2.3 (n = 6), M4.3 (n = 6), 5c.c7 (n = 5), AND (n = 5), αmL26-TCR (n = 4). **(F)** 4102-MCC-GFP bearing C3H $Rag^{-/-}$ mice were treated with TCR-engineered $CD4^+$ T cells: M2.3 (n = 6), M4.3 (n = 6), 5c.c7 (n = 5), AND (n = 5), αmL26-TCR (n = 3). **(G)** Mice from both tumor models (6132A-MCC and 4102-MCC) were combined and analyzed for long-term survival. Group 1: Mice treated with TCRs characterized by convergent recombination M2.3 and M4.3 (n = 24). Group 2: Mice treated with single clonotype TCRs with shared elements 5c.c7 and AND (n = 20). Control group: Mice treated with control TCR αmL26 (n = 7). Mice treated with TCRs from group 1 (M2.3 or M4.3) survived significantly longer (**$p \leq 0.01$) than mice treated with TCRs from group 2 (5c.c7 or AND) or the control group (***$p \leq 0.001$). Mice treated with TCRs from group 2 (5c.c7 or AND) survived longer (**$p \leq 0.01$) than mice treated with the αmL26 TCR (control group). Statistical significance was determined using log-rank test.

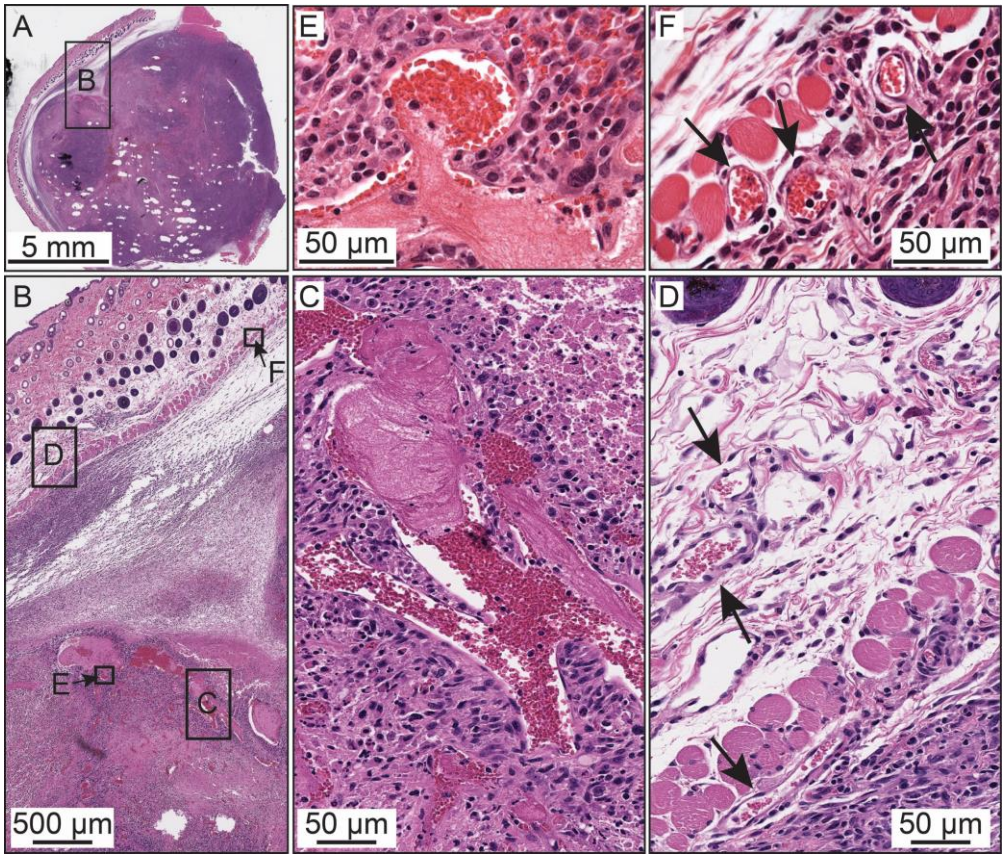

Fig. S7. Destruction of tumor vessels but not of pre-existent vasculature after T cell transfer. Histological analysis of a 6132A-tumor grown in C3H $Rag^{-/-}$ mice 6 days after adoptive transfer of H6-engineered $CD4^{+}$ T cells. Multiple H&E stained slides were analyzed. Shown are representative examples. **(A)** Slide of the entire tumor with an area at the tumor margin in the upper left delineated with "B" and further magnified in (B). **(B)** A higher magnification outlines the areas C, D, E and F. **(C)** Large clogged and destroyed vessels within the tumor. **(D)** Healthy, intact tissue with functional vessels along the panniculus carnosus which indicates the rim of the tumor. At this location, healthy cancer cells can be detected. Black arrows indicate pre-existing vessels with intact epithelia. **(E)** Shown is an example of blocked blood flow by a thrombus within the tumor. **(F)** Healthy margin showing smaller intact vessels encircled by undamaged endothelia at the tumor margin.

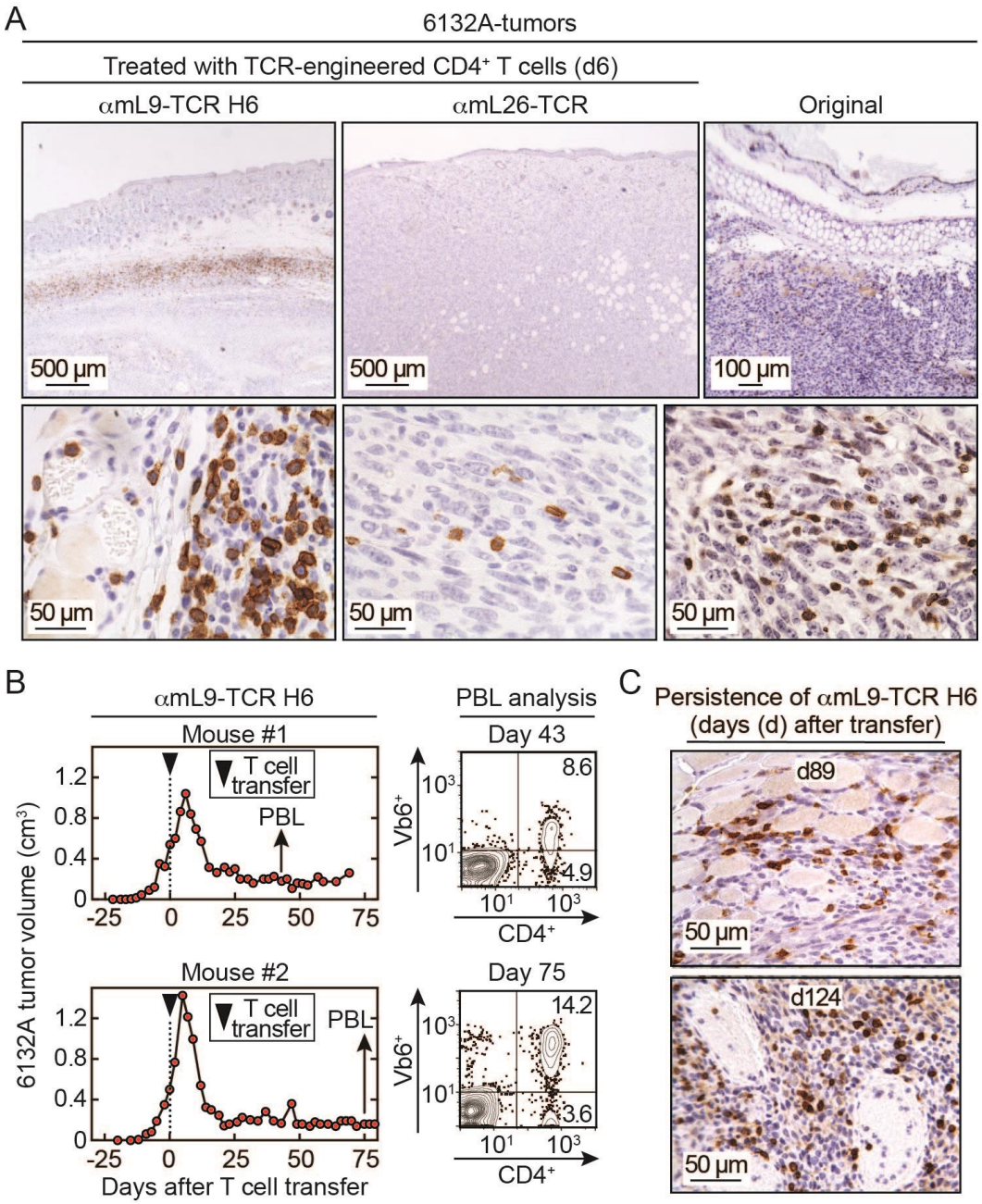

Fig. S8. Persistent detection of T cells in the original 6132A tumor as well as transplanted 6132A tumors. (A) CD3 stain of slides from 6132A-tumors grown in C3H Rag$^{-/-}$ mice 6 days after adoptive transfer of either H6- or αmL26-TCR-engineered CD4^{+} T cells. Spleens of C3H CD8$^{-/-}$ mice were used as CD4^{+} T cell source for TCR-engineering. Additionally, the original autochthonous 6132A tumor was also analyzed by CD3-stain. Multiple sections were evaluated and a representative location is shown. Left panels**:** H6-treated tumor. Accumulation of T cells forming a line at the tumor rim where cancer cells survived. Fewer T cells can be detected inside the destroyed tumor. Middle panels: αmL26-treated tumor. Lower magnification of the tumor

margin (upper middle panel) fails to reveal a rim of dense T cell infiltration. Very few of the control T cells infiltrated the 6132A-tumor at this stage (lower middle panel). Right panels: The original 6132A tumor. The upper right panel (lower magnification) fails to show a distinctive rim of T cell infiltration at the tumor margin. The structures in the upper part of the section represent the skin overlaying the auricicular cartilage of the ear from which the cancer originated. Despite failing to show a distinctive rim of T cell infiltration, the original autochthonous 6132A tumor was diffusely and heavily infiltrated with $CD3^+$ T cells (lower right panel). **(B – C)** C3H $CD8^{-/-}$ mice were used as $CD4^+$ T cell source. 6132A tumor-bearing C3H $Rag^{-/-}$ mice were treated with H6-engineered T cells. **(B)** Left panels: Timepoints of T cell transfer and analysis of peripheral blood are indicated by the arrow heads. Right panels: The H6-T cell population was detected by flow cytometry via αVβ6 and αCD4 stain in peripheral blood several weeks after T cell transfer. Percentages are of $V\beta6^+$ and $CD4^+$ positive cells are indicated. Upper right panel: 43 days after T cell transfer. Shown is one out of three independent mice where blood was analyzed 40 to 50 days after T cell transfer. Bottom right panel: 75 days after T cell transfer. Shown is one out of two independent mice where peripheral blood was analyzed 70 to 80 days after T cell transfer. **(C)** Histochemical demonstration of persisting ($CD3^+$ stained) T cells infiltrating the growth-arrested remaining 6132A tumor tissue 89 days (top) and 124 days (bottom) after transfer of H6-T cells.

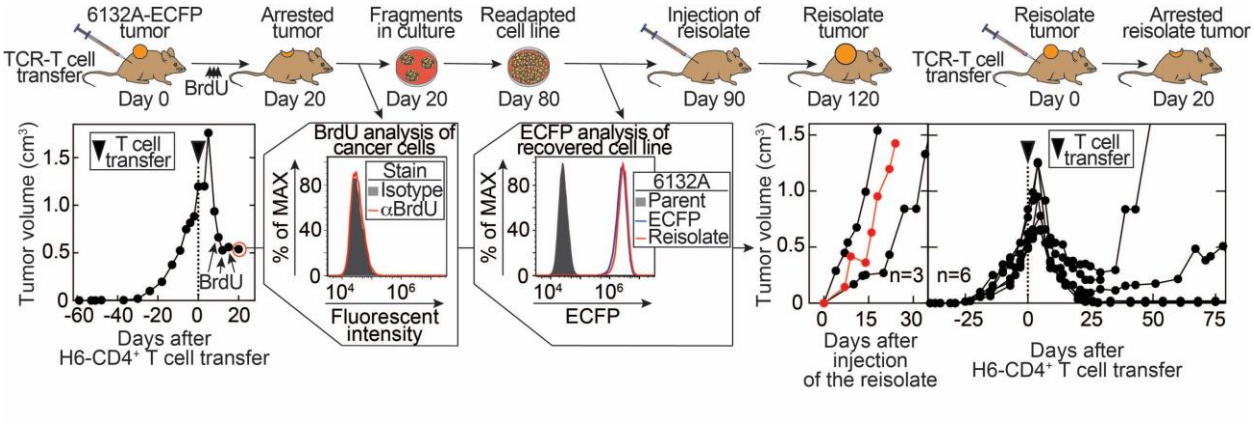

Fig. S9. Non-proliferative, growth-arrested 6132A cancer cells can be recovered *in vitro* and form again treatable tumors *in vivo*. 6132A-ECFP was injected into a C3H Rag$^{-/-}$ mouse and the tumor was treated with H6-T cells. The mouse was injected with BrdU twice a day for three consecutive days before tumor tissue was isolated at day 20 (circled red) after T cell transfer. Arrested 6132A-ECFP cancer cells were analyzed by flow cytometry for frequency of BrdU incorporation and tumor fragments were taken in culture on the same day. 60 days later, a stable cell line was recovered which was analyzed by flow cytometry for ECFP expression and then transferred into another C3H Rag$^{-/-}$ mouse to determine whether these cells can still form a tumor. A tumor developed (indicated in red) and after 25 days fragments were transferred into two additional C3H Rag$^{-/-}$ mice (indicated in black) to analyze whether the developed tumor was still transplantable. Aggressively growing tumors were formed again. Lastly, established tumors (total n = 6) which developed from the recovered 6132A-ECFP cancer cell line, were treated with H6-T cells which caused again tumor destruction followed by long-term growth arrest. This process, readaption of growth-arrested tumor fragments *in vitro*, recovering of a 6132A-ECFP cancer cell line and H6-T cell retreatment of established tumors developed by the *in vitro* recovered cell line, was repeated in a second independent experiment. Both *in vitro* recovered 6132A-ECFP cancer cell lines were used for whole-exome sequencing as indicated in **Table S2**.

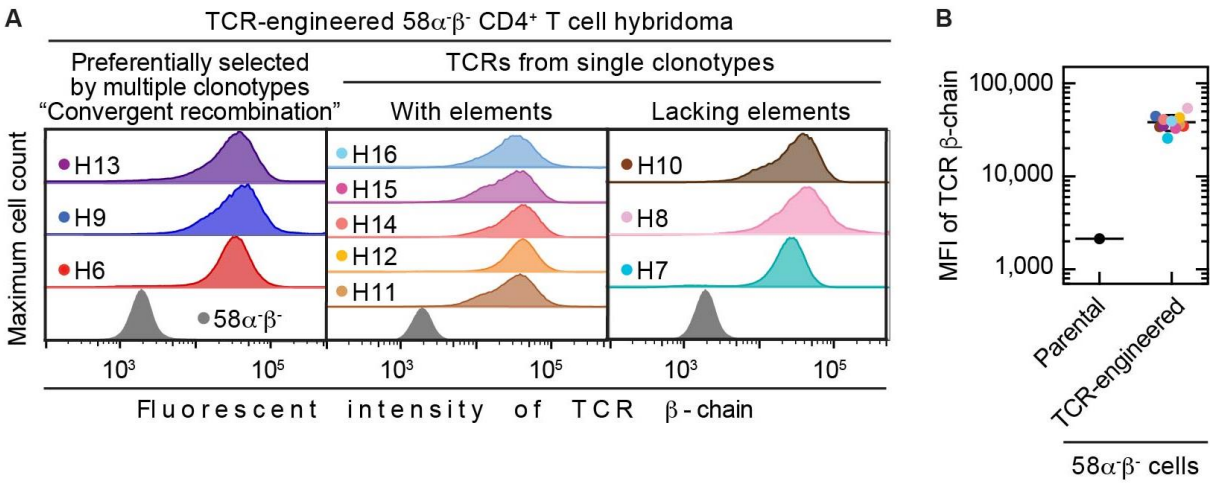

Fig. S10. The TCR-engineered 58α-β- CD4+ T cell hybridomas express the different CD4TCRs similarly. The 58α-β- CD4+ T cell hybridoma was used to generate 11 different cell lines, each expressing one TCR: H6, H7, H8, H9, H10, H11, H12, H13, H14, H15 or H16. Cell lines were sorted for similar TCR expression. **(A)** TCR expression was determined using an antibody recognizing a part of the constant region of the TCR β-chain. **(B)** Mean fluorescent intensity (MFI) of the TCR β-chain showing similar expression between the 11 generated TCR-engineered 58α-β- CD4+ T cell hybridoma cell lines. Parental 58α-β- CD4+ T cell hybridoma which lacks TCR expression was used as control.

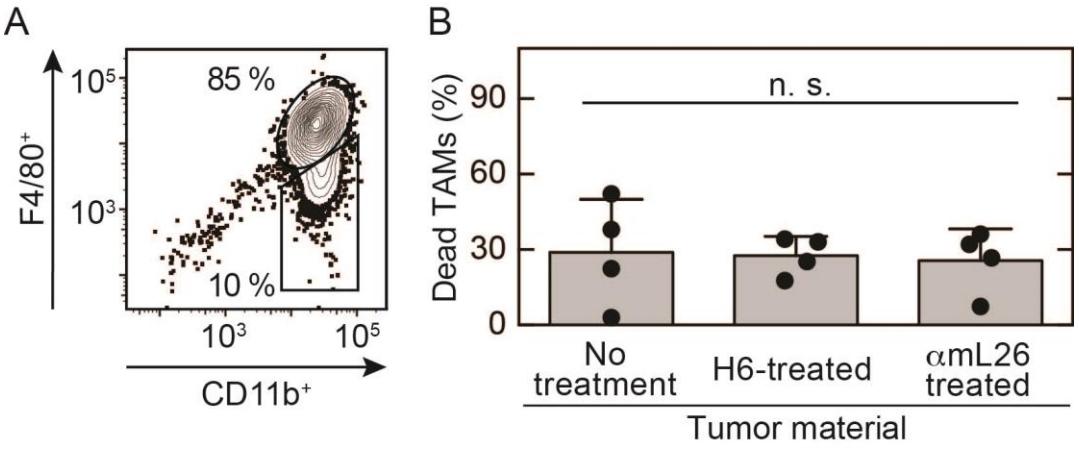

Fig. S11. Proportion of dead stromal macrophages is similar in growing and arrested tumors. **(A)** Proportion of F4/80^{+} cells of bulk CD11b^{+} cells isolated from a representative 6132A tumor grown in C3H Rag$^{-/-}$ mice analyzed by flow cytometry. **(B)** Spleens from C3H CD8$^{-/-}$ mice were used as CD4^{+} T cell source for H6- or αmL26-TCR engineering. C3H Rag$^{-/-}$ mice bearing 6132A tumors were treated 21 to 23 days after cancer cell injection. TAMs (CD11b^{+}, F4/80^{+}) were analyzed by flow cytometry. Tumors were left untreated (n = 4) or treated with either H6- (n = 4) or αmL26-T cells (n = 4). Tumor tissue was isolated at day 20 – 25 after T cell transfer. Frequency of dead TAMs is indicated. Significance (n.s. – not significant) was determined using a multiple comparison one-way ANOVA test. Number (n) indicates total number of analyzed tumors from independent mice. Data are compiled from three independent experiments.

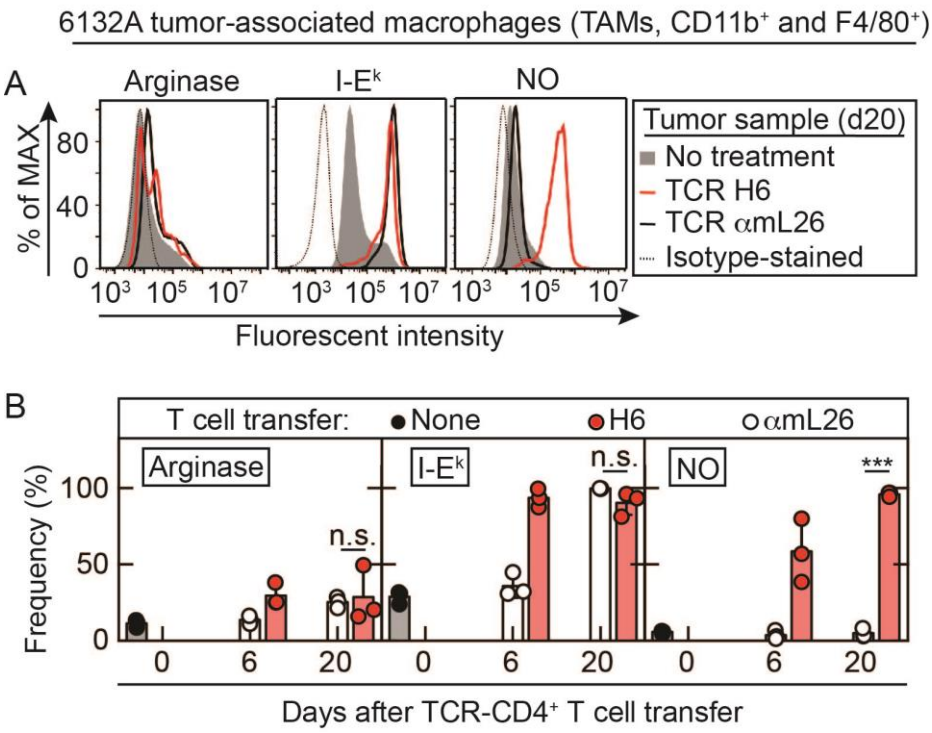

Fig. S12. Production of NO is selectively induced in TAMs following treatment with the therapeutically effective and preferentially selected TCR H6. By contrast, there were no significant differences in the upregulation of MHC Class II or arginase in TAMs from tumors treated with either the H6-TCR or αmL26 control TCR. **(A – B)** Spleens from C3H CD8$^{-/-}$ mice were used as CD4^{+} T cell source for TCR engineering. C3H Rag$^{-/-}$ mice bearing 6132A tumors were treated 21 to 23 days after cancer cell injection. TAMs (CD11b^{+}, F4/80^{+}) were analyzed by flow cytometry. Tumors were treated with either H6- (n = 3) or αmL26-T cells (n = 3) or left untreated (n = 3). Number (n) indicates total number of tumors analyzed from independent mice. Tumor tissue was isolated at day 0, 6 or 20 – 22 after T cell transfer. Tumor single cell suspensions were analyzed by flow cytometry for frequency of TAMs expressing arginase, I-E^{k} and NO. **(A)** Representative flow cytometry analysis at day 20 after T cell transfer. **(B)** Change of TAMs expressing arginase, I-E^{k} and NO over time after T cell transfer. Significance was determined using an unpaired, two-tailed Student's t-test (***$p \leq 0.001$, n.s. – not significant). Data are compiled from two independent experiments.

Table S1. Number of sorted mL9-tetramer^{+} CD4^{+} T cells and identified TCRs based on CDR3 amino acid sequences among tumor and spleen from 6132A tumor-bearing mice.

Mouse	Tumor		Spleen	
	Number of T cells	Number of TCRs	Number of T cells	Number of TCRs
1	63	25	104	41
2	175	74	99	54
3	25	14	285	55
4	7	7	372	83
5+6	543	108	149	42
Average	162.6	45.6	201.8	55

Table S2. Analysis of expressed nsSNVs in reisolated progressing or arrested 6132A tumors.

6132A reisolate[A]	Treatment[B]	mL9 expression (RNA FPKM)	Expressed nsSNV (RNA FPKM ≥ 5)
#4718	None	548.493	1779
#4719[C]	H6	466.526	1769
#7855[D]	H6	625.942	1710
#4720	αmL26	619.572	1768
#7854	αmL26	570.551	1705

[A]All 6132A reisolates were from mice injected with tumor cells 45 days earlier
[B]TCR-engineered $CD4^+$ T cells were transferred 21 days after cancer cell injection
[C]Readapted from mouse shown in Fig. S9, indicated by the red circle in the far left panel
[D]Experimental repeat of #4719

Materials Design Analysis Reporting (MDAR)
Checklist for Authors

The MDAR framework establishes a minimum set of requirements in transparent reporting applicable to studies in the life sciences (see Statement of Task: doi:10.31222/osf.io/9sm4x.). The MDAR checklist is a tool for authors, editors, and others seeking to adopt the MDAR framework for transparent reporting in manuscripts and other outputs. Please refer to the MDAR Elaboration Document for additional context for the MDAR framework.

For all that apply, please note where in the manuscript the required information is provided.

Materials:

Newly created materials	indicate where provided: page no/section/legend)	n/a
The manuscript includes a dedicated "materials availability statement" providing transparent disclosure about availability of newly created materials including details on how materials can be accessed and describing any restrictions on access.	Materials and data availablility statement included on page 32.	

Antibodies	indicate where provided: page no/section/legend)	n/a
For commercial reagents, provide supplier name, catalogue number and RRID, if available.	RRID are provided under "material and methods", sections: "mice" page 15, "longitudinal confocal imaging" page 20 – 21, "flow cytometry and antibodies" page 21, "TCR sequencing analysis" page 22 and "statistics" page 23.	

DNA and RNA sequences	indicate where provided: page no/section/legend)	n/a
Short novel DNA or RNA including primers, probes: Sequences should be included or deposited in a public repository.	Sequencing dat are deposited at Sequence Read Archive (SRA). Project ID's are included in the data availability statement on page 32.	

Cell materials	indicate where provided: page no/section/legend	n/a
Cell lines: Provide species information, strain. Provide accession number in repository **OR** supplier name, catalog number, clone number, **OR** RRID.	Provided under material and methods, section "cell lines", page 16.	
Primary cultures: Provide species, strain, sex of origin, genetic modification status.	Provided under material and methods, section "TCR-engineering of primary $CD4^+$ T cells", pages 17 – 18	

Experimental animals	indicate where provided: page no/section/legend)	n/a
Laboratory animals or Model organisms: Provide species, strain, sex, age, genetic modification status. Provide accession number in repository **OR** supplier name, catalog number, clone number, **OR** RRID.	Provided under material and methods, section "Mice", page 15	
Animal observed in or captured from the field: Provide species, sex, and age where possible.		n/a

Plants and microbes	indicate where provided: page no/section/legend)	n/a
Plants: provide species and strain, ecotype and cultivar where relevant, unique accession number if available, and source (including location for collected wild specimens).		n/a
Microbes: provide species and strain, unique accession number if available, and source.		n/a

Human research participants	indicate where provided: page no/section/legend) or state if these demographics were not collected	n/a
If collected and within the bounds of privacy constraints report on age, sex and gender or ethnicity for all study participants.		n/a

Design:

Study protocol	indicate where provided: page no/section/legend)	n/a
If study protocol has been pre-registered, provide DOI. For clinical trials, provide the trial registration number **OR** cite DOI.		n/a

Laboratory protocol	indicate where provided: page no/section/legend)	n/a
Provide DOI **OR** other citation details if detailed step-by-step protocols are available.		n/a

Experimental study design (statistics details)		
For in vivo studies: State whether and how the following have been done	**indicate where provided: page no/section/legend. If it could have been done, but was not, write not done**	**n/a**
Sample size determination		n/a
Randomisation	Mice were randomized on the day of adoptive TCR-T cell transfer. Described in material and methods, under "study design" page 15	
Blinding		n/a
Inclusion/exclusion criteria		n/a

Sample definition and in-laboratory replication	indicate where provided: page no/section/legend	n/a
State number of times the experiment was replicated in laboratory.	Each experiment was replicated at least twice, some even a third time. Number of replicates are included in figure legends, pages 33 – 36.	
Define whether data describe technical or biological replicates.	All data are biological replicates, described in "material and methods" section "statistics", page 23.	

Ethics	indicate where provided: page no/section/legend	n/a
Studies involving human participants: State details of authority granting ethics approval (IRB or equivalent committee(s), provide reference number for approval.		n/a
Studies involving experimental animals: State details of authority granting ethics approval (IRB or equivalent committee(s), provide reference number for approval.	Animal experiments were approved by The University of Chicago according to Institutional Animal Care and Use Committee (IACUC), included in material and methods, under "study design" page 15.	
Studies involving specimen and field samples: State if relevant permits obtained, provide details of authority approving study; if none were required, explain why.		n/a

Dual Use Research of Concern (DURC)	indicate where provided: page no/section/legend	n/a
If study is subject to dual use research of concern regulations, state the authority granting approval and reference number for the regulatory approval.		n/a

Analysis:

Attrition	indicate where provided: page no/section/legend	n/a
Describe whether exclusion criteria were preestablished. Report if sample or data points were omitted from analysis. If yes report if this was due to attrition or intentional exclusion and provide justification.		n/a

Statistics	indicate where provided: page no/section/legend	n/a
Describe statistical tests used and justify choice of tests.	Figure legends include which statistical tests were used, pages 33 – 36.	

Data availability	indicate where provided: page no/section/legend	n/a
For newly created and reused datasets, the manuscript includes a data availability statement that provides details for access or notes restrictions on access.	Materials and data availablility statement included on page 32	
If newly created datasets are publicly available, provide accession number in repository **OR** DOI **OR** URL and licensing details where available.	Sequencing data are deposited at Sequence Read Archive (SRA). Project ID for TCR-sequencing PRJNA1113628. Project ID for whole-exome-sequencing PRJNA1113704	
If reused data is publicly available provide accession number in repository **OR** DOI **OR** URL, **OR** citation.		n/a

Code availability	indicate where provided: page no/section/legend	n/a
For all newly generated custom computer code/software/mathematical algorithm or re-used code essential for replicating the main findings of the study, the manuscript includes a data availability statement that provides details for access or notes restrictions.		n/a
If newly generated code is publicly available, provide accession number in repository, **OR** DOI **OR** URL and licensing details where available. State any restrictions on code availability or accessibility.		n/a
If reused code is publicly available provide accession number in repository **OR** DOI **OR** URL, **OR** citation.		n/a

Reporting

MDAR framework recommends adoption of discipline-specific guidelines, established and endorsed through community initiatives. Journals have their own policy about requiring specific guidelines and recommendations to complement MDAR.

Adherence to community standards	**indicate where provided: page no/section/legend**	**n/a**
State if relevant guidelines (e.g., ICMJE, MIBBI, ARRIVE) have been followed, and whether a checklist (e.g., CONSORT, PRISMA, ARRIVE) is provided with the manuscript.	The ARRIVE guidelines were followed when animal experiments were described in material and methods, section “Study design” and section “Mice”, page 15. A checklist is not provided.	

		Days after cancer injection	Tumor volume #351-CPA11	#126-CPA17	#4846-#6-CPA22
		-1	0	0	0
		0			
		1			
		2			
		3			
		4			
		5			
		6		546	
		7			
		8			
		9		1056	
		10			1071
	Code CPA-11, CPA-17, CPA-22 and CPA-23 Outgrowth of 6132A-PRO 2.2 in wt mice	11		955	
		12			
Fig. 1A		13	273	2145	1495
		14			
		15		2754	
		16	189		2475
		17		3480	
		18			3536
		19	243		
		20			3627
		21	288		
		22			
		23	283		
		24			
		25			
		26	495		
		27			
		28	885		
		29			
		30			

Fig. 1B	Code CPA-17 FACS sort	Mouse #126	

		Mouse 1		
	Tumor		Spleen	
	TCR	Number	TCR	Number
	H6	31	H6	33
	H7	6	H7	13
		3	H13	8
		2		7
	H13	1		5

1	2
1	2
1	1
1	1
1	1
1	1
1	1
1	1
1	1
1	1
1	1
1	1
1	1
1	1
1	1
1	1
1	1
1	1
1	1
1	1
	1
	1
	1
	1
	1
	1
	1
	1
	1
	1
	1
	1
	1
	1
	1
	1
	1

Fig. 1C

Code CPA-11, CPA-17, CPA-22 and CPA-23 TCR frequency

Fig. 1D	Code CPA-11, CPA-17, CPA-22	Sequencing data available at SRA	Project number PRJNA1113628			
			Clone 1	Clone 2	Clone 3	
		Mouse 1				
		Mouse 2				
		Mouse 3				
		Mouse 4				
		Mouse 5+6	63		25	
						Spl
			Clone 1	Clone 2	Clone 3	
Fig. 1E	Code CPA-11, CPA-17, CPA-22 and CPA-23 T cell clonotype prevalence (%)	Mouse 1				
		Mouse 2				
		Mouse 3	80	20		
		Mouse 4				
		Mouse 5+6				
						Spl
			Clone 1	Clone 2	Clone 3	
		Mouse 1				
		Mouse 2				
		Mouse 3				
		Mouse 4				
		Mouse 5+6	100			

of each mouse		
#4854-#8-CPA220	#7752-CPA230	#7746-CPA230
	440	156
	504	456
	462	672
616	539	833
1400	864	1024
	1134	1140
2112		
	1540	1580
2244		
2925		

	Mouse 2				Mou
	Tumor		Spleen	Tumor	
TCR	Number	TCR	Number	TCR	Number
H6	41	H9	9	H9	8
H8	15		9	H10	5
	8		7		1
	8	H6	6		1
	6	H8	6		1

	5	4	1
	5	3	1
	3	3	1
	3	2	1
	3	2	1
	3	2	1
	3	2	1
	2	2	1
	2	2	1
	2	1	
	2	1	
	2	1	
	2	1	
	2	1	
	2	1	
	2	1	
	2	1	
	1	1	
	1	1	
H9	1	1	
	1	1	
	1	1	
	1	1	
	1	1	
	1	1	
	1	1	
	1	1	
	1	1	
	1	1	
	1	1	
	1	1	
	1	1	
	1	1	
	1	1	
	1	1	
	1	1	
	1	1	
	1	1	
	1	1	
	1	1	
	1	1	
	1	1	
	1	1	
	1	1	
	1	1	

1	1
1	1
1	1
1	1
1	
1	
1	
1	
1	
1	
1	
1	
1	
1	
1	
1	
1	
1	
1	
1	
1	
1	
1	

			H6			
Spleen						
	Clone 4	Clone 5	Clone 6	Clone 7	Clone 1	Clone 2
			100			
			100			
	21	79				
	12				60	19
			H9			
een						Tun
	Clone 4	Clone 5	Clone 6	Clone 1	Clone 2	Clone 3
	78	11	11			
				75	25	
						100
			H13			
een						Tun
	Clone 4	Clone 5	Clone 6	Clone 1	Clone 2	Clone 3
	75		25			
	61	39				
	100					
				53	35	12

ıse 3				Mouse 4			
Spleen		Tumor		Spleen		Tur	
TCR	Number	TCR	Number	TCR	Number	TCR	
H9	60		14	H14	99	H15	
H6	33	H10	14	H12	83	H6	
H13	28		14	H8	32	H16	
H10	27		14		21		
H11	27		14	H13	19	H13	

19	14	9	
11	14	7	
9		6	
8		6	
6		6	
4		5	
4		4	
2		3	
2		2	
2		1	
1		1	
1		1	
1		1	H9
1		1	
1		1	
1		1	
1		1	
1		1	
1		1	
1		1	
1		1	
1		1	
1		1	
1		1	
1		1	
1		1	
1		1	
1		1	
1		1	
1		1	
1		1	
1		1	
1		1	
1		1	
1		1	
1		1	
1		1	
1		1	
1		1	
1		1	
1		1	
1		1	
1		1	
1		1	
1		1	

1
1
1
1
1

1
1
1
1
1
1
1
1
1
1
1
1
1
1
1
1
1
1
1
1
1
1
1
1
1
1
1
1
1
1
1
1
1
1
1
1
1
1
1
1
1
1
1
1
1

	Tumor			
Clone 3	Clone 4	Clone 5	Clone 6	Clone 7
	3		94	3
			100	
18	3			
nor				
Clone 4	Clone 5	Clone 6		
100				
nor				
Clone 4	Clone 5	Clone 6		
100				

Mouse 5+6			
nor		Spleen	
Number	TCR	Number	
124	H6	57	
103	H16	21	
98		10	
35		6	
17		6	

12	H13	5
11		4
8		2
7		2
5		2
4		2
3		2
3		1
3		1
3		1
3		1
3		1
3		1
2		1
2		1
2		1
2		1
2		1
2		1
2		1
2		1
1		1
1		1
1		1
1		1
1		1
1		1
1		1
1		1
1		1
1		1
1		1
1		1
1		1
1		1
1		1
1		1
1		1
1		
1		
1		
1		
1		
1		
1		
1		

1
1
1

1
1
1
1
1
1
1
1
1
1
1
1
1

Fig. 2A Treatment overview

Days after T cell transfer	#609	#851	T(
-26			0
-25			
-24			
-23			
-22			
-21			0
-20	0		
-19			
-18			9
-17			
-16			28
-15	0		
-14			
-13			
-12	8		72
-11			
-10			
-9	63		126
-8			
-7	84		160
-6			
-5	189		200
-4			
-3			360
-2	350		
-1			
0	500		700
1			
2	768		
3			1365
4			
5	1425		
6			1365
7	1215		
8			
9	997		643
10			
11			
12	540		572
13			

		14	325	
		15		480
		16	300	
		17		
		18		390
		19	247	
		20		
		21	144	300
	Treatment	22		
Fig. 2B	in C3H Rag	23	160	390
	2-/- Mice	24		
		25		248
		26	180	
		27		
		28	225	220
		29		
		30		
		31	202	144
		32		
		33		
		34	192	
		35		192
		36		
		37	283	
		38		162
		39		
		40	192	
		41		175
		42		
		43	168	195
		44		
		45		
		46		180
		47	360	
		48		260
		49	160	
		50		
		51	160	577
		52		
		53		462
		54	140	
		55		728
		56	180	
		57		784
		58	160	

59		
60		832
61	160	
62		
63		1008
64	140	
65		
66	192	
67		
68	192	
69		
70	192	
71		
72	140	
73		
74		
75	160	

		TCR H7, CRA-
Days after T cell transfer	6903	Mou 6950
-26		
-25		
-24		
-23		
-22	0	0
-21		
-20		
-19		
-18		
-17		
-16		
-15		
-14	12	12
-13		
-12		
-11		
-10	28	28
-9		
-8		
-7	54	42
-6		
-5	132	54
-4		
-3	144	100
-2		

		-1		
		0	227	210
		1		
		2		
		3	367	273
		4		
		5		
		6		
		7	512	364
		8		
		9	535	367
		10		
		11	680	409
		12		
		13		
		14	836	472
		15		
		16	891	577
		17		
		18	912	918
		19		
		20		
		21		
		22	960	1071
		23		
		24		
Fig. 2C	Treatment in C3H Rag 2-/- Mice	25	1170	1470
		26		
		27		
		28	1228	1485
		29		
		30	1430	2024
		31		
		32	1800	
		33		
		34		
		35		
		36		
		37		
		38		
		39		
		40		
		41		
		42		
		43		

				44
				45
				46
				47
				48
				49
				50
				51
				52
				53
				54
				55
				56
				57
				58
				59
				60
				61
				62
				63
				64
				65
				66
				67
				68
				69
				70
				71
				72
				73
				74
				75
				76
				77
				78
				79
				80
Fig. 2D	Code CPA-11, CPA-17,	Sequencing data	Project number PRJNA1113628	
		TCR	Mouse	Death after T cell transfer
			6963	91
			6962	69
		H13 Code:	6961	91
		CRA-67,	6960	69
		CRA-69,	6959	52

Fig. 2E	Survival overview	CRA-70	7902	102
			6993	75
			6991	124
			7993	98
		H9 Code: CRA-58, CRA-61	7985	70
			7984	108
			7982	115
			7980	98
			609	125
		H6 Code: CRA-3, CRA-12, CRA-14	851	63
			834	57
			37	69
			45	72
			167	72
			7996	32
		H12 Code: CRA-58, CRA-61	7990	98
			7969	95
			7965	112
			7957	112
			7933	29
		H11 Code: CRA-58, CRA-65, CRA-70	7997	35
			7989	28
			7937	38
			7095	30
			7094	75
			7092	48
			6976	32
		H14 Code: CRA-72, CRA-73	7099	52
			7046	91
			7039	93
			7038	93
			7091	28
			7090	48
		H15 Code: CRA-72, CRA-73	6977	69
			7045	74
			7041	46
			7040	44
			7100	41
			7098	94
		H16 Code: CRA-72, CRA-73	7089	97
			7044	98
			7043	98
			7042	93
			6903	32
		H7 Code: CRA-65	6950	30

CRA-65, CRA-67	7906	33
	7905	33
H8 Code: CRA-65, CRA-67	7921	25
	6934	28
	7923	32
H10 Code: CRA-58, CRA-65	6901	49
	6902	25
	7995	21
	7987	21
12.2 Code: CRA-48, CRA-49, CRA-65	7922	27
	4779	27
	4776	25
	4778	19
	4767	21
Outgrowth Code: CRA-12, CRA-13 CRA-49, CRA-65	36	14
	878	12
	881	14
	4777	21
	6949	27
	7920	24
	7935	24

	Mouse	Death after T cell transfer
H13 Code: CRA-67, CRA-69, CRA-70	6963	91
	6962	69
	6961	91
	6960	69
	6959	52
	7902	102
H9 Code: CRA-58, CRA-61	6993	75
	6991	124
	7993	98
	7985	70
	7984	108
	7982	115
	7980	98
H6 Code: CRA-3, CRA-12, CRA-14	609	125
	851	63
	834	57
	37	69
	45	72
	167	72
H12 Code:	7996	32
	7990	98

Fig. 2F	Relapse after T cell transfer	CRA-58, CRA-61	7969	95
			7965	112
			7957	112
		H11 Code: CRA-58, CRA-65, CRA-70	7933	29
			7997	35
			7989	28
			7937	38
			7095	30
			7094	75
		H14 Code: CRA-72, CRA-73	7092	48
			6976	32
			7099	52
			7046	91
			7039	93
		H15 Code: CRA-72, CRA-73	7038	93
			7091	28
			7090	48
			6977	69
			7045	74
			7041	46
		H16 Code: CRA-72, CRA-73	7040	44
			7100	41
			7098	94
			7089	97
			7044	98
			7043	98
		H7 Code: CRA-65, CRA-67	7042	93
			6903	32
			6950	30
			7906	33
			7905	33
		H8 Code: CRA-65, CRA-67	7921	25
			6934	28
			7923	32
		H10 Code: CRA-58, CRA-65	6901	49
			6902	25
			7995	21
			7987	21

CR H6, Code CRA-2, CRA-3, CRA-12, CRA-14

Mouse				
#834	#037	#045	#167	#4779
0				
	0	0	0	0
0				
	0	0	0	
9				
	0	4	0	0
15				
	4	6	4	4
	16	20	16	
42				
	45	37	45	
				84
62				
	90	70	125	
90				
	120	108	157	144
240				
	351	175	210	
384				283
	324	231	352	
715	539	416	480	455
	600	540	567	
1456				
	864	660	770	546
1456	1040	832	960	728
	840	660	810	784
840				
	693	351	650	
				892
540	572	192	396	
				1008

480	315	120	396	998
484	264	132	280	1050
484	315	105	270	1280
480	270	105	210	1496
462	300	81	210	1890
420	200	72	112	2070
330	200	72	175	
	160	54	120	
297	200	36	140	
300	200		157	
270	225	36	144	
252	180	36	175	
270	200	16	175	
243	108	16	135	
	160	16	135	
202	154	16	135	
243	140	16	135	
160				
144	220	16	112	

	175	16	112	
	175	16	112	
	260	16	231	
		30	120	

-65, CRA-67			TCR H8, CRA-65, CRA-67	
use			Mouse	
7906	7905	7921	7922	7923
		0	0	0
0	0			
0	0	20	20	20
16	16			
16	20	52	37	20
25	45	100	87	30
		144	120	42
157	60	216	168	56

252	269	336	210	140
273	384	459	283	192
441	408			
540	468	731	550	288
675	630	731	600	280
825	700	1092	605	308
960	900	1092	605	264
1072	990	1449	780	420
1260	1144	1449	792	420
1350	1248	1989	1080	576
1402	1456			
1768	1456	2772	1092	624
1878	1638		1352	910
				910
				1125
	2793			

Convergent TCR	Convergent elements	Non-Convergent	No treatment	
1				
1				1 - High tumo
1				0 - Neither hig
1				
1				

0
1
0
0
0
0
0
1
0
1
0
0
0
0

0
0
0
0
1
1
1
0
0
1
1
0
1
0
0
0
1
1
1
1
1
1
1
1
0
1
0
0
1

1
1

		1		
		1		
		1		
		1		
		1		
		1		
		1		
		1		
		1		
			1	
			1	
			1	
			1	
			1	
			1	
			1	
			1	
			1	
			1	
			1	
			1	

Relaspe defined as tumor growth in 3 consecutive measurrements		D40 Convergent TCRs	D40 Converegent elements	D40 Non-Convergent
Relapse Day 40	Relapse Day 80			
No	No	0/19	10/24	11/11
No	Yes	0	41.7	100
No	Yes			
No	Yes	D80 Convergent TCRs	D80 Converegent elements	D80 Non-Convergent
No	Yes			
No	No	6/19	13/24	11/11
No	Yes	31.5	54.2	100
No	No			
No	No			
No	No			
No	No			
No	No			
No	No			
No	No			
No	Yes			
No	No			
No	No			
No	No			
No	No			
No	No			
No	No			

No	No
No	No
No	No
Yes	Yes
Yes	Yes
Yes	Yes
/	/
/	/
No	Yes
Yes	Yes
/	/
Yes	Yes
No	No
No	No
No	No
Yes	Yes
Yes	Yes
No	Yes
No	Yes
Yes	Yes
Yes	Yes
Yes	Yes
/	/
/	/
No	No
No	No
No	No
Yes	Yes
Yes	Yes
Yes	Yes
Yes	Yes
Yes	Yes
Yes	Yes
Yes	Yes
Yes	Yes
Yes	Yes
Yes	Yes

amL26, CRA-48, CRA-49			No treatment, CRA-12, CRA-13, CRA-49			
Mouse			Mouse			
#4776	#4778	#4767	#036	#878	#881	#4777
	0	0	0	0	0	
0						0
			0			
				0	0	
	0	0	4			
0				4	4	0
	4	4	6			
4				20	20	4
			28			
			30	30	25	
	64	63				
28				30	30	54
			120			
				60	45	
	160	168	220			
175				122	70	140
			315			
	288	315		192	189	
285			616			364
				315	315	
	378	392	792	315	350	
630	490	504				441
			1300			480
				528	572	
	676	510	1470			
805				624	1080	720
	819	756	2145			
966						816
	1008	864	2242			
1104				1170	1500	936
			2400			
	1275	980	2448			
1288				1309	2431	1064
	1615	1176		1568		
1440						1280

	1805	1200	3000	2808	
1500					1964
	1976	1472			
1560					2346
	2457	1920			
2016					2925
		2592			2592
2240					
2610					

	TCR H9, CRA-58, CRA-61 Mouse					TCR H10, CRA Mou	
7993	7985	7984	7982	7980	6901	6902	
					0	0	
0	0	0	0	0			
12	12	20	20	20	12	12	
18	20						
		20	20	25	52	20	
45	63						
120	140	36	40	63	120	52	
					157	126	
156	324						
		90	182	189	192	157	

315	525	168	360	283	192	175
448	600	224	432	320	192	269
720	816	350	648	486		
432	825	283	665	486	280	318
294	375	112	540	315	210	318
227	234	73	318	192	169	318
210	210	54	315	112	231	343
224	180	45	192	112	336	480
227	162	45	168	72	308	600
245	148	20	140	60	352	648
227	121					
224	144	20	120	60	396	769
208	132	20	72	45	526	
					600	
208	132				650	
252	148	20	72	45		
350	162	20	54	45		

350	162			
280	198	25	54	45
300	195	25	54	45
300	195	25	54	45
300	195	30	54	60
300		30	54	60

r burden or relapse when died
gh tumor burden nor relapse when died

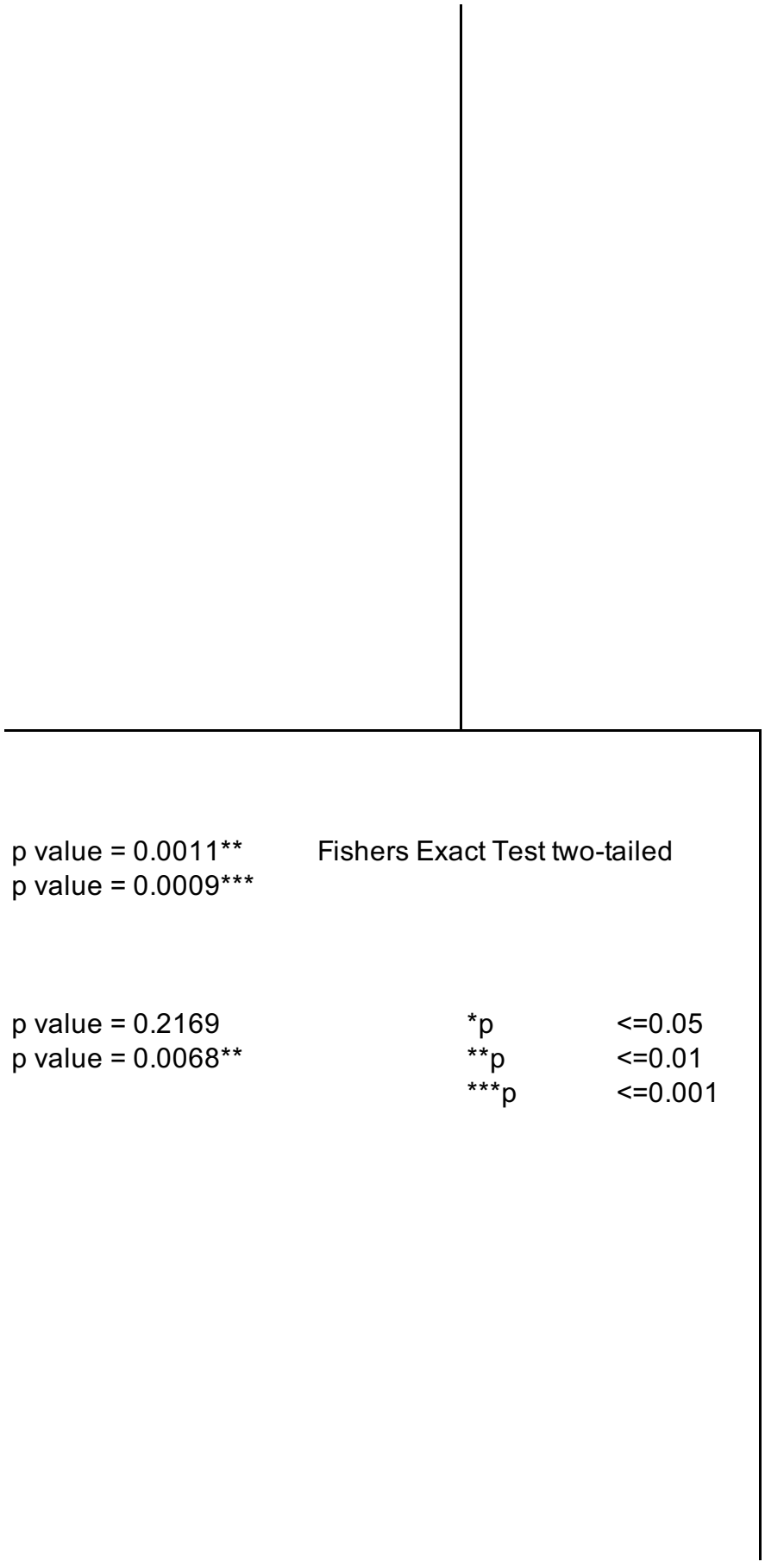

p value = 0.0011** Fishers Exact Test two-tailed
p value = 0.0009***

p value = 0.2169 *p <=0.05
p value = 0.0068** **p <=0.01
***p <=0.001

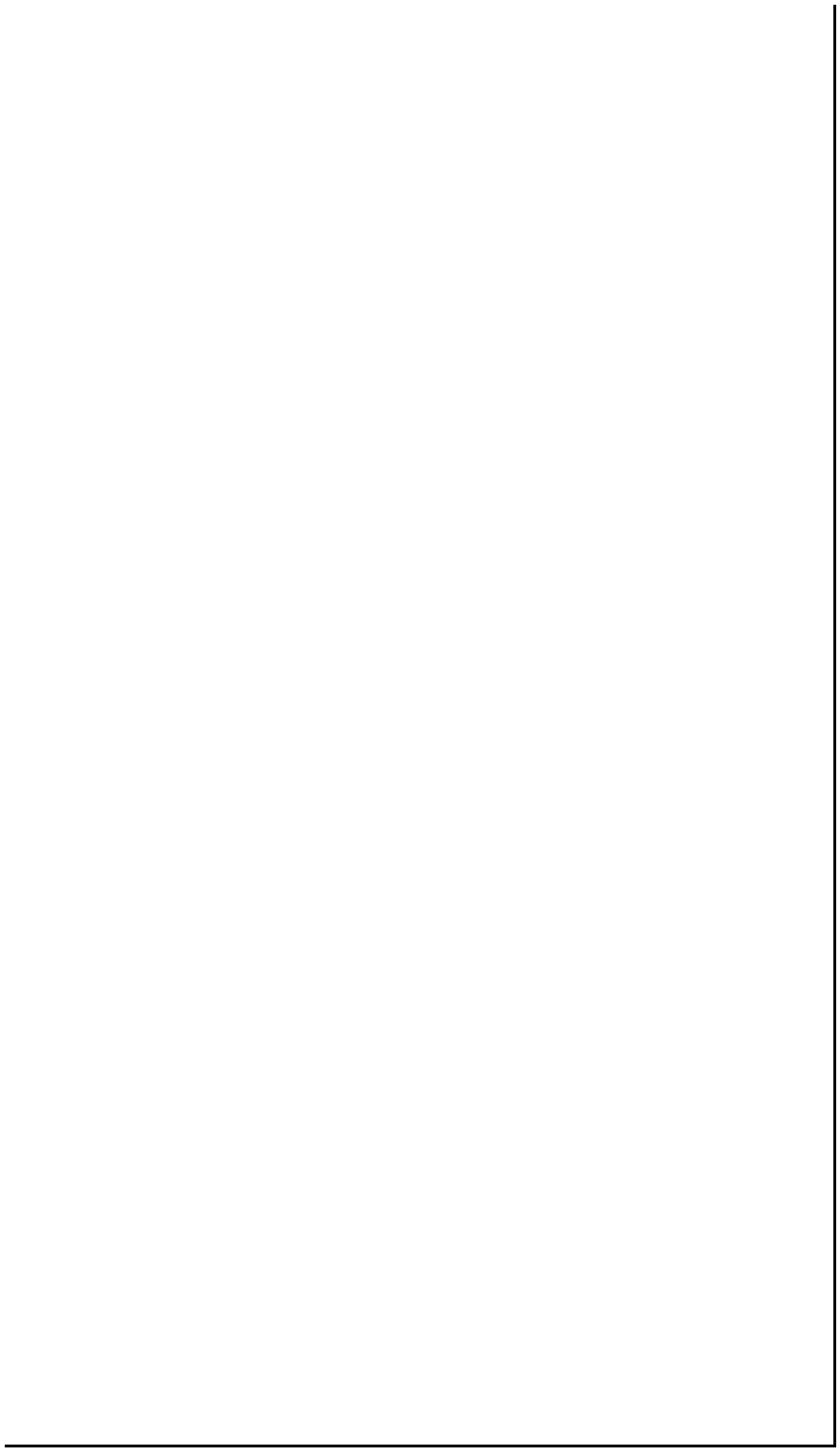

A-58, CRA-65			TCR H11, CRA-58, CRA-65, CRA-70			
use			Mouse			
7995	7987	7933	7997	7989	7937	7095
0	0	0	0	0	0	0
12	12	20	12	12	20	0
28	30	56	24	20	36	42
112	126	63	100	90		
157	160	100	108	140	100	137
324	360	125	200	283	112	216
		180			192	

528	500	252	560	484	240	273
702	637	392	630	660	409	318
810	877		792	858		318
910	1260	416	864	929	350	367
847	1275	360	440	756	208	294
1170	1275	346	346	648	192	273
1365	1350	280	325	756	192	252
1456	1530	283	300	756	270	231
1530	1683	256	363	929	216	210
2340	1938	360	462	1170	216	198
			495	1237		198
		605	648	1768	176	
		780	648	1912	216	292
		858			234	252
			780		216	
			1040			
					216	

TCR H12, CRA-58, CRA-61 Mouse						
7094	7996	7990	7969	7965	7957	6963
						0
0	0	0	0	0	0	
0						
	12	12	20	20	20	12
30	28	54				
						120
			20	20	20	
	60	154				135
70						
	132	192	20	40	45	180
196						
	180	300				231
			96	132	112	
252						392

320	472	588	157	252	270	560
432	600	672	216	312	350	720
486	792	960	315	455	441	891
600	526	1008	264	441	432	1080
360	468	660	200	364	220	792
280	360	660	157	210	135	768
243	260	490	126	120	157	600
112	240	455	96	126	112	392
94	240	490	96	126	112	294
84	220	455	70	112	80	351
108	240	455				308
	240	455	60	70	80	378
96	275	440	60	70	80	378
94						
108	240	385				312
		297	54	54	36	351
162						336
		297	20	20	28	292

315	297				275
	264	20	20	28	225
423					225
	250	20	20	28	200
546					202
819	240	20	20	28	250
980					250
	240	20	25	35	
1232					300
	264	30	25	35	360
					363

TCR H13, CRA-67, CRA-69, CRA-70

Mouse

6962	6961	6960	6959	7902	6993	6991
0	0	0	0			
				0	0	0
					0	0
18	13	13	12	0		
				16	30	30
63	45	189	180			
				24		
63	67	210	252			
					80	54
63	96	164	273	45		
					231	140
150	135	409	409			
				180		
234	252	585	441		336	189

294	280	630	748	294	378	280
				420	455	352
297	283	720	972			
				544	572	585
598	462	936	1134		780	585
598	480	936	1170	480		
				315	468	154
306	308	616	768			
				252	360	126
270	240	624	577			
					252	105
187	270	500	616	210		
				180	252	81
154	180	400	576			
				110	280	105
112	126	288	390			
					220	94
135	189	455	462	108		
				48	308	94
140	202	423	462			
				48		
156	202	504	420			
					308	94
135	240	420	385	48		
					308	94
196	202	462	423		264	94
192	247	360	500	27		
210	243	420	462			
				48	308	94
280	275	462	507			

280	225	396	637	18	378	84
384	225	396	784			
336	350	396	1020	27	539	84
416	346	325		31		
392	330	325		7 2	660	84
535	330	504		2	900	84
855	385	637			1215	84
1039	420	936		15	1920	84
	773			15		
	952					

TCR H14, CRA-72, CRA-73 Mouse						
7099	6976	7092	7046	7039	7038	6977
0	0	0				0
			0	0	0	
16	16	20				16
42	28	36	0	0	0	20
147	122	144				48
245	220	288	108	220	45	140
350	315	409				196
440	346	567	175	392	94	210

585	420	630	336	598	157	346
624	468	880	336	760	245	440
780	693	1248	336	960	336	560
675	616	1028	504	1056	409	462
720	616	840	378	918	220	420
594	420	756	378	660	264	324
440	484	660	315	704	264	220
600	346	756	280	660	231	240
468	346	756	210	468	140	105
384	308	756	157	441	126	105
350	346	847	140	336	54	105
810	420	810	96	200	36	120
896	308	810	70	100	28	120
			52	75	8	
			24	75	8	
			8	90	4	
1020		975	8	35	4	220

		8	50	2	
1309	1878				240
		20	234	20	
1530					357
					325
		20	80	16	
					588
					350
					350
		20	80	16	
					350
					588
					819
		20	28	16	
		16	28	16	

TCR H15, CRA-72, CRA-73

Mouse

7090	7091	7045	7041	7040	7098	7100
0	0				0	0
		0	0	0		
20	20				16	16
36	49				24	20
		0	0	0		
120	192				84	132
168	364	231	36	245	192	409
220	409				210	455
252	526	231	100	294	420	490

350	742	336	196	472	504	600
455	825	416	196	472	665	880
560	1215	540	224	504	731	1235
700	900	441	320	595	960	1134
535	1056	318	288	567	425	1400
337	864	409	252	476	440	1105
337	1071	288	360	476	126	940
255	884	192	252	476	156	880
306	1071	192	360	476	136	1026
240	1309	168	450	416	120	1053
405	1980	175	432	476	94	1358
450	2244	308	495	630	94	1330
540		247	540	450	84	1824
		157	786	540		
		135	700	749		
		135	924	749		
912		112	1070	1092 1232	84	2016

112 1232 1485

1530

1540 84

245

30

6

396

2

1

1

432

1

1

520

4

616

4

TCR H16, CRA-72, CRA-73 Mouse			
7089	7044	7043	7042
0			
	0	0	0
16			
28			
	0	0	0
147			
280	192	105	157
280			
396	352	280	245

495	432	441	294
594	526	490	364
594	630	630	600
840	643	405	337
780	409	280	292
780	297	210	168
572	225	160	168
594	180	90	154
643	126	90	154
378	94	52	115
315	63	30	94
315	36	36	105
378	30	20	70
	4	6	31
	2	6	70
	2	4	33
385	2	2	44

2	2	40
4	4	192
4	4	192
4	4	192
4	4	216
16	4	234

Fig 3A	Code WI-8	Mouse #7517			
				Cancer area	
		Mouse	Day 4	Day 5	Day 6
Fig 3B	Code WI-7 and WI-8	#594	100	32,08	25,08
		#591	100	20,46	20,49
		#578	100	55,13	26,64
		#7517	100	13,87	15,06
		#7247	100	30,26	13,48
		#7510 (control)	100	58,8	120,92
Fig. 3C	Code CRA-39 and CRA-42 Dead endothelial cells		H6	12,2	
			26,8	4,35	
			13,9	4,8	
			20,3		
			14,5		
			32,1		
			15,5		
			31,8		
Fig. 3D	Code CRA-39 and CRA-42 IFNg in ng/mg	Analyzed in MA-18	H6	12,2	
			6,49	0,72	
			6,49	0,06	
			2,28	0,84	
			8,61		
			9,60		
			1,86		
			1,57		
			6,23		
Fig. 3E	Code CRA-39 and CRA-42 TNF in ng/mg	Analyzed in MA-18	H6	12,2	
			2,13	0,94	
			3,82	0,57	
			2,2	0,64	
			3,28		
			3,71		
			1,41		
			1,44		
			3,71		
		Mouse	Treatment	Cell type	BrdU %
		#7945	12,2	Cancer cell	11
				TAM	/
				T cell	19,4
		#7943	No treatent	Cancer cell	49,7
				TAM	/
		#7938	12,2	Cancer cell	54,6
				TAM	/
				T cell	58,8

Fig. 3F and 3G	Code CRA-52 for 3F, CRA-63, CRA-56 and CRA-52 BrdU and cleaved Caspase 3 for Fig. 3G	#7947	No treatment	Cancer cell TAM T cell	54,2 / 14,9
		#7977	H6	Cancer cell TAM T cell	4,94 / 1,01
		#7978	H6	Cancer cell TAM T cell	2,93 / 5,71
		#7942	H6	Cancer cell TAM T cell	23,4 / 23,4
		#7841	12,2	Cancer Cell TAM T cell	38,1 / 27,9
		#7840	No treatment	Cancer Cell TAM T cell	6,99 / 7,17
		#4720	12,2	Cancer Cell TAM T cell	0,3 / 8,98
		#4719	H6	Cancer Cell TAM T cell	8,98 / 5,71
		#4718	No treatment	Cancer Cell TAM T cell	5,71 / 6,25

		TUNEL negative		TUNEL positive	
		H6	amL26	H6	amL26
Fig 3H and 3I	Code CRA-77 for 3H and CRA-53 for Fig. 3I	411	392	2	4
		351	410	3	5
		542	385	5	5
		508	493	6	7
		531	473	0	5
		424	463	3	6
		548	388	4	8
		451	407	4	5
		471	298	1	3
		406	283	3	3
		430	343	3	6
		382	284	1	2
		427	352	4	4
		493	354	3	6
		390	361	6	0
		373	356	1	5

		Days after cancer injection	#4704	#4724 w/o	#4723
		-48	0	0	0

-47			
-46			
-45			
-44			
-43			
-42			
-41	4	4	4
-40			
-39			
-38			
-37			
-36			
-35	9	4	4
-34			
-33	18	4	15
-32			
-31			
-30			
-29			
-28	18	4	21
-27			
-26			
-25			
-24	20	4	21
-23			
-22			
-21			
-20			
-19			
-18			
-17	67	4	54
-16			
-15			
-14	126	4	98
-13			
-12			
-11			
-10	175	20	200
-9			
-8			
-7	240	67	288
-6			
-5	364	108	364
-4			
-3			

		-2			
		-1			
		H6-T cell transfer	640	245	704
		1			
		2	720	308	792
		3			
		4	918	441	891
		5			
		6			
		7	378	572	720
		8			
	Code CRA-47 and CRA-55	9	220	630	560
Fig. 3J	Treatment of 6132A MHC	10			
	II KO	11	270	693	315
		12			
		13			
		14	84	1120	220
		15			
		16	140	1386	192
		17			
		18	154	1584	168
		19			
		20			
		21	96	2194	120
		22			
		23	52		99
		24			
		25			
		26			
		27			
		28	67		90
		29			
		30			
		31			
		32	67		82
		33			
		34			
		35	67		81
		36			
		37			
		38			
		39			
		40			
		41			
		42			105

	43	
	44	
	45	
	46	
	47	94
	48	
	49	
	50	94
	51	
	52	
	53	
	54	
	55	
	56	
	57	
	58	81
	59	
	60	
	61	
	62	
	63	
	64	
	65	81
	66	
	67	81
	68	
	69	
	70	

Vessel area		
Day 4	Day 5	Day 6
100	15,66	9,77
100	57,59	36,09
100	67,69	60,24
100	38,04	21,46
100	66,58	58,92
100	107,17	104,28

cCsp3 %
0,1
0,08
/
0,2
0,04
1,62
0,003
/

0,24
0,002
24,1
7,09
/
27,3
1,41
/
14,1
5,21
/
1,87
6,54
/
0,93
1,79
13,5
2,09
/
49,9
10,4
/
7,64
0,84

Tumor volume of each mouse						
#4722	#4721	#7853	#7852	#7851	#7850 w/o	#7849
0	0					

4	4	0	0	0	0	0
4	4	0	0	0	0	0
4	9					
		12	12	12	12	12
4	20	16	20	25	16	24
4	20	20	30	25	20	24
		20	30	25	28	24
20	45					
28	80					
112	192	45	147	98	90	140
140	283	105	224	189	120	198
200	315	144	283	269	162	308
		196	400	432	262	468

500	742	320	420	630	384	715
539	810	484	462	675	540	1008
756	972	594	616	1050	630	1436
480	480	480	504	780	800	924
224	346	252	360	360	968	715
140	243	300	360	330	1320	526
98	175	168	225	216	1925	495
84	140	162	200	150		450
84	157	120	200	175		400
42	144	112	154	165		378
42	175					
		54	140	150		175
35	120	72	132	135		210
35	200					
42	150		140	175		150
42	150		140	180		84

	240	
36		
	100	108
36		
	100	80
	100	90
		108

Fig. 4A	mL9 and wtL9 peptide stimulation	Relative IFN-g release (%)	Concentration in (nM)		
			mutant L9 (L9)		H6, Code T-33, T-36
			None	11,8	14,8
			0,001	30,2	38,7
			0,01	39	26,5
			0,1	50,6	48,7
			1	82,5	79,8
			10	100,7	93
			100	100,8	96,1
			1,000	101,5	92,6
			10,000	94,2	93,6
			wild type L9 (wtL9)		H6, Code T-33, T-36
			None	6	1,6
			0,001	4	4
			0,01	7,4	6,8
			0,1	8,2	12
			1	12	10,4
			10	6,3	7,6
			100	6,7	6,7
			1,000	4	10,3
			10,000	12,5	11,3
			Concentration in (nM)		
			TNF		H6, Code R-35
			None	2	1
			0,001	2	1
			0,01	2	2
			0,1	3	1
			1	5	3
			10	15	10
			100	19	23
			1,000	18	21
			10,000	17	18
			IL-2		H6, Code R-35
			None	4	3
			0,001	3	2
			0,01	3	3
			0,1	3	2
			1	5	3
			10	17	9
			100	27	33
			1,000	30	39
			10,000	29	36

			IL-4		H6, Code R-35
			None	1	1
			0,001	0	1
			0,01	1	1
			0,1	1	2
			1	2	5
			10	8	7
			100	19	18
			1,000	29	16
Fig. 4B	mL9 peptide stimulation	Relative Cytokine release (%)	10,000	30	9
			IL-10		H6, Code R-35
			None	3	3
			0,001	2	4
			0,01	2	4
			0,1	3	3
			1	9	4
			10	24	10
			100	27	16
			1,000	26	15
			10,000	28	15
			IL-17		H6, Code R-35
			None	1	2
			0,001	1	2
			0,01	1	2
			0,1	2	4
			1	3	7
			10	9	16
			100	12	40
			1,000	16	40
			10,000	15	58
			IL-22		H6, Code R-35
			None	2	6
			0,001	2	2
			0,01	1	6
			0,1	2	6
			1	5	15
			10	16	29
			100	14	49
			1,000	16	43
			10,000	18	46
	TCR signaling MFI			H6	H

Fig. 4C	of pERK after stimulation with either mutant L9 (mL9 or wild type L9 (wtL9) peptide	Experiment #1 #2	wtL9 720 0	L9 3237 499	wtL9 148 197
Fig. 4D	mutant L9 (mL9) and wild type L9 (wtL9) peptide stimulation of TCR-engineered 58 cells	Relative IL-2 release (%)	Concentration in (nM) mutant L9 (L9) None 0,001 0,01 0,1 1 10 100 1,000 10,000 wild type L9 (wtL9) None 0,001 0,01 0,1 1 10 100 1,000 10,000	 0 0 0 0 7 37 52 56 43 0 0 0 0 0 0 1 0 1	H6, Code 0 0 0 0 3 33 52 46 46 H6, Code 1 0 0 0 0 0 1 1 1

		Convergent TCRs				
, R-34		H9, Code T-33, T-36			H13, Code T-36, R4-34	
9,6	26,4	6,1	7,2	12	4	2
24	0,9	13,5	74,2	20	7	10
19,4	6	2,6	13,1	36	8	13
66,3	5,2	5,2	11,9	42	22	13
101,6	4,2	9,9	20,6	95	39	32
133,1	25,6	64,4	56,2	111	77	70
112,9	75,3	82,6	132,7	103	84	80
108,9	89	90,3	84	106	79	82
107,9	94,7	103,5	81,9	108	96	81

, R-34		H9, Code T-33, T-36			H13, Code T-36, R4-34	
26,4	0	3,8	1,6	9	3	1
14,9	2,1	6,4	7	35	5	7
10,7	0	2	34,1	19	8	9
11,1	0	4,8	5,6	5	4	6
17,8	0	4,6	30,6	65	9	9
27,2	5,1	6,1	4	6	8	6
63	10	1,3	18,4	9	5	7
9,3	0	2,8	8,2	10	9	14
20,9	9,6	3,7	4,7	1	6	3

		Convergent TCRs				
		H9, Code R4-35			H13, R4-35	
1	6	2	2	3	2	2
1	7	1	1	3	4	3
1	5	1	1	4	3	3
1	6	1	1	4	5	3
3	6	3	1	9	7	6
9	6	6	4	16	16	12
19	7	9	6	22	22	22
26	13	10	9	23	31	30
20	13	14	9	22	27	22

		H9, Code R4-35			H13, R4-35	
3	3	2	2	4	4	3
3	2	1	2	2	13	10
2	3	1	1	3	9	11
2	3	2	1	3	13	11
3	3	3	1	11	14	14
11	4	6	4	29	28	21
30	6	9	5	43	58	47
48	13	13	8	49	79	74
35	12	15	8	42	62	52

		H9, Code R4-35			H13, R4-35	
1	0	0	0	0	1	1
1	0	0	0	0	2	1
1	0	0	0	0	1	1
2	0	0	0	0	2	2
4	0	1	0	1	4	3
11	1	1	1	2	7	4
11	1	2	1	4	14	10
13	3	2	1	6	24	20
12	4	3	2	5	18	15

		H9, Code R4-35			H13, R4-35	
3	1	1	1	1	2	2
3	2	1	0	1	4	2
2	1	1	1	1	3	2
2	1	1	0	2	5	5
5	1	3	1	19	18	10
12	5	4	3	40	75	41
17	9	8	5	33	93	62
23	15	10	8	41	88	85
20	20	18	10	31	57	45

		H9, Code R4-35			H13, R4-35	
1	1	1	0	1	0	0
1	1	0	0	1	0	0
1	1	0	0	1	0	0
1	1	0	0	1	1	0
5	2	2	1	6	3	2
11	4	4	3	11	6	5
25	6	7	5	15	16	11
55	10	10	10	24	37	22
40	8	21	11	19	29	16

		H9, Code R4-35			H13, R4-35	
2	2	1	0	1	4	2
2	4	0	0	1	11	3
2	4	0	0	1	3	3
3	2	1	0	2	9	3
12	2	5	2	9	35	6
26	4	7	5	22	60	27
40	11	16	10	21	92	29
55	18	21	25	25	100	49
39	12	45	22	16	55	17

9	H13	H11	H12

L9	wtL9	L9	wtL9	L9	wtL9	L9
446	243	606	12	1074	226	2137
338	0	464	0	674	383	1650

			Convergent TCRs			
Γ-54, T-55			H9, Code T-49, T-54			
0	0	0	0	0	0	5
0	11	0	0	0	0	0
1	3	0	0	0	0	1
0	1	0	0	0	0	0
0	1	0	0	0	0	0
0	4	0	0	0	0	4
29	46	0	0	0	0	25
70	74	0	0	0	0	56
84	100	0	0	0	0	89
Γ-54, T-55			H9, Code T-49, T-54			
0	0	0	0	0	0	0
0	0	0	0	0	3	0
0	0	0	0	0	0	0
0	0	0	0	0	0	24
0	0	0	0	0	0	0
0	0	0	0	0	0	0
0	0	0	1	0	0	0
0	0	1	0	0	0	0
0	0	0	0	0	0	0

						Single clonoty
H11, Code T-33, T-36, R4-34			H12, Code T-33, T-36			H14 C
9,6	19	4	7,6	12,9	40	4
13,7	14,2	18,5	4,4	2,1	56,8	25
20,5	19,2	11	3,6	2,9	46,8	2
24,5	26,7	24,9	32,7	35,3	28,6	21
53,1	157,8	67,9	58,4	52,4	107,6	59
121,3	94,5	119,8	76,3	116	136,5	88
89,6	93,7	112,6	75,4	91	187,1	93
128,9	88,2	116,1	76,3	98,7	106,3	92
91,5	94,7	114,4	75,2	87,6	102,7	116

H11, Code T-33, T-36, R4-34			H12, Code T-33, T-36			H14 C
6	25,2	14,5	19,7	4,8	24	0
9	15,6	0,3	11,5	4,7	39,7	0
10	29,3	3,7	8,2	0	17,1	0
5	26,3	1,3	13,9	9,3	12,2	1
9	26,5	1,7	8,2	3,1	14,3	0
5	27,4	5,7	10,9	19,6	16,2	0
7	24,6	0,2	12,5	11	14,2	0
8	66,9	0,3	15,7	9,5	22,3	0
12	45,7	1,3	14,1	7,8	18,3	0

	H11, Code R4-35			H12, Code R4-35		
3	2	2	2	1	1	3
2	1	1	1	0	0	3
2	2	1	1	0	0	3
3	2	1	1	1	0	4
7	4	3	3	2	1	10
15	14	11	9	8	3	20
24	23	31	17	16	11	27
23	24	36	18	22	15	25
24	24	31	21	18	13	23

	H11, Code R4-35			H12, Code R4-35		
7	1	1	5	3	3	8
6	1	1	6	1	1	5
7	1	1	5	1	1	6
6	1	1	4	1	1	7
7	1	1	4	2	2	6
18	3	4	12	9	4	18
42	13	19	27	26	18	52
49	17	27	30	34	25	56
50	18	26	34	29	22	49

	H11, Code R4-35			H12, Code R4-35		
1	1	0	1	0	0	1
1	1	0	1	0	0	1
1	1	0	2	0	0	1
1	1	0	1	0	0	2
2	1	1	2	1	0	3
6	3	1	8	2	1	12
12	3	4	32	6	2	100
16	4	5	55	8	4	100
17	7	7	62	8	4	100

	H11, Code R4-35			H12, Code R4-35		
7	5	4	8	3	3	9
9	4	2	9	1	1	7
7	4	3	12	1	1	5
13	6	2	11	2	1	14
20	9	5	19	7	4	28
41	16	11	36	21	9	45
51	20	33	52	32	22	68
51	18	34	49	39	26	53
60	22	34	54	35	24	56

	H11, Code R4-35			H12, Code R4-35		
1	2	1	0	1	1	1
1	1	0	0	0	0	1
1	2	1	0	1	0	1
1	4	1	0	1	1	4
4	16	6	2	4	4	8
10	27	13	4	14	9	16
19	41	52	12	25	22	23
21	47	65	20	41	38	26
27	66	65	22	49	39	22

	H11, Code R4-35			H12, Code R4-35		
2	5	4	1	2	1	1
2	4	1	2	1	0	2
1	7	1	1	1	1	2
1	8	2	2	2	1	6
3	24	10	4	9	6	14
6	40	21	9	30	13	29
14	45	58	15	41	28	47
21	41	58	20	43	32	44
25	41	44	21	40	27	42

H14 H15 H16 H

wtL9	L9	wtL9	L9	wtL9	L9	wtL9
266	2906	436	849	399	669	654
457	6788	1051	2225	0	5149	321

H13, Code T-49, T-55				H-11, Code T-50, T-81		
0	0	0	8	4	0	0
0	0	0	2	15	0	0
0	0	0	2	8	0	0
0	0	0	3	2	0	0
0	0	0	6	5	1	0
5	0	0	4	9	35	32
18	0	0	38	47	100	100
46	0	0	60	66	91	98
68	0	0	102	110	92	79

H13, Code T-49, T-55				H-11, Code T-50, T-81		
0	0	0	0	0	88	0
0	0	0	0	3	0	0
0	0	0	0	0	0	0
0	0	0	0	0	0	0
0	0	0	0	0	0	0
0	0	0	0	0	0	0
0	3	0	0	0	0	0
0	0	0	0	0	0	0
0	0	0	0	0	0	0

ypes with shared elements

Code R4-38, R4-40		H15 Code R4-38, R4-40			H16 Code R4-38, R	
0	15	0	5	0	6	0
22	21	0	3	0	0	0
0	12	0	22	0	0	0
20	24	0	24	0	5	0
72	73	93	69	0	52	51
88	104	96	129	62	105	103
96	112	82	89	65	119	105
87	110	94	104	62	111	116
100	103	98	99	52	120	109

Code R4-38, R4-40		H15 Code R4-38, R4-40			H16 Code R4-38, R	
5	20	3	0	0	1	0
0	7	0	16	0	10	1
4	15	0	17	6	6	1
0	6	0	13	4	12	0
3	11	0	36	2	0	0
0	14	0	13	12	6	2
0	2	0	9	3	5	1
0	17	0	9	0	13	9
10	7	0	0	0	22	18

Single clonotypes with shared elements

H14, Code R4-38, R4-40				H15, Code R4-38, R4-40		
3	3	3	2	1	3	3
3	3	2	2	1	3	3
2	2	2	1	1	3	2
3	3	3	2	1	3	3
10	10	9	4	4	4	5
21	21	21	16	16	18	13
26	28	25	26	24	27	36
30	29	29	27	25	35	25
25	27	24	25	25	30	29

H14, Code R4-38, R4-40				H15, Code R4-38, R4-40		
9	3	2	2	2	2	3
7	2	1	2	2	2	3
6	1	1	2	2	2	2
6	2	2	1	2	2	1
7	3	2	1	2	1	2
23	8	8	3	4	5	4
46	18	15	7	10	11	16
91	24	27	14	15	18	16
63	29	25	12	13	21	19

H14, Code R4-38, R4-40

1	2	2	1
1	2	1	1
1	1	1	1
1	2	1	1
3	2	2	2
13	6	5	24
51	10	11	100
100	16	14	100
100	16	10	100

H15, Code R4-38, R4-40

1	2	2
1	2	1
1	2	1
1	1	1
2	2	1
24	5	3
100	10	16
100	19	11
100	15	15

H14, Code R4-38, R4-40

7	0	0	3
8	0	0	5
8	0	0	8
11	0	0	5
27	11	0	13
64	35	35	28
64	74	75	54
86	60	98	64
65	47	45	65

H15, Code R4-38, R4-40

3	8	9
4	6	5
6	11	5
3	0	0
15	7	11
34	45	26
57	78	72
66	108	56
74	81	67

H14, Code R4-38, R4-40

1	2	1	0
1	0	1	0
1	0	1	0
2	1	2	1
7	7	7	3
15	17	17	7
14	28	26	14
32	30	49	26
20	40	38	26

H15, Code R4-38, R4-40

1	1	3
1	2	2
1	3	2
1	2	3
4	5	6
9	25	15
16	36	35
27	55	54
30	67	72

H14, Code R4-38, R4-40

2	5	2	1
1	2	1	1
4	2	3	1
5	4	3	2
14	15	10	6
54	30	24	13
40	44	32	24
59	49	54	49
44	27	42	44

H15, Code R4-38, R4-40

1	7	9
2	8	6
2	8	5
1	7	7
8	10	14
22	29	24
45	49	34
51	52	45
44	54	64

L9	wtL9	L9	wtL9	L9		
1572	446	319	444	805		
351	1363	2017	0	581		
					Single clonotypes with shared ele	
	H-12, Code T-54, T-55				H-14, Code T-49, T-58	
0	0	0	0	0	0	0
0	0	0	0	0	0	0
0	0	0	0	0	0	0
0	0	5	0	17	0	0
0	0	0	0	0	0	0
8	4	4	0	77	8	0
24	28	10	0	31	20	25
31	30	71	51	60	38	71
23	20	96	100	66	55	78
	H-12, Code T-54, T-55				H-14, Code T-49, T-58	
1	0	0	0	0	0	0
0	0	0	0	55	1	0
0	0	0	0	1	4	0
0	5	0	1	1	0	0
0	0	0	0	0	0	0
1	0	0	0	0	0	0
0	0	0	0	0	0	0
0	0	0	0	0	0	0
1	0	0	0	0	0	0

				Single clonotypes lacking shared element		
:4-40	H7, Code T-36, MA-34			H8, R4-38, R4-40		
11	3,2	7,2	2,6	0	2	0
11	22,6	27,7	12	3,7	10,6	3
8	18,2	21,1	1,5	13,3	4,2	9
10	12,2	24	5,9	5	4,7	5
27	17,4	24,6	2,1	20,3	6,1	1
97	13,2	18,5	3,3	11,8	6,6	0
102	20,1	22,6	2,6	8,8	13,4	0
99	20	20,1	2	14,8	38,9	0
100	27,5	21,9	1,8	13,8	12,4	0
:4-40	H7, Code T-36, MA-34			H8, R4-38, R4-40		
0	14,3	9	9,6	0	0	0
1	3,9	13,7	16,2	7,1	8,5	15
1	20,7	11,1	1,6	1,9	5,1	4
0	9,3	11,1	8,6	9,5	9,4	3
0	18,9	15,1	3,2	5,1	4,4	6
2	15,7	14,2	21,7	4,8	7,8	8
1	12,3	10,4	28,4	20	19,8	1
9	11	15,8	3,2	12,9	25,1	0
18	15,7	17,5	1	16,9	29,3	0
	H16, Code R4-38, R4-40			H7, Code R4-35, MA-34		
1	2	2	2	7	1	1
1	1	1	1	7	1	1
1	1	1	2	6	1	0
1	2	1	2	6	1	1
4	4	3	3	7	2	1
14	18	11	11	7	1	1
28	28	25	24	6	0	0
29	30	30	33	5	0	1
27	37	32	33	3	0	1
	H16, Code R4-38, R4-40			H7, Code R4-35, MA-34		
4	3	3	3	3	0	0
4	3	2	2	3	0	0
3	4	2	2	2	0	0
4	3	2	2	3	0	0
4	4	2	2	4	0	0
11	9	3	4	2	0	0
33	25	12	13	2	0	0
48	43	23	27	2	0	0
55	63	31	34	2	0	0

	H16, Code R4-38, R4-40			H7, Code R4-35, MA-34		
0	0	1	1	2	0	0
0	0	1	0	2	0	0
0	0	1	0	2	0	0
0	0	1	1	1	0	0
1	1	1	1	1	0	0
4	4	2	2	1	0	0
24	28	6	5	1	0	0
100	56	9	9	1	0	0
100	100	12	12	2	0	0

	H16, Code R4-38, R4-40			H7, Code R4-35, MA-34		
8	7	0	0	3	0	0
8	7	0	0	3	0	0
8	7	0	0	3	0	0
8	7	0	0	3	0	0
8	11	0	0	3	0	0
37	37	9	10	3	0	0
66	59	36	29	3	0	0
55	50	42	44	3	0	0
57	56	56	59	3	0	0

	H16, Code R4-38, R4-40			H7, Code R4-35, MA-34		
0	0	1	1	1	0	1
0	0	1	1	1	1	1
0	0	1	1	0	1	0
1	1	1	1	0	0	0
4	5	3	3	1	1	1
8	11	12	9	0	0	0
23	23	26	19	1	0	0
32	28	39	33	1	0	1
29	41	48	53	0	0	1

	H16, Code R4-38, R4-40			H7, Code R4-35, MA-34		
2	1	3	2	7	0	0
2	1	2	2	7	0	0
1	1	2	2	7	0	0
1	1	3	1	7	0	0
7	4	9	6	7	0	0
25	10	30	19	7	0	0
37	28	51	35	7	0	0
38	25	56	47	7	0	0
55	34	68	58	7	0	0

ɛments

		H-15, Code T-49, T-58				H-16, Code
0	10	1	0	0	0	0
0	0	0	0	0	0	0
0	52	0	0	0	0	0
0	0	0	0	0	0	0
0	0	0	0	0	0	0
0	18	8	0	0	0	3
19	26	22	0	0	7	18
78	74	55	0	5	30	45
101	120	77	0	0	46	63

		H-15, Code T-49, T-58				H-16, Code
0	0	0	0	0	0	0
0	4	7	0	0	0	3
0	0	0	0	0	0	3
0	0	0	0	0	0	0
0	0	0	0	0	0	32
0	0	6	0	0	0	0
0	0	0	0	0	0	0
0	0	0	0	0	0	0
0	0	0	0	0	0	0

:s

H10, Code T33, T36		
34,8	0	16,4
0	4,6	16,4
34,6	6,4	10,2
0	6,5	16,1
19	6,9	37,7
1,4	14,7	24,3
43,8	42,1	19,4
79,8	77,8	35,1
113	82,9	35,2

H10, Code T33, T36		
0	0	7,4
0	0	5,5
0	5	14,2
0	1,6	17,7
0	27,2	10,8
9,7	2,1	3
0	2,7	12,9
0	0	14,5
0	0,3	15,2

Single clonotypes lacking shared elements

H8, Code R4-38, R4-40				H10, Code R4-35		
1	1	4	1	5	2	2
1	2	2	1	5	2	2
1	1	2	1	6	1	2
1	1	1	1	5	1	2
1	2	2	1	7	1	2
1	1	1	1	4	1	2
1	2	1	1	5	3	7
1	1	1	1	6	5	10
1	1	1	1	7	4	14

H8, Code R4-38, R4-40				H10, Code R4-35		
4	4	2	1	3	3	3
4	5	2	1	3	1	3
2	4	2	1	4	1	4
3	4	1	1	3	1	4
2	4	2	1	2	2	2
3	3	1	0	3	1	3
3	4	1	0	3	3	8
2	3	1	1	6	5	14
2	3	1	0	7	3	19

	H8, Code R4-38, R4-40				H10, Code R4-35	
1	1	2	0	0	0	0
1	1	2	0	0	0	0
1	0	1	1	0	0	1
1	1	1	1	0	0	0
1	1	1	1	0	0	0
1	1	1	0	0	0	1
1	1	1	0	0	1	2
1	0	1	1	0	1	3
1	1	1	0	1	1	3

	H8, Code R4-38, R4-40				H10, Code R4-35	
7	4	0	0	1	2	1
6	5	0	0	1	1	1
5	5	0	0	1	0	2
7	4	0	0	1	0	1
3	4	0	0	1	1	0
5	4	0	0	1	1	2
4	4	0	0	1	3	8
3	4	0	0	6	6	13
3	4	0	0	6	3	16

	H8, Code R4-38, R4-40				H10, Code R4-35	
1	1	1	1	1	2	1
0	1	1	1	1	0	1
0	0	1	1	1	0	1
0	0	1	1	0	0	1
0	0	1	1	1	1	1
0	0	0	0	1	1	2
0	1	0	0	2	4	14
0	0	0	1	4	8	19
0	0	0	1	5	5	49

	H8, Code R4-38, R4-40				H10, Code R4-35	
1	1	1	1	4	2	1
1	2	1	1	3	0	1
1	3	1	1	1	0	3
1	1	1	1	1	0	1
1	2	1	1	4	1	1
2	2	0	1	1	2	2
1	1	0	1	3	9	23
1	1	1	1	6	18	42
1	1	1	1	5	12	87

						Single cl
T-49, T-58			H7, Code T-49, T-81			
0	0	0	0	0	0	0
0	0	0	0	0	0	0
0	0	0	0	0	15	0
0	0	0	-7	0	1	0
0	0	0	0	0	0	0
0	0	0	0	0	0	0
3	0	5	-70	1	17	0
32	24	0	-320	0	1	0
78	40	0	0	21	0	0
T-49, T-58			H7, Code T-49, T-81			
0	0	0	0	0	0	0
0	0	0	0	0	0	0
0	0	0	0	0	0	0
0	0	0	0	0	26	0
0	0	0	0	0	0	0
0	0	0	0	0	0	0
0	0	0	0	0	0	0
0	0	0	0	0	0	0
0	0	0	0	0	0	0

lonotypes lacking shared elements						
H-8, Code T-49, T-81				H-10, Code T-50, T-54		
0	0	0	0	0	16	7
0	0	9	0	0	5	3
0	0	4	0	0	7	7
0	0	3	0	0	5	4
0	0	2	0	0	3	5
0	0	21	0	0	3	5
0	0	13	0	1	4	3
0	0	2	0	0	6	4
0	0	0	0	0	2	2
H-8, Code T-49, T-81				H-10, Code T-50, T-54		
18	0	0	0	0	0	0
0	0	24	0	0	6	0
0	0	0	0	0	0	0
2	0	0	0	0	0	0
0	0	0	0	0	0	0
0	0	0	0	0	0	0
0	0	0	0	0	0	0
0	0	0	0	0	0	0
0	0	0	0	0	0	0

		Number of TAMs			
		IFN-g	H6, Code R4-36, R4-37		
		None	5	1	1
		70	2	3	0
		200	2	2	0
		600	4	2	1
		1800	5	6	2
		5500	10	11	9
		16600	35	40	22
		50000	100	100	47
		150000	100	100	62
		IL-2	H6, Code R4-36, R4-37		
		None	6	4	4
		70	4	3	4
		200	5	3	3
		600	5	2	4
		1800	6	4	10
		5500	6	3	23
		16600	10	6	45
		50000	22	14	84
		150000	61	40	123
		IL-4	H6, Code R4-36, R4-37		
		None	0	0	0
		70	0	0	0
		200	0	0	0
		600	0	0	0
		1800	0	1	0
		5500	0	1	2
		16600	1	1	3
	T cell stimulation with 6132A-TAMs cytokine panel	50000	1	2	4
Fig. 5A		150000	1	2	2
		IL-10	H6, Code R4-36, R4-37		
		None	5	4	3
		70	3	3	3
		200	3	3	2
		600	3	2	2
		1800	5	3	5
		5500	7	5	12
		16600	17	13	17
		50000	34	32	23
		150000	126	117	20

IL-17	H6, Code R4-36, R4-37		
None	1	0	0
70	1	0	0
200	1	1	0
600	1	1	0
1800	1	1	2
5500	2	2	3
16600	4	3	5
50000	7	6	8
150000	10	10	9

IL-22	H6, Code R4-36, R4-37		
None	1	0	0
70	1	1	0
200	2	1	0
600	1	1	0
1800	2	1	1
5500	3	2	3
16600	6	6	8
50000	18	13	15
150000	29	27	21

Fig. 5B 6132A-TAMS flow cytometry markers after TCR-therapy, CRA-71, CRA-75

	Arginase		CD1
TCR	Effective	Failing	Effective
H6	41,5		1,96
H6	71,2		0,24
H6	42,1		1,77
H6	63,6		4,32
H9	58,7		0,38
H9	69		0,78
H9	69,3		0,36
H9	43,2		0,71
H12	19,2		0,23
H12	25,2		6
H12	56,4		0,7
H12	41,2		0
H13	57,3		0,1
H13	79,8		0,54
H13	58,4		0
H13	57,7		0,55
H10		81,6	
H10		62,2	
H10		30,3	
H10		27,4	
amL26		18,2	

		amL26		20,4	
		amL26		32,2	
		amL26		53	
				Failing	
			Day 6	Day20	
Fig 5C	Kinetic of NO in 6132A-TAMs flow cytometry individual TCRs CRA-59, CRA-60, CRA-71, CRA-75	I-Ek positive TAMs	amL26	amL26	H10
		Arginase+	9,7	27,83	34,1
		NO+	4,1	7,43	4,56
		NO+ and Arginase+	1,7	5,02	5,65
		Alone	84,5	59,73	55,73
				TAMs NO+ and I-Ek+	
				Arginase +	Argin
		TCR	Effective	Failing	Effective
		H6	67,1		31,6
		H6	45		55
		H6	54,8		45,2
		H6	15,8		5,26
		H9	8,81		5,04
		H9	16,1		12
		H9	26		29,9
		H9	21,2		13,6
		H12	74		20,5
Fig. 5D	NO TAM comparison CRA-71, CRA-75	H12	81		11,5
		H12	67,7		32,3
		H12	50		50
		H13	9,36		10,6
		H13	50,2		45,1
		H13	41,7		58,3
		H13	29,2		30,8
		H10		4,16	
		H10		9,51	
		H10		0	
		amL26		7,71	
		amL26		7,18	
		amL26		12,6	
		amL26		2,21	

Convergent TCRs						
H9, Code R4-36, R4-37			H13, Code R4-36, R4-37			H11,
2	3	0	10	6	2	2
2	4	0	12	11	2	2
24	5	0	23	15	1	2
4	2	1	4	72	1	2
3	2	0	11	6	2	3
2	4	0	13	9	7	3
4	3	1	25	32	20	10
4	3	2	67	70	52	39
17	18	5	100	100	92	100

H9, Code R4-36, R4-37			H13, Code R4-36, R4-37			H11,
1	1	1	3	3	1	4
1	1	2	2	2	1	6
1	1	2	2	2	1	6
1	1	2	3	2	2	5
1	1	2	2	2	3	6
1	1	3	3	3	7	7
1	1	4	5	6	21	9
1	1	6	11	11	52	17
1	1	9	42	40	99	58

H9, Code R4-36, R4-37			H13, Code R4-36, R4-37			H11,
0	0	0	0	0	0	0
0	0	0	0	0	0	0
0	0	0	0	0	0	0
0	0	0	0	0	0	0
0	0	0	0	0	0	0
0	0	0	0	0	0	1
0	0	0	0	0	1	1
0	0	0	1	1	1	1
0	0	0	1	0	1	1

H9, Code R4-36, R4-37			H13, Code R4-36, R4-37			H11,
1	1	0	4	3	1	6
1	1	1	4	4	2	6
1	1	0	5	5	2	7
1	1	1	4	8	1	7
1	1	1	4	3	2	9
1	1	3	5	4	6	9
3	2	12	11	11	26	15
7	7	55	30	26	82	41
34	29	147	113	87	171	125

H9, Code R4-36, R4-37			H13, Code R4-36, R4-37			H11,
1	1	1	0	1	0	0
1	0	1	1	1	0	0
1	1	1	1	1	0	1
1	0	1	1	2	0	1
1	0	0	1	1	1	1
0	0	1	2	1	2	1
1	1	2	4	4	6	3
1	1	4	8	7	10	6
2	2	6	17	13	13	14

H9, Code R4-36, R4-37			H13, Code R4-36, R4-37			H11,
1	1	0	1	1	0	0
1	1	0	1	1	0	0
1	1	0	2	1	0	1
1	0	0	2	2	0	1
1	1	0	3	1	1	2
0	1	0	3	2	1	4
1	1	0	8	9	10	4
1	1	2	19	16	29	20
7	6	3	38	27	31	28

L63	CD204		CD206		IDO	
Failing	Effective	Failing	Effective	Failing	Effective	Failing
	92,2		15,7		83,6	
	95,7		12,5		38	
	93,6		2,47		96,9	
	86,7		1,82		62,9	
	98,9		15		95,4	
	96,8		20,8		6,86	
	95,6		4,04		86,6	
	98,4		0,33		45,6	
	90		1,52		62,1	
	91,9		11,8		8,98	
	92		0,42		90,6	
	74,2		0		35	
	99,1		6,09		91,8	
	95,7		14,2		16,2	
	85,4		0		89	
	97		0,88		37,9	
0,28		99,7		19,1		97,5
0		75,8		12,1		8,64
0,53		97,9		1,07		85,2
0,75		97,8		0,51		36,8
0,8		99,6		10,5		94,6

0,68	97,4	35,1	35,8
0,59	96,5	1,16	93,9
0,51	97,5	6,97	73,4

Effective				
Day 6	Day 20			
H6	H6	H9	H12	H13
16,1	9,2	31,3	0,87	10,33
44,1	45,68	18,03	68,18	32,62
10,8	34,27	15,14	27,33	36,2
28,9	10,84	35,48	2,39	27,81

ıase - Failing
12,6
4,36
0
3,77
3,92
6,61
5,76

						Single
Code R4-36, R4-37			H12, R4-36, R4-37			H14, Code R4
2	1	2	2	1	0	1
2	1	3	2	0	0	0
1	1	2	3	1	0	0
6	1	2	3	1	1	1
2	1	3	3	1	1	1
3	2	6	7	4	2	2
8	5	19	20	12	5	5
30	17	55	50	34	11	12
100	34	100	100	57	19	19
Code R4-36, R4-37			H12, R4-36, R4-37			H14, Code R4
4	3	3	3	2	8	10
3	2	3	3	2	6	6
3	2	3	3	2	6	6
2	3	3	3	3	9	7
4	4	4	4	3	6	10
4	8	4	4	6	13	14
5	17	5	6	14	29	30
11	50	9	10	36	59	73
42	99	28	35	67	102	121
Code R4-36, R4-37			H12, R4-36, R4-37			H14, Code R4
0	0	0	0	0	1	1
0	0	0	0	0	1	1
0	0	0	0	0	1	1
0	0	0	0	0	1	1
0	0	0	0	0	1	1
0	1	0	0	0	1	2
1	1	0	1	1	3	3
1	1	1	1	1	3	3
1	1	0	1	1	1	1
Code R4-36, R4-37			H12, R4-36, R4-37			H14, Code R4
6	2	2	3	1	2	2
3	2	3	3	1	2	2
4	3	3	3	1	2	2
6	3	3	3	2	2	2
5	3	3	4	2	2	2
8	8	5	6	5	5	6
10	28	9	9	17	26	27
31	97	21	22	53	101	119
87	214	67	75	108	279	303

Code R4-36, R4-37		H12, R4-36, R4-37				H14, Code R4
0	0	0	0	0	0	0
0	0	0	0	0	1	1
0	1	0	0	0	1	1
1	1	0	1	0	1	2
0	1	1	1	0	4	4
1	3	1	1	2	12	11
2	7	2	2	4	20	17
5	11	4	3	5	29	32
12	17	8	8	7		

Code R4-36, R4-37		H12, R4-36, R4-37				H14, Code R4
1	0	1	0	0	1	1
1	0	1	1	0	1	1
1	0	1	1	0	1	1
0	0	2	1	0	1	1
1	1	2	3	0	1	2
2	1	2	2	1	2	3
3	4	5	5	3	10	7
8	15	10	10	7	39	34
20	26	28	23	11	67	105

IL-10		CD40		IL-12		N
Effective	Failing	Effective	Failing	Effective	Failing	Effective
9,54		54,6		2,29		98,7
0,78		64,6		0,25		98,9
0,61		20,8		2		95,4
0,19		37		0,44		37,1
0,02		53,5		0,097		39,6
0,055		50,9		0,13		34
0,088		17,8		0,13		52,3
0,066		65,7		0,12		47,8
0,29		37,6		3,24		94,7
1,91		31,3		0,64		90,9
0,28		7,03		1,02		97,8
0		25,8		0,74		86,8
1		46,1		0,44		23,1
1,3		50,4		0,12		92,9
0,22		14,6		0,87		98,8
0		16,8		0		66
	0,12		54,3		0,73	
	5,46		19		0,35	
	0,037		2,56		0,1	
	0,031		53,4		0,032	
	0,04		49,8		0,17	

0,051	51,6	0,029
0,073	7,07	0,2
0,036	69	0,05

clonotypes with shared elements

4-37, MA-34			H15, Code R4-37, MA-34			
2	2	0	1	3	3	1
2	2	1	1	3	3	1
2	2	1	1	3	5	2
2	3	1	1	4	4	1
5	5	1	1	6	5	2
11	18	2	2	12	17	2
21	32	7	5	23	21	6
52	53	17	16	50	55	22
75	79	41	36	95	96	33

4-37, MA-34			H15, Code R4-37, MA-34			
1	1	2	3	1	1	3
1	1	2	1	1	1	2
1	1	2	2	1	1	3
1	1	2	2	1	1	2
1	1	3	2	1	1	3
2	4	4	5	2	2	5
4	6	7	3	2	2	6
9	11	12	12	5	4	12
15	19	29	25	11	11	23

4-37, MA-34			H15, Code R4-37, MA-34			
1	1	0	0	1	0	0
1	1	0	0	1	1	0
1	1	0	0	1	1	0
1	1	0	0	1	1	0
1	1	0	0	1	1	0
1	3	0	0	2	2	0
2	3	0	0	1	1	0
2	3	0	0	2	1	0
1	1	0	0	1	1	0

4-37, MA-34			H15, Code R4-37, MA-34			
4	5	1	1	4	5	1
4	9	1	1	11	3	1
4	5	1	1	9	11	1
3	7	1	1	4	5	1
7	7	1	1	5	8	1
13	31	2	2	22	29	3
55	72	11	5	44	25	10
153	242	44	41	143	124	43
360	453	113	93	295	309	97

4-37, MA-34			H15, Code R4-37, MA-34			
1	1	0	0	1	1	0
1	1	0	0	1	4	0
2	2	0	0	3	2	0
4	3	0	0	3	3	1
6	8	2	2	8	8	2
13	13	4	2	9	7	6
20	21	9	11	17	17	11
26	28	14	15	28	37	15

4-37, MA-34			H15, Code R4-37, MA-34			
1	1	0	0	2	2	0
2	1	0	0	1	2	0
2	2	0	0	3	5	0
2	2	0	0	7	3	0
6	5	0	0	3	5	1
11	11	2	2	10	13	2
17	17	3	2	15	10	4
27	24	12	14	25	20	13
26	30	33	23	31	40	23

O		TNF
Failing	Effective	Failing
	1,89	
	9,62	
	18,4	
	4,44	
	25,4	
	4,23	
	14,3	
	0,33	
	1,5	
	23	
	14,5	
	18,1	
	8,9	
	8,54	
	13,3	
	2,26	
		9,81
19,7		2,52
9,33		16,4
0,57		0,21
13,4		3,79

11	0,76
15	14,3
15,5	2,2

Single cl

H16, Code R4-37, MA-34			H7, Code R4-36, R4-37			
1	2	1	0	1	2	1
1	1	1	0	1	1	1
2	2	2	0	2	1	1
2	2	2	0	1	5	1
1	4	3	0	3	1	1
2	9	12	1	1	1	0
6	25	24	0	3	1	1
16	79	62	1	2	7	1
41	100	94	1	4	3	1

H16, Code R4-37, MA-34			H7, Code R4-36, R4-37			
3	2	1	3	2	1	5
2	1	1	3	2	2	5
2	1	1	3	2	1	2
3	1	1	2	2	1	3
3	2	1	2	2	1	3
4	2	3	2	1	1	3
7	4	4	1	1	2	2
13	13	9	2	1	1	2
31	18	16	4	1	2	3

H16, Code R4-37, MA-34			H7, Code R4-36, R4-37			
0	0	0	0	0	0	0
0	0	1	0	0	0	0
0	1	0	0	0	0	0
0	0	1	0	0	0	0
0	1	1	0	0	0	0
0	1	1	0	0	0	0
0	2	2	0	0	0	0
0	3	2	0	0	0	0
0	1	1	0	0	0	0

H16, Code R4-37, MA-34			H7, Code R4-36, R4-37			
1	4	6	1	2	2	1
1	2	5	1	2	2	1
1	6	6	1	2	2	1
1	5	4	1	2	2	1
1	11	6	1	2	2	1
2	11	11	1	2	2	1
10	56	62	9	5	5	5
44	277	269	57	11	13	26
115	486	622	150	54	62	96

H16, Code R4-37, MA-34			H7, Code R4-36, R4-37			
0	1	1	0	0	0	0
0	1	1	0	0	0	0
1	1	1	0	1	0	0
0	3	2	0	0	1	0
1	4	4	0	0	0	0
3	7	7	0	0	0	0
7	15	16	0	0	0	0
10	25	20	0	0	0	0
			0	0	0	0

H16, Code R4-37, MA-34			H7, Code R4-36, R4-37			
0	1	0	0	0	0	0
0	1	1	0	0	0	0
0	1	1	0	1	0	1
1	2	2	0	0	1	1
0	5	2	0	0	1	0
2	7	8	0	0	0	0
3	15	16	0	0	0	0
13	36	27	0	0	1	0
34	32	30	1	1	2	1

lonotypes lacking shared elements

H8, R4-37, MA-34			H10, R4-36, R4-37		
1	2	1	1	4	0
1	2	2	1	1	0
1	2	1	1	1	0
1	1	1	1	1	0
1	1	1	2	1	0
0	1	1	1	1	0
1	1	1	3	1	0
0	1	1	2	2	1
1	2	2	4	4	1

H8, R4-37, MA-34			H10, R4-36, R4-37		
6	1	1	2	1	4
3	1	1	2	1	2
4	2	1	1	1	3
3	0	1	2	1	3
4	1	1	2	1	3
4	1	1	2	1	4
5	1	0	2	1	4
3	1	1	1	1	4
2	1	1	2	1	6

H8, R4-37, MA-34			H10, R4-36, R4-37		
0	1	1	0	0	0
0	2	1	0	0	0
0	1	1	0	0	0
0	1	1	0	0	0
0	0	1	0	0	0
0	1	1	0	0	0
0	0	0	0	0	0
0	0	0	0	0	0
0	0	0	0	0	0

H8, R4-37, MA-34			H10, R4-36, R4-37		
1	1	1	3	2	1
1	0	0	3	2	1
1	0	0	3	2	1
1	1	0	3	2	0
1	1	2	3	2	2
1	0	2	3	2	3
6	4	3	7	5	14
26	15	23	18	16	70
90	10	10	74	65	204

H8, R4-37, MA-34				H10, R4-36, R4-37	
0	1	1	0	0	0
0	1	0	0	0	0
0	1	1	0	0	1
0	1	0	0	0	0
0	0	0	1	0	1
0	0	0	0	0	0
0	0	0	0	0	0
0	0	1	0	1	1
0	1	1	1	1	2

H8, R4-37, MA-34				H10, R4-36, R4-37	
0	1	1	0	0	0
0	1	0	0	0	0
0	1	0	1	1	0
0	1	0	1	0	0
0	0	0	1	0	0
1	0	0	0	1	0
0	1	0	0	0	0
0	0	1	1	1	0
1	2	3	4	3	1

	TIL	Flow Cytometry, mouse #2 from Fig. 1A		
	combined	CD3	CD4	mL9-Tetramer
Fig. S1A	analysis	36,5	68,7	19,3
	(%), CPA-	26	41,7	1,4
	11, -17, -22,	9,82	42,5	0,6
	-23	26,3	13,7	1,37

Schematic of Ward et al.	TCR clonotype	Number of T cells
Original 6132 Spleen CPA-25		5
	H13	2
		2
		2
		1
		1
		1
		1
		1
		1
		1
		1
		1
		1
		1
		1
		1
		1
		1
		1
		1
		1
		1
		1
		1
		1
		1
		1
		1
		1
		1
		1
		1
		1
		1
		1
		1
		1
		1
		1
		1
		1
		1

Fig. S2

1
1
1
1
1
1
1
1
1
1
1
1
1
1
1
1
1
1
1
1
1
1
1
1
1
1
1
1
1
1
1
1
1
1
1
1
1
1
1

Fig. S3	Code CPA-11, CPA-17, CPA-22 and CPA-23 Convergent TCR recombination	Sequencing data available at SRA

Project number
PRJNA1113628

Days after T cell transfer	H6			
	3317	3318	3372	5520
-34				
-33				
-32	0	0	0	0
-31				
-30				
-29				
-28				
-27				
-26	2	12	12	16
-25				
-24	2	9	12	
-23				
-22				
-21	18	20	28	
-20				
-19				140
-18				
-17	24	33	54	
-16				
-15				
-14	45	90	120	280
-13				
-12				
-11				
-10	66	144	195	405
-9				
-8				
-7	140	210	360	540
-6				
-5				
-4				700
-3	225	367	525	
-2				
-1				
0	378	535	600	825
1				
2	532	728	765	1056
3				
4	560	900	1080	
5				1224
6	990	990	1296	

Fig. S4	4102-mL9 treatment FOT-1, FOT-3	7				
		8				
		9	576	720	960	768
		10				
		11	504	472	693	360
		12				
		13	441	392	693	
		14				160
		15				
		16	378	392	572	96
		17				
		18	332	273	643	73
		19				
		20				
		21	297	288	480	45
		22				
		23				20
		24				
		25	204	269	420	20
		26				
		27				
		28	204	162	420	20
		29				
		30				
		31				12
		32	180	96	420	
		33				
		34				12
		35	140	84	346	
		36				
		37				12
		38				
		39	96	84	240	
		40				
		41				
		42				
		43				
		44				
		45	120		240	
		46				12
		47				
		48				
		49				
		50				
		51	132			

	52		
	53		12
	54		
	55		
	56		
	57		
	58	52	12
	59		
	60		
	61		
	62		
	63	42	
	64		
	65		
	66		
	67	36	16
	68		
	69		
	70		
	71		
	72		16
	73		
	74	36	
	75		
	76		
	77		
	78		
	79		0
	80	36	

5519	5518	3329	3330	H10 3328	5524	5525
0	0	0	0	0	0	0
16	16	6	9	6	20	20
		9	12	6		
		12	24	12		
90	126				108	54
		32	30	20		
192	364	72	42	52	126	54
273	441	180	80	84	126	130
472	648	294	157	192	273	273
595	841	441	270	210	385	343
680	864	576	336	409	455	557
765	1045	595	472	441	525	504
990	1140	748 972	540 841	560 616	675	567

1020	864	918	900	595	1020	810
720	768	1020	864	654	1122	855
720	630	1020	792	616	1122	855
720	525	1020	880	525	1122	855
720	450	1170	935	525	1215	940
540	315	1287	1122		1215	940
540	245				1287	855
612	292	1482	1188		1386	1045
512	234		1188		1386	1045
420	105		1368		1638	1254
441	105					1254
324	84					1440
288	37					

168	20
90	16
90	16
90	16
0	0

TCR			H12			
5516	3326	3373	3375	5527	5526	5523
0	0	0	0	0	0	0
16	9	9	9	20	20	20
	21	17	9			
	33	20	30			
64				154	105	90
	45	35	75			
135	120	75	110	252	200	231
195	318	132	154	288	390	273
343	540	231	260	525	462	441
540				768	624	504
	726	288	504			
576	760	560	560	768	819	675
648	990	600	640	918	1120	935
	1573	704	891			
765				1105	1536	1020
	1716	841	972			

1089	891	525	600	616	728	616
1188	616	409	560	420	600	468
1296	560	351	441	270	480	346
1254	286	312	351	162	320	346
1368	162	210	251	108	252	297
1368	94	132	312	84	140	210
1089				63	122	180
1188	73	94	220	63	122	144
1188	52	105	140	63	98	144
1254	37	60	84	36	70	73
1320	24	60	80	36	98	73
1440	24	52	80	36	98	73
	24	52	81	36	98	73
	24	52	81			

			36	98	73
30	52	52	36	73	73
25	30	48			
25	30	48	30	63	73
			30	63	73
25	30	48			
			0	0	0
25	30	48			

amL26 3320	3374	3327	5522	5521	5517
0	0	0	0	0	0
12	9	9	16	16	16
12	12	9			
27	24	12			
			67	157	108
36	24	28			
54	28	28	100	157	210
72	60	52	126	196	240
130	110	70	294	245	432
240	234	189	448	364	526
315	392	264	476	448	630
480	540	264	648	648	825
616	688	396			
704	900	504	810	850	907

661	990	504	1080	1090	1040
724	1188	624	1134	1296	1152
920	1188	624	1452	1368	1190
960	1254	624	1573	1368	1215
1080	1254	676		1482	1404
1200	1320	728			
1188	1440	945			
1320	1452	1008			
1452		1071			
		1309			

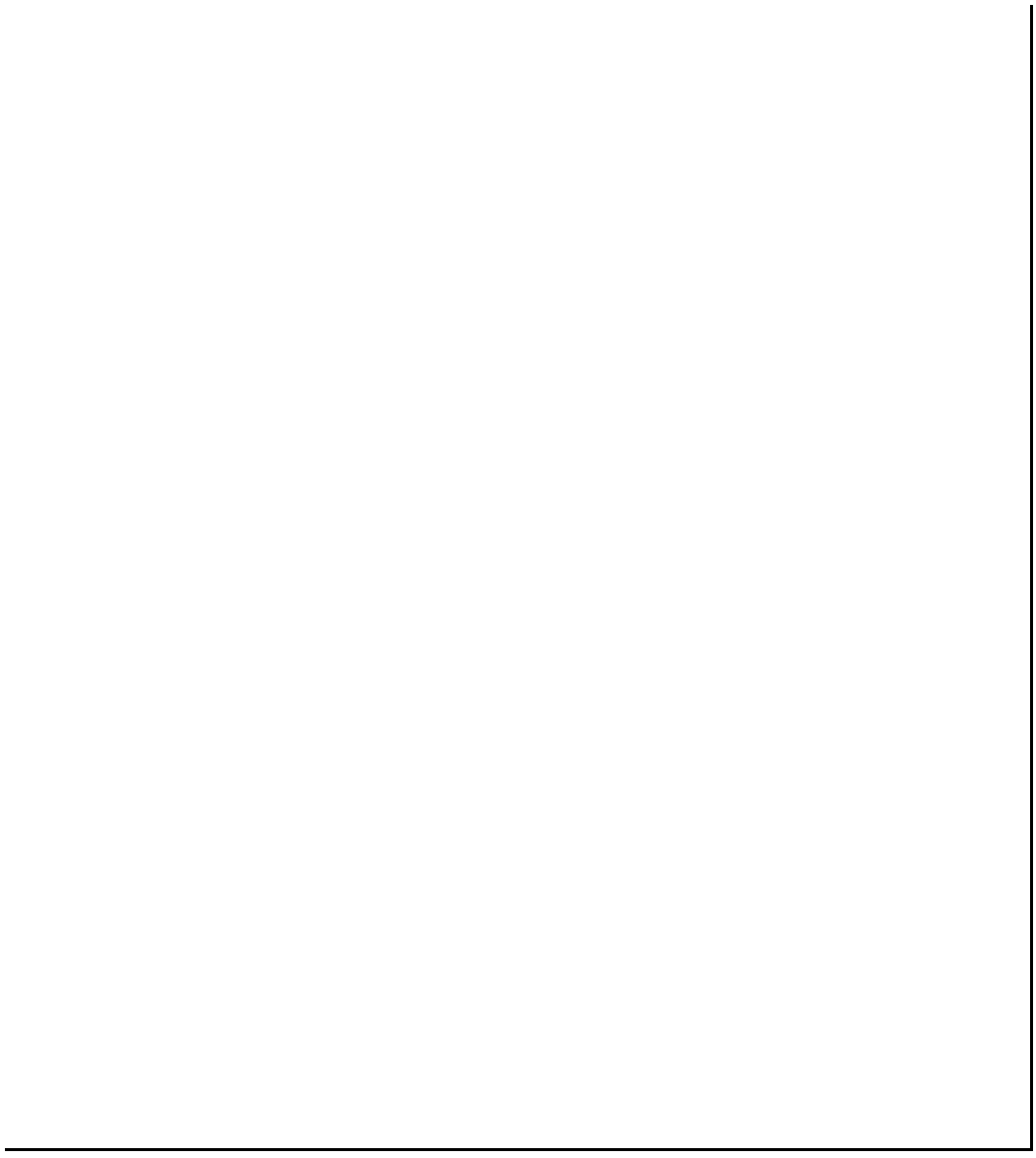

Fig. S5	MCC-TCR sec	Published in McHeyzer-Williams et. al. (22).

Fig. S6A MCC sequences

Fig. S6B MCC-TCRs recognition, R4-39, R4-40

	TCR			
MCC peptide	AND	5c.c7	M2.3	M4.3
None	0	0	0	0
0,001	919	183	1417	1154
0,01	1011	0	171	347
0,1	935	0	558	1365
1	1470	1999	2725	4713
10	2556	4207	4154	5085
100	2074	4267	3259	4481
1,000	1624	3880	2592	4311
10,000	1919	3570	2849	4764

Fig. S6C Vectr construct

Fig. S6D Treatment overview

	5c.c7			
Days after T cell transfer	3331	3332	3366	3365
-34	0	0		
-33			0	0
-32				
-31				
-30				
-29				
-28	12	12		
-27				
-26				
-25				
-24	30	30	24	24
-23				
-22				
-21	54	30		
-20				
-19				
-18				
-17	108	84	30	30
-16				
-15				
-14	108	84		
-13				
-12				
-11				
-10	168	126	84	84
-9				
-8				

Fig. S6E	Treatment of 6132A-MCC-GFP, CRA-76, CRA-78	-7	196	168	105	220
		-6				
		-5				
		-4				
		-3	318	280	196	294
		-2				
		-1				
		0	343	315	224	336
		1				
		2	540	315	252	416
		3				
		4	607	360	252	630
		5				
		6				
		7	640	495	280	630
		8				
		9	576	350	252	392
		10				
		11	540	346	360	504
		12				
		13				
		14	448	400	385	560
		15				
		16	640	400	440	560
		17				
		18	816	400	462	577
		19				
		20				
		21	864	544	576	704
		22				
		23				
		24			676	773
		25	1026	648		
		26				
		27			676	936
		28	1330	780		
		29				
		30			780	1064
		31	1700	1078		
		32				
		33			784	1282
		34				
		35				
		36				
		37			1008	

		38			
		39		1402	
		40			
		41			
		42			

		Days after T cell transfer	3369	3370	5c.c7 3371
		-34	0	0	0
		-33			
		-32			
		-31			
		-30	0	0	0
		-29			
		-28			
		-27			
		-26			
		-25			
		-24			
		-23	20	20	20
		-22			
		-21			
		-20			
		-19			
		-18			
		-17			
		-16	36	36	66
		-15			
		-14			
		-13			
		-12			
		-11			
		-10			
		-9	112	96	189
		-8			
		-7			
		-6	144	104	364
		-5			
		-4			
		-3			
		-2	245	130	600
		-1			
		0	416	245	640
	Treatment of 4102-MCC-GFP	1			
Fig. S6F		2			

Fig. 3bF	MCC-GFP, FOT-2, FOT-3	3	476	315	841
		4			
		5	612	392	1020
		6			
		7	476	270	994
		8			
		9			
		10	448	270	1215
		11			
		12	448	367	1215
		13			
		14			
		15	448	343	1326
		16			
		17			
		18			
		19	367	318	1309
		20			
		21			
		22	367	175	1344
		23			
		24			
		25			
		26	420	137	1428
		27			
		28			
		29	392	156	1547
		30			
		31			
		32			
		33	367	52	
		34			
		35			
		36	367	60	
		37			
		38			
		39		81	
		40			
		41			
		42		72	

	TCR	Mouse	after T cell t	nvergent TC ergent elem
		3325	39	0
		3324	28	0
	AND	3356	30	1
	Code:	3354	37	1

		CRA-76, CRA-78, FOT-2, FOT-4	3353	30		1
			3379	36		0
			5505	48		1
			3377	45		1
			3798	48		1
			3367	52		1
			3332	31		1
			3331	31		1
		5c.c7 Code: CRA-76, CRA-78, FOT-2, FOT-4	3365	33		1
			3362	30		1
			3369	36		1
			5501	26		1
			3366	39		1
			5503	34		1
			3370	106		0
			3371	29		1
Fig. S6G	MCC Survival overview	M2.3 Code: CRA-76, CRA-78, FOT-2, FOT-4	3323	28	0	
			3322	46	1	
			3321	46	1	
			3352	46	1	
			3382	80	1	
			3384	64	1	
			5574	74	1	
			3799	53	1	
			3368	106	1	
			3797	62	1	
			3800	82	1	
			5573	62	1	
			5550	39	1	
			3351	42	1	
			3334	39	1	
		M4.3 Code: CRA-76, CRA-78, FOT-2, FOT-4	3381	68	0	
			3333	39	1	
			3385	64	1	
			3364	37	1	
			5508	41	1	
			5507	53	1	
			5506	122	0	
			3383	106	1	
			3363	33	1	
			3336	31		
		12.2 Code: CRA-76, CRA-78, FOT-2,	3361	30		
			3360	30		
			3359	27		
			3376	29		

	FOT-4	5504	26
		3378	36

			AND			
3362	3324	3325	3356	3354	3353	3321
0	0	0	0	0	0	0
	12	12				12
24	30	30	20	20	20	30
	30	54				30
52	42	72	36	36	36	72
	70	87				90
140	87	168	75	50	90	125

175	100	168	147	144	147	157
288	220	224	196	171	196	294
336	245	288	256	288	288	364
364	336	320	324	324	364	364
416	245	288	486	364	405	392
520	269	196	585	450	405	416
455	269	288	486	405	495	336
504	231	252	396	405	405	231
560	269	350	540	605	550	210
540	269	283	630	665	660	231
693	269	270	600	605	840	210
675	294	270	816	665	1144	231
1020	269	270	1080	936	1248	336
1170	294	315	1235	1014	1326	336
1567		243	1358	1176	1755	416
		315		1260		540
		385		1462		567

		385				675
						880

				AND		
5501	5503	3367	3377	3379	5505	3798
		0	0	0		
0	0	0	0	0	0	0
9	9				9	9
		20	40	20		
112	56				96	157
		112	125	42		
540	198	252	336	112	280	512
		324	392	80		
572	318				409	576
693	392				504	765
		420	525	182		
720	472	455	640	273	600	900

		572	792	343		
832	640				847	1080
		616	918	607		
832	720				1080	1296
		572	768	441		
588	504				700	1248
		572	600	312		
864	616				756	1170
		693	577	312		
810	560				756	1326
		715	577	273		
864	654				810	1404
884	748				810	1326
		675	577	227		
1105	816				616	1326
		520	616	132		
1170	864				756	1326
1287	864	600	660	168	560	900
1170						
	1053	693	540	168	650	1020
1287						
	1235				770	1020
		660	577	168		
	1463					
		720	672	168		
		832	672			
		864	994			

Control

1 - High tumor burden or relapse when died

0 - Neither high tumor burden nor relapse when died

1
1
1
1
1

1
1

		TCR M2.3				
3322	3323	3352	5574	5573	3333	3334
0	0	0	0	0	0	0
12	12				12	12
30	30	25	25	25	30	30
54	42				30	42
70	70	45	45	45	72	56
105	87				90	87
122	108	80	80	90	126	120

147	168	108	120	90	171	168
171	245	189	220	196	252	294
256	308	336	336	308	320	343
256	308	409	416	364	360	448
288	308	643	468	364	360	480
283	308	352	352	320	324	392
252	269	220	308	240	283	318
122	269	240	189	220	283	273
122	231	231	245	196	350	336
122	210	210	210	168	350	336
122	210	175	245	157	423	409
196	240	175	189	189	423	409
224	336	240	168	189	702	441
220	308	280	189	168	676	560
224		440	157	189	676	660
		576	175	252		
400					784	1020
495		572	175	396	1050	1215

660		756	231	396	1360	1428
720		1050	308	396		

TCR M2.3

3368	3382	3384	3800	3799	3797	3381
0	0	0				0
0	0	0	0	0	0	0
20	20	20	9	9	9	20
73	72	96	75	80	90	122
112	216	270	269	343	360	168
140	357	448				294
			416	384	498	
294	535	535	504	504	630	607
343	720	567	640	535	630	700

420	940	684				960
			768	792	918	
472	1140	1045				1028
			768	792	1140	
480	1140	760				825
			441	560	1020	
392	935	760				675
			560	560	972	
364	680	810				600
			490	560	748	
392	612	648				600
			420	472	810	
			472	510	841	
273	504	576				560
			525	535	816	
252	595	476				567
			525	400	680	
231	648	476	472	405	680	504
165	680	476	360	425	680	504
			441	360	567	
112	476	360				500
96	525	384				546
94	432	384				676
73	535	476				572

M4.3					amL26	
5550	3351	3364	3363	3336	3361	3360
0				0		
	0	0	0		0	0
12				12		
30	25	24	24	30	16	16
30				30		
67	45	30	30	56	36	36
90				80		
108	98	60	60	96	70	70

210	168	189	140	140	122	140
252	224	308	245	294	171	220
364	252	378	336	336	224	220
416	315	468	364	416	252	320
392	400	567	504	336	288	320
336	500	700	675	567	360	445
273	405	526	504	630	544	445
294	252	384	441	630	648	540
231	283	409	600	630	720	600
364	405	490	525	693	715	650
364	360	490	600	742	840	786
336	450	490	864	864	975	924
420	500	672	1020	960	1050	1170
472	440	720	864	1105	1200	1170
616	786	900	1170	1235	1408	1365
841	858	1105	1567			
1170	1092	1425				

1358	1260					
	1440					

		M4.3				aml
3383	3385	5528	5507	5506	3319	3376
0	0				0	0
0	0	0	0	0	0	0
20	20	9	9	9	20	35
56	80	80	100	112	36	157
160	150	252	294	270	100	294
210	357	409	367	378	108	378
409	612	268	525	420	175	672
409	504	540	560	490	231	616

648	665				320	936
		1080	748	616		
742	880				352	936
		1170	748	660		
880	836				384	1040
		675	612	409		
742	760				308	1040
		1056	535	472		
504	720				336	1144
		880	340	275		
504	535				346	1215
		1020	340	350		
		850	340	375		
416	576				396	1215
		765	360	378		
416	535				396	1326
		990	360	350		
432	535	946	360	292	396	1428
384	535	935	360	216	396	1547
		1224	396	216		
432	535				396	
				160		
336	504				396	
				140		
315	640				396	
				94		
315	680				396	

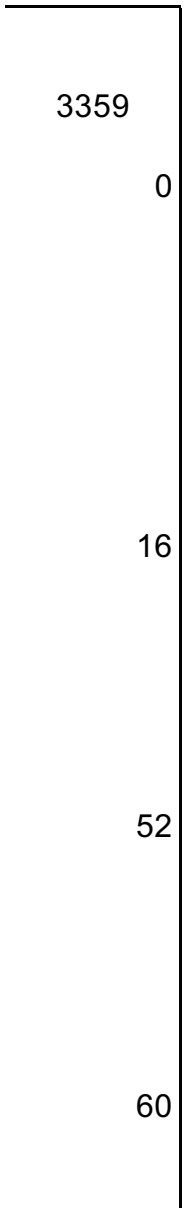
3359
0
16
52
60

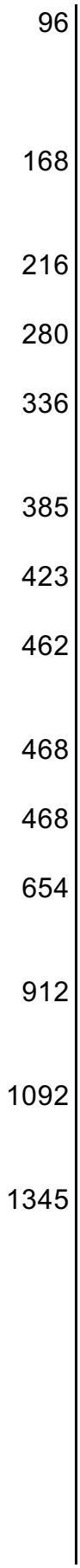
96
168
216
280
336
385
423
462
468
468
654
912
1092
1345

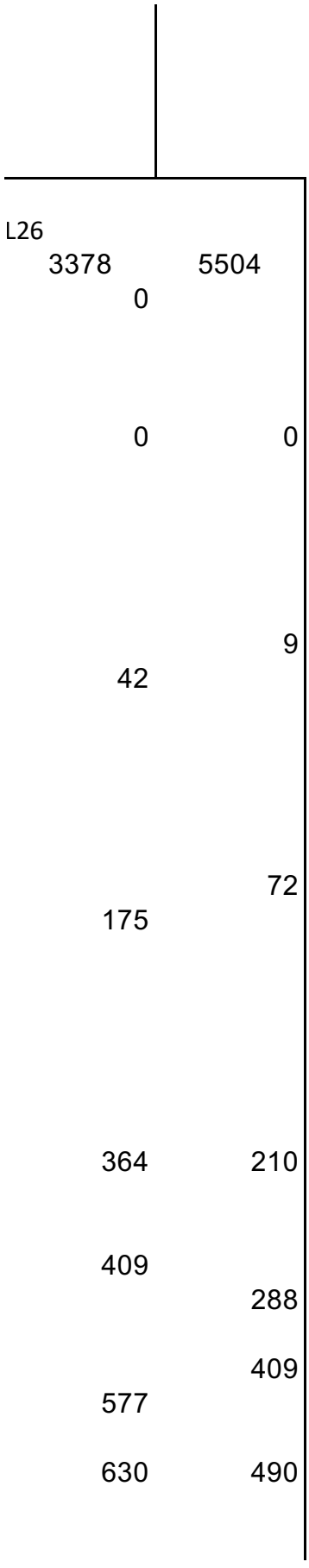
L26
3378
5504
0
0
0
9
42
72
175
364
210
409
288
409
577
630
490

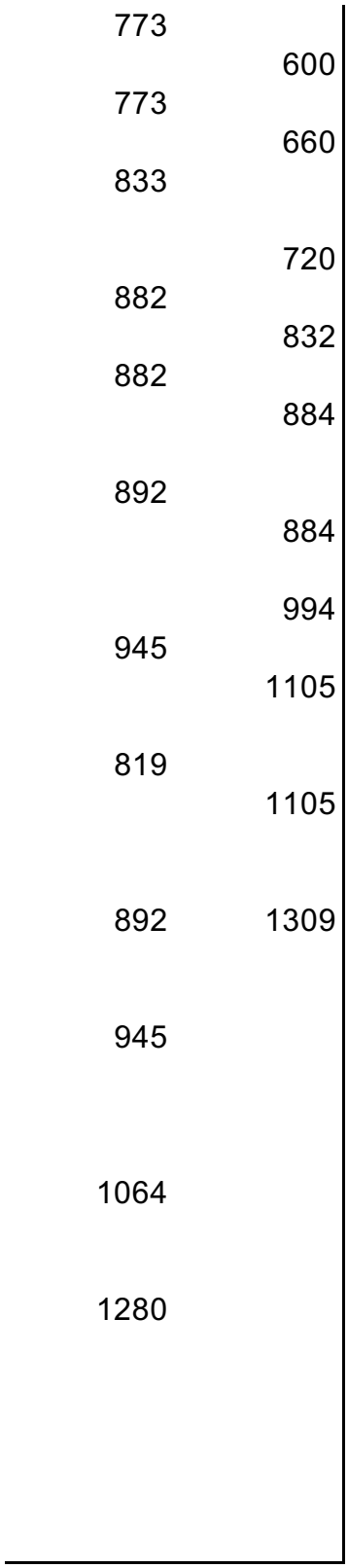
773
600
773
660
833
720
882
832
882
884
892
884
994
945
1105
819
1105
892
1309
945
1064
1280

Fig. S7 Histology Day 6 after H6-T cell transfer, CRA-53, CRA-81

Fig. S8A	Histology Day 6 after H6-T cell transfer, CRA-53, CRA-81	
Days after T cell transfer	Tumor growth, H6-treatment Mouse #1, 037	Mouse #2, 609
-25		
-24		
-23		
-22	0	
-21		
-20		0
-19	0	
-18		
-17	0	
-16		
-15	4	0
-14		
-13	16	
-12		8
-11	45	
-10		
-9		63
-8	90	
-7		84
-6	120	
-5		189
-4	351	
-3		
-2	324	350
-1		
0	539	500
1		
2	600	768
3		
4	864	
5		1425
6	1040	
7		1215
8	840	
9		997
10	693	
11		
12	572	540
13		
14		325
15	315	

Fig. S8B	Analyzing peripheral blood, CRA-3, CRA-12	16		300
		17		
		18	264	
		19		247
		20		
		21	315	144
		22		
		23	270	160
		24		
		25	300	
		26		180
		27	200	
		28		225
		29		
		30	200	
		31		202
		32	160	
		33		
		34		192
		35		
		36	200	
		37		283
		38	200	
		39		
		40	225	192
		41		
		42		
		43	180	168
		44		
		45	200	
		46		
		47	108	360
		48		
		49	160	160
		50		
		51	154	160
		52		
		53	140	
		54		140
		55		
		56		180
		57	220	
		58		160
		59	175	
		60		

	61		160
	62		
	63		
	64	175	140
	65		
	66		192
	67		
	68		192
	69	260	
	70		192
	71		
	72		140
	73		
	74		
	75		160
	76		
	77		160
	78		
	79		160
	80		
	81		160
Fig. S8C	Histology, Day 89 and Day 124 after H6 T cells, CRA-12 #045, #167		

#4719 used for Fig. S9, CRA-52 Repeat CRA-57 Treatment

Original tumor and treatment		BrdU Fflow analysis
Days after H6 T cell transfer	4719	FACS data
-60		
-59	0	
-58		
-57		
-56		
-55		
-54		
-53	0	
-52		
-51	0	
-50		
-49		
-48	4	
-47		
-46		
-45		
-44		
-43		
-42		
-41		
-40		
-39		
-38		
-37	4	
-36		
-35		
-34		
-33		
-32		
-31		
-30	20	
-29		
-28		
-27		
-26		
-25		
-24	99	
-23		
-22		
-21		

-20	
-19	
-18	196
-17	
-16	
-15	
-14	
-13	375
-12	
-11	
-10	
-9	525
-8	
-7	
-6	748
-5	
-4	816
-3	
-2	884
-1	
0	1197
1	
2	
3	1200
4	
5	1760
6	
7	
8	936
9	
10	663
11	
12	528
13	
14	
15	561
16	
17	
18	
19	
20	540
21	
22	
23	
24	

Fig. S9 dapted and r

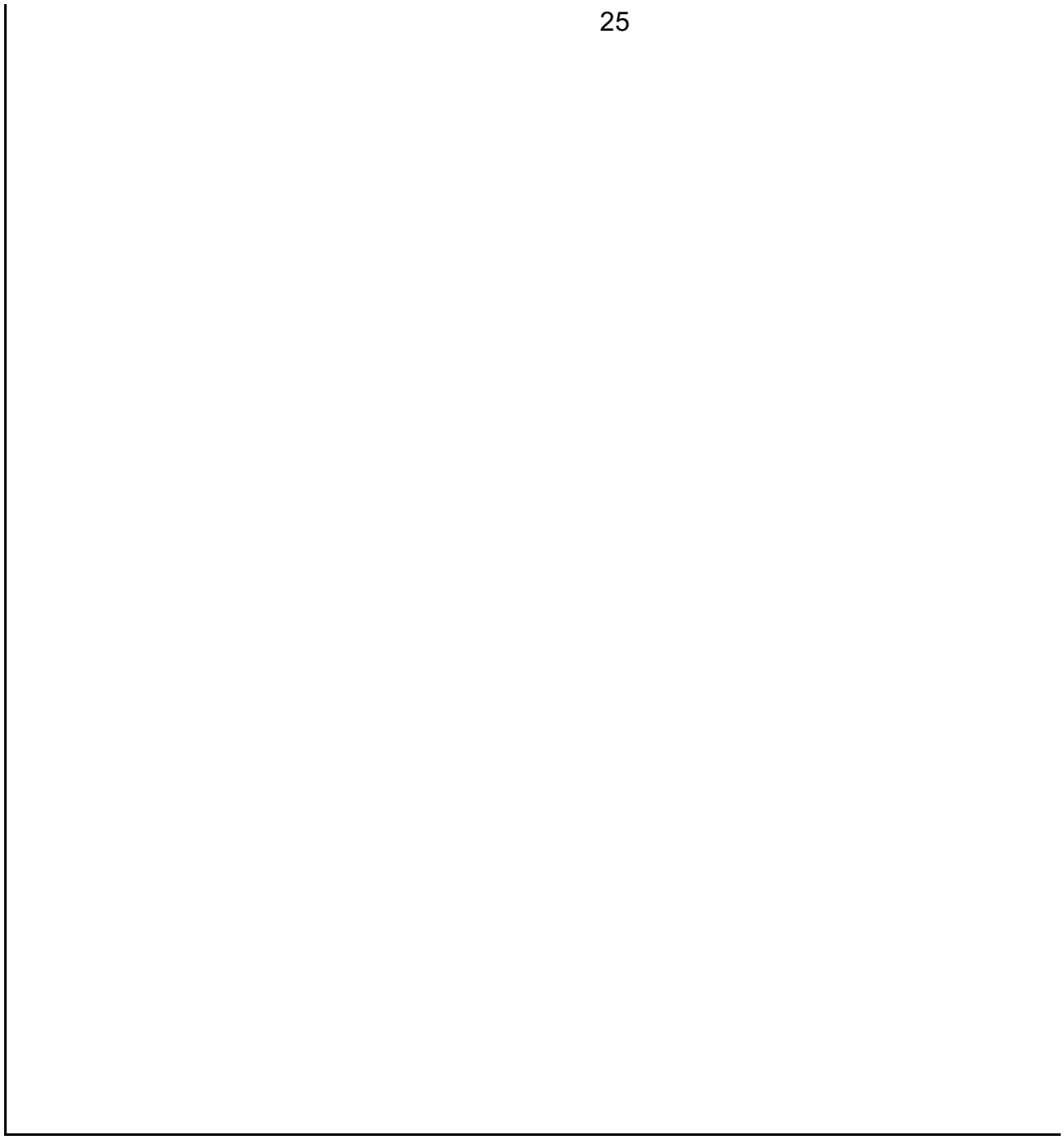

: of 4719 CRA-70, CRA-74

Readadapted cell line flow analysis		Outgrowth of readapted 4719 cell l
FACS data	Days after cancer cell injection	#800 indicated in red
	0	0
	1	
	2	
	3	
	4	
	5	
	6	
	7	144
	8	
	9	416
	10	
	11	
	12	
	13	
	14	362
	15	
	16	630
	17	
	18	952
	19	
	20	
	21	
	22	1197
	23	
	24	1425
	25	
	26	
	27	
	28	
	29	
	30	
	31	
	32	
	33	
	34	
	35	
	36	
	37	
	38	
	39	

line			Retreatment of 4719 tumors with H6 T		
#749	#350	Days after H6 T cell transfer	7049	7048	7047
0	0	-39			
		-38			
		-37	0	0	0
		-36			
	288	-35			
		-34			
		-33			
	448	-32			
	540	-31			
		-30			
168		-29	0	0	0
	675	-28			
		-27			
245		-26			
252	994	-25			
		-24			
		-23	20	20	20
		-22			
	1540	-21			
		-20			
270	1890	-19			
		-18			
432		-17			
		-16			
		-15	94	108	63
		-14			
		-13			
842		-12			
		-11			
		-10			
		-9			
842		-8			
		-7	220	192	157
		-6			
1330		-5	320	318	252
		-4			
		-3	320	343	378
1710		-2			
		-1			
		0	486	504	620

1			
2	600	576	660
3			
4			
5	660	648	780
6			
7			
8			
9	315	378	360
10			
11			
12			
13	240	220	315
14			
15	160	182	180
16			
17			
18			
19			
20	35	81	72
21			
22	28	68	56
23	14	45	56
24			
25			
26	10	18	18
27			
28	2	4	8
29			
30			
31			
32			
33	4	20	20
34			
35			
36			
37			
38			
39			
40			
41	4	20	16
42			
43			
44			
45			

46			
47	4	20	16
48			
49			
50			
51			
52			
53			
54	4	20	16
55			
56			
57			
58			
59			
60			
61	4	20	12
62			
63			
64			
65			
66			
67			
68	4	20	12
69			
70			
71			
72			
73			
74			
75		20	12
76			
77			
78			
79			

Γ cells		
6988	6987	6986
0	0	0
0	0	0
0	0	0
16	16	16
80	56	100
157	140	252
346	288	273
400	409	343
540	441	540
840	560	768